NASA CONTRACTOR REPORT

NASA CR-1713

STUDY AND DEVELOPMENT OF TURBOFAN NACELLE MODIFICATIONS TO MINIMIZE FAN-COMPRESSOR NOISE RADIATION

Volume III - Concept Studies and Ground Tests

Prepared by
THE BOEING COMPANY
Seattle, Wash. 98124
for Langley Research Center

NATIONAL AERONAUTICS AND SPACE ADMINISTRATION • WASHINGTON, D. C. • JANUARY 1971

1. Report No.	2. Government Accession No.	3. Recipient's Catalog No.
NASA CR-1713		

4. Title and Subtitle	5. Report Date
STUDY AND DEVELOPMENT OF TURBOFAN NACELLE MODIFICATIONS TO MINIMIZE FAN–COMPRESSOR NOISE RADIATION. VOLUME III – CONCEPT STUDIES AND GROUND TESTS.	January 1971
	6. Performing Organization Code
7. Author(s)	8. Performing Organization Report No.
	10. Work Unit No.
9. Performing Organization Name and Address The Boeing Company Seattle, Wash. 98124	11. Contract or Grant No. NAS 1-7129
	13. Type of Report and Period Covered Contractor Report May 1, 1967 to November 1, 1969
12. Sponsoring Agency Name and Address National Aeronautics and Space Administration Washington, D.C. 20546	14. Sponsoring Agency Code

15. Supplementary Notes

16. Abstract The program objective was the reduction by 15 PNdB of Boeing 707-320B/C airplane noise during landing approach. It was determined that this goal could be achieved by attenuating the fan noise of the P & W JT3D engines by acoustically treating the engine nacelle. The nacelle fan exhaust duct design was required to contribute the full 15-PNdB attenuation, while the inlet need only attenuate 10 PNdB, since forward noise radiation was 5 PNdB lower. Various configurations of the inlet and fan duct, with acoustic treatment, were studied. The inlet design selected has two concentric rings supported from the cowl by struts at eight radial locations. Polyimide fiberglass acoustic sandwich material is used integrally with the structure of the concentric rings, inner cowl wall, and centerbody. A full length fan exhaust duct with annular nozzle essentially coplanar with the primary nozzle was selected. Acoustic treatment was applied to approximately one-third of the duct length in which inner and outer duct walls as well as four radial flow channel splitters are of polyimide fiberglass acoustic/structural sandwich materials. Ground test results, compared with baseline ground test data on the 707 airplane production nacelle, showed approximately 2 percent increase in thrust due to the new duct design. This gain is offset by increased recovery loss of the new inlet. A take-off thrust noise reduction of 5 to 6 PNdB was predicted from the test results.

17. Key Words (Suggested by Author(s))	18. Distribution Statement
707 Airplane Noise, aircraft Acoustically treated engine nacelles	Unclassified - Unlimited

19. Security Classif. (of this report)	20. Security Classif. (of this page)	21. No. of Pages	22. Price*
Unclassified	Unclassified	85	$3.00

*For sale by the National Technical Information Service, Springfield, Virginia 22151

STUDY AND DEVELOPMENT OF TURBOFAN NACELLE MODIFICATIONS TO MINIMIZE FAN-COMPRESSOR NOISE RADIATION

OVERALL REPORT ORGANIZATION

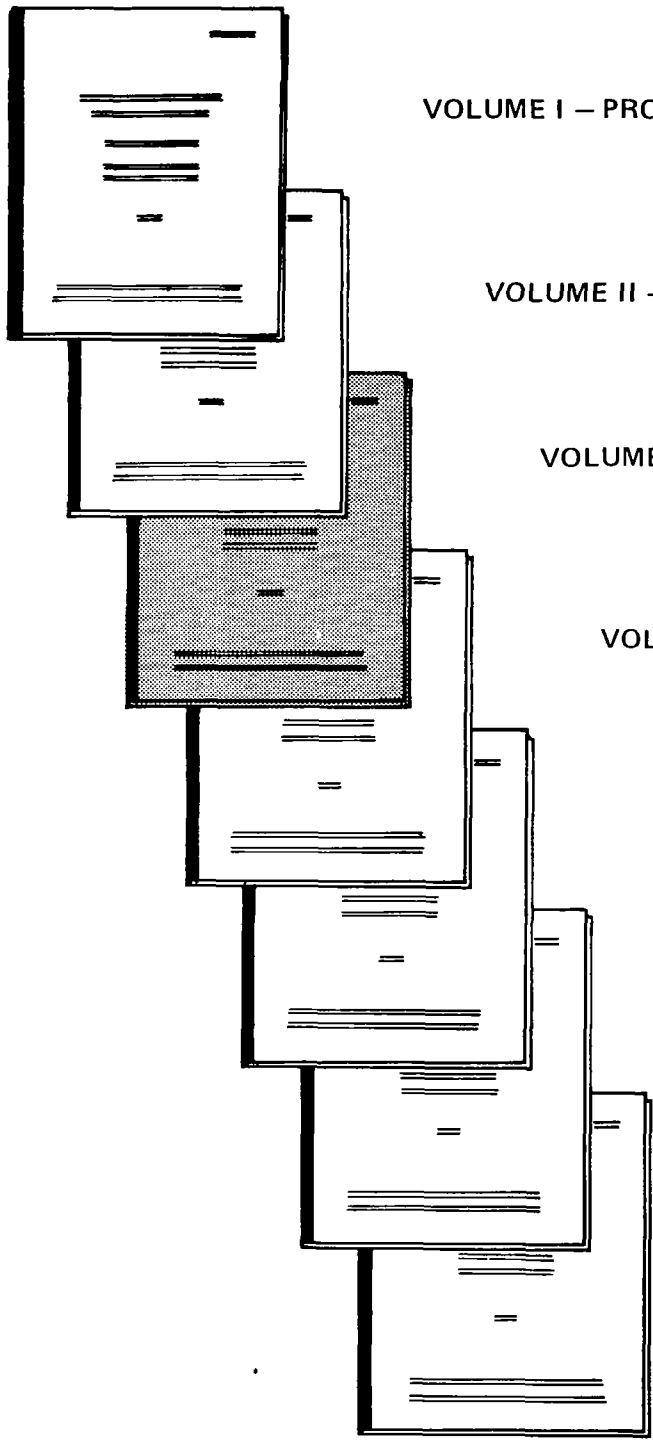

VOLUME I – PROGRAM SUMMARY

VOLUME II – ACOUSTIC LINING DEVELOPMENT

VOLUME III – CONCEPT STUDIES AND GROUND TESTS

VOLUME IV – FLIGHTWORTHY NACELLE DEVELOPMENT

VOLUME V – SONIC INLET DEVELOPMENT

VOLUME VI – ECONOMIC STUDIES

VOLUME VII – SUBJECTIVE EVALUATION TESTS

CONTENTS

TABLES

FIGURES

FIGURES—Continued

FIGURES—Continued

FIGURES—Concluded

STUDY AND DEVELOPMENT OF TURBOFAN NACELLE MODIFICATIONS TO MINIMIZE FAN-COMPRESSOR NOISE RADIATION

VOLUME III

CONCEPT STUDIES AND GROUND TESTS

The Boeing Company
Seattle, Washington

SUMMARY

Initial program studies of perceived noise level (PNL) associated with the JT3D turbofan engine established the relative noise level of each contributing noise source for the full range of engine power settings. It was determined from these studies that the basic program objective of 15-PNdB reduction in perceived noise level during landing approach could be achieved through fan noise suppression only. To achieve this total noise suppression, a 10-PNdB reduction of fan inlet noise and a 15-PNdB reduction in fan discharge duct noise would be required. Preliminary designs of alternate approaches were made and studied for the fan inlet and fan discharge ducts. The basic approach was to install acoustically absorptive structure in both the inlet and fan duct.

Evaluation of treated inlet design concepts resulted in selection of a configuration with two concentric rings supported from the cowl by eight radial struts. Polyimide-fiberglass acoustic sandwich material was used as the integral structure of the rings, the inner cowl wall, and the surface of the standard centerbody. Inlet length was increased approximately 9 in. over the 707 airplane baseline inlet to provide the required length of acoustic treatment for the candidate inlet concepts. The blow-in doors of the baseline inlet were eliminated. The configuration selected satisfied noise reduction objectives with the least acoustical treatment and inlet weight. Also, it provided minimum loss in pressure recovery (1.2 percent at cruise) which resulted in smallest thrust loss over the existing inlet.

The fan exhaust duct design selected from seven concepts evaluated is a full long nacelle duct with annular nozzle essentially coplanar with the primary jet nozzle. Acoustically treated areas were located in two separate parts of the duct. The forward section had double-wall lining plus eight lined flow-dividing splitters over a 69-in. length of duct. The aft section had outer wall lining plus the eight lined splitters over a 30-in. length of duct. All acoustically treated areas were constructed of polyimide-fiberglass sandwich material. This configuration was adjudged to provide the best balance in terms of its effect on airplane range and its capability to achieve the noise reduction objective. The coplanar configuration also had

promise of providing some primary jet noise attenuation. One set of boilerplate treated fan exhaust ducts was fabricated and tested with a JT3D turbofan engine mounted on an engine test stand. Results were compared with a baseline test which used a 707 airplane existing short duct. To evaluate the design, far-field sound pressure levels and engine and aerodynamic performance data were obtained. Test results indicated that this configuration would provide a reduction of 15 PNdB at approach power conditions. Engine thrust measurements indicated an increase in fan thrust of approximately 2 percent over the 707 airplane baseline short duct.

It was concluded that the inlet and fan duct configurations outlined above would achieve the required noise suppression with little airplane performance loss other than that due to the increased nacelle weight. In addition, it was estimated from ground test results that a 5- to 6-PNdB reduction in takeoff noise would result from the boilerplate long duct configuration. These configurations of treated inlet and treated duct were selected for flightworthy design, construction, and test on a Boeing 707-320B/C airplane.

INTRODUCTION

The purpose of this volume is to describe the engineering design concept studies and configuration selection process culminating in the choice of the two-ring, eight-strut, treated inlet and the full long, treated fan exhaust duct. Model tests used to evaluate configuration performance aspects and boilerplate/prototype tests of the full-scale treated fan duct are described, and test results are presented.

The program to reduce turbofan engine compressor noise was begun with simultaneous initiation of concept studies and the materials development activities reported in volume II. In accordance with contract direction, concept studies were organized to investigate sonic or near-sonic inlets and acoustically treated fan exhaust ducts. After completion of the basic design of the boilerplate/prototype sonic inlet (reported in vol. V) and fan exhaust duct, the program was redirected to include the study and development of a treated inlet. A parallel NASA engine noise reduction investigation helped to establish confidence that the mechanically simpler treated inlet could achieve the required noise attenuation. The sonic inlet work was to be carried through development fabrication and ground testing. Flight testing only was planned for the treated inlet. Along with introduction of the treated inlet, the program schedule was revised to reschedule the flight test period 4 mo earlier. The timing of treated inlet design initiation and the acceleration of the flight test program reduced the time period available for inlet development to a minimum. In the interest of completing the program in accordance with the revised schedule, it was decided to limit model tests and eliminate boilerplate/prototype tests of the treated inlet. First full-scale testing was scheduled during ground calibration of the flightworthy nacelle inlet. The judgment to proceed in this manner was born out by the successful performance of the flightworthy treated inlet, as reported in volume IV.

The aerodynamic, acoustic, and structural design considerations that went into the concept studies, as well as a brief summary of the fabrication processes for the boilerplate/ prototype fan exhaust duct, are provided in this section. In addition to containing the description and results of concept studies for both treated inlet and fan exhaust duct of the treated nacelle, this volume describes supporting model tests and results. Model test work is followed by a description of the ground test of the full-scale boilerplate fan duct, including the test configuration, plan, and instrumentation together with the acoustic, propulsion, and aerodynamic test results.

SYMBOLS

A	area, inches^2
A_M	area per unit length of model wake, inches^2/inch
BL	buttock line, a plane that is parallel at a fixed distance from a centerline
C_D	drag coefficient
C_L	lift coefficient
C_V	velocity coefficient
C_{f_w}	average skin friction coefficient
dB	decibel
F_g	gross thrust, pounds
Hz	hertz (cycles/second)
L	length, inches
M	Mach number
n. mi.	nautical mile
P	pressure, pounds/inch^2
PNdB	unit of PNL
PNL	perceived noise level, PNdB

PNLM	maximum perceived noise level, PNdB
q	dynamic pressure, pounds/inch^2
R_e	Reynolds number
SPL	sound pressure level, dB re 2 x 10^{-4} μbar
T	temperature, °R or °F
u	acoustic particle velocity, centimeters/second
U	velocity, feet/second
W_A	engine airflow, pounds/second
X	distance downstream of reference point, inches
δ	pressure ratio, P/P_o
θ	temperature ratio, T/T_o
μbar	microbar
ν	kinematic viscosity, feet^2/pound

Subscripts:

amb	ambient
F_4	fan duct exit plane
S	static
T	total
w	model wake
o	sea level standard

2	engine entrance station
2.5	fan duct entrance station
7	turbine discharge station
∞	freestream

CONCEPTUAL STUDIES

Treated Inlet

At the start of the program to develop technology to reduce fan-generated noise of the Boeing 707-320B/C airplane, it was expected that a sonic or near-sonic inlet would be required to achieve the necessary inlet attenuation. Initial inlet development was limited to the sonic inlet configuration covered in volume V.

Tests conducted during parallel NASA program investigations indicated that sufficient noise reduction could be accomplished with an inlet properly treated with acoustic absorbing material. Because of the schedule advantage which results from the treated inlet's simpler design and fabrication, it was decided to limit sonic inlet development to ground testing. The program was redirected to include design and flight test of a treated inlet in combination with the acoustically treated fan ducts already under development at Boeing.

Attenuation criteria.—Studies of perceived noise levels associated with the JT3D turbofan engine indicate that with an aircraft at an altitude of 400 ft, the contribution of the inlet noise to the total maximum perceived noise level (PNLM) is approximately 5 PNdB lower than that of the fan exhaust noise at approach power (fig. 1). To meet a target of 15-PNdB reduction in maximum perceived noise, therefore, it is required to reduce the forward radiated noise contribution by only 10 PNdB.

Typical sound pressure level (SPL) spectra of the maximum noise attributed to the forward radiation from the baseline untreated inlet are shown in figure 2. When a target attenuation of 20 dB is applied to the inlet noise spectra and is centered near the fan fundamental frequency, the resulting reduction in PNLM is 10 PNdB.

Design constraints.—In evaluating inlet concepts designed to meet the target attenuation, consideration must be given to the effect on propulsion performance. In general, inlet performance is influenced by the amount of acoustic material used, how it is positioned, the length of the inlet required, and the flow diffusion efficiency. Small decreases in pressure recovery can cause significant changes in takeoff and cruise performance of the airplane. It is therefore desirable to use the least amount of acoustic material to provide the required attenuation. The material must also be arranged in a configuration that provides minimum pressure loss.

At the outset, inlet conceptual studies were given direction by the need to avoid wake-generated engine fan blade excitation frequencies. Coordination with Pratt & Whitney established that without recourse to extensive testing and analysis, a minimum of eight struts was required to avoid adverse effects on engine fan blades.

Prior investigation conducted during sonic inlet design studies provided a maximum inlet length of 50 in. This constraint is a function of both engine structural and wing structural limitations for the 707 airplane.

Acoustic treatment.—The quantity of treatment required in an inlet to meet the target noise reduction depends on (1) the radial distribution of the acoustic pressure level in the inlet, (2) the cross-sectional areas of the flow channels formed by the insertion of the acoustic material, (3) the separation distance of the acoustic material, and (4) the type of acoustic material selected. Experimental data showed that the SPL in the 1/3-octave bandwidth containing the fundamental fan frequency was 10 dB higher close to the outer wall than close to the centerbody. To obtain uniform acoustic performance across the inlet, the amount of attenuation provided must vary across the inlet. The material selected for application to the inlet and fan duct of the JT3D engine was a porous polyimide-fiberglass laminate. This laminate was backed by a honeycomb core and nonporous backing sheet to form an acoustic liner. A full description of this material and liner is provided in volume II.

Since the effect of acoustic lining in an engine inlet depends on the distribution of treatment across the inlet, studies were conducted initially to evaluate the merits of a number of different design concepts. Various combinations of radial struts and concentric rings (fig. 3) were studied. All the concepts included acoustic treatment on the inner cowl wall and centerbody.

Each configuration was evaluated by estimating the amount of acoustic treatment required to meet the target attenuation. Results, shown in table I, indicate that treated radial struts require more acoustic treatment than treated rings to produce the same attenuation. Increased treatment is required because the radial splitters have excessively large treatment separation distance at the cowl wall where the maximum attenuation is required.

Aerodynamic performance.—Inlet pressure loss for each concept was estimated by computing the friction drag of the inlet from the flow velocity, the wetted area, and the local skin friction coefficient. Velocity distribution through the inlet was based on one-dimensional net area distribution. The skin friction coefficient for the acoustic material was based on experimental data. These data indicated a coefficient 1.5 times greater than that of a smooth flat plate. Results are tabulated in table I, along with the estimated weight increases of the various concepts.

Inlet selection.—Trade studies indicated that the two-ring concept with untreated struts required significantly less acoustic treatment to meet the objective than any of the designs using treated radial struts. Also, the inlet flow losses were smaller and the weight increase less for the two-ring inlet with untreated radial struts. Consequently, this basic concept was selected for detail design development.

Treated Fan Duct

Various treated fan duct concepts evolved concurrently with the development of model test data and acoustical lining technology (vol. II). These studies permitted determination of the effect of treatment length and duct geometry on acoustic attenuation and performance. The selection of the boilerplate/prototype and flightworthy fan duct configuration was based on a detailed acoustical and airplane performance evaluation of the more promising fan duct concepts studied.

Attenuation criteria.—During landing approach of a Boeing 707-320B/C airplane, the perceived noise level is dominated by noise radiated from the fan discharge ducts. The basic program objective was a reduction of 15 PNdB in maximum perceived noise level during landing approach. The reduction was to be accomplished by attenuation of the predominant, discrete component of engine fan noise.

Development of acoustical treatment to meet the noise reduction objective required that landing approach noise be analyzed. This analysis determined the needed frequency bands requiring attenuation, the amount of noise reduction required, and the possible limitation of attenuation due to other landing approach noise sources. Measured data from the experimental duct tests and predicted jet noise levels enabled a landing approach noise spectrum to be divided into component contributions (fig. 4).

For a reduction in PNLM of 15 PNdB, a reduction of approximately 22 dB is required in the 1/3-octave band containing the blade passage frequency. To ensure that the SPL of this band is established by broadband noise, the discrete fan noise component must be attenuated by an additional 8 dB. Therefore, an attenuation of 30 dB in the fan blade passage frequency range (2200 to 4000 Hz) during engine operation is required. Similarly, adequate attenuation of the second and third harmonics of the discrete fan component

requires reductions of approximately 25 and 20 dB, respectively. A target attenuation spectrum was therefore set (fig. 5). This target attenuation would attenuate the discrete fan noise components over the entire operating range of the engine, but with maximum reduction in fan noise PNL occurring at the landing approach condition.

Preliminary design study.—The existing fan duct on the 707 airplane, shown in figure 6, is very short. It was designed to minimize the weight and external drag of the nacelle. To obtain insight into the most reasonable compromise of fan duct length, cross-sectional area, and shape that could achieve the 15-PNdB acoustic attenuation goal without imposing severe penalties on the performance of the airplane, a preliminary design trade study was undertaken. Four basic configurations were selected for evaluating the amount of acoustic treatment required and the effect on performance.

Figure 7 shows a short fan duct, standard for the 707 airplane, but incorporating a translating sleeve. The sleeve, with its acoustically lined inner surface, would be stowed in the forward position for cruise and translated aft to provide noise attenuation during approach.

The fan duct shown in figure 8 extends to about three-quarters of the nacelle length and has a kidney-shaped nozzle. It is representative of the design flight tested by Boeing prior to this program. This configuration allows considerably more acoustic treatment than the duct shown in figure 7. It also incorporates changes in contours and flow areas to improve aerodynamic performance over the fan duct previously flight tested.

The fan duct shown in figure 9 extends to about seven-eighths of the nacelle length. It also has a kidney-shaped nozzle. Increased length facilitates fan reverser design without complication to the primary reverser. The added length is also expected to decrease boattail drag. Potential for increase in acoustic treatment, if required, is also provided.

Figure 10 shows a full-length fan duct with an annular nozzle. This concept is similar to the seven-eights long duct with the exception that the fan air nozzle has been extended aft to be essentially coplanar with the primary nozzle. Of the four study concepts, it provides for the maximum amount of acoustic treatment.

The following general conclusions were reached from analysis of these designs and evaluation of the results of both full-scale engine and flow duct tests of acoustic materials (see vol. II).

- It did not appear likely that the primary goal of 15-PNdB reduction could be achieved with the limited acoustic treatment shown in figure 7. Although the three-quarters long duct shown in figure 8 had more treatment capability, a 15-PNdB reduction appeared marginal.

- The scrubbing drag of the short fan duct, which is caused by high-velocity fan discharge over the nacelle afterbody, is reduced by the full long duct. This gain tends to offset the weight penalty and increased internal and external drag of the full long duct. With proper duct and nacelle design, equivalent airplane performance appeared possible.

- Attainment of 15-PNdB attenuation appeared possible with well-designed, acoustically treated long ducts.

- Acoustic theory indicated that coplanar fan and primary nozzles would produce some attenuation of primary jet noise. For evaluation of this effect, see volume IV.

Further study was therefore confined to performance analysis of versions of the seven-eighths and full long duct designs.

Acoustic treatment.—As indicated in volume II, the attenuation of individual lining configurations is affected by many parameters, including airflow velocity in the duct channels, number of channel walls treated, distance between opposing channel walls, length of treatment, and type of treatment. Application of these design criteria to a full long duct for determining the peak noise attenuation as a function of treatment length and treatment separation distance is shown in figure 11. All duct channel walls were assumed treated. The acoustic material and liner used was the same as described previously for the inlet. The 30-dB maximum attenuation target can be met with a full treatment length of 69 in. for a configuration having a treatment separation distance of 7 in., whereas an additional treatment length of 15 in. is required for a 9-in. treatment separation. The downstream sections principally attenuate grazing waves, for comparatively small incremental attenuation. The more upstream sections attenuate most of the oblique incident waves as well. However, use of additional acoustic treatment was considered advisable to compensate for possible loss in acoustic effectiveness due to manufacturing variation or contamination while in service.

The nominal flow resistances for the various sections of the duct linings were calculated from SPL measurements. These measurements were made at the fan duct walls of the full-scale, three-quarters long duct engine rig (vol. II) for the maximum approach power condition. The resulting flow resistances and treatment distributions are shown in figure 12.

Single-layer linings on all walls of flow channels will provide adequate attenuation of the peak frequency. However, to obtain adequate bandwidth of attenuation for the required range of approach conditions, some double-layer lining was desirable. Accordingly, a mixed lining configuration was selected. A double-layer treatment 1-in. deep on the outer wall and a 1/2-in.-deep, single-layer treatment on the inner wall and the splitters was used. A honeycomb core cell size of 3/8 in. was selected because of its availability and near-optimum performance.

Performance.–Fan duct performance evaluation was conducted on two versions of the seven-eighths long duct and three versions of the full long duct design concepts, listed below:

- Seven-eighths long duct, kidney nozzle (fig. 9)
- Full long duct, full annular nozzle (fig. 10)
- Seventh-eighths long duct, nearly annular nozzle (fig. 13)
- Full long duct, nearly annular nozzle (fig. 14)
- Full long, annular duct (fig. 15)

Both versions of the seven-eighths long duct (figs. 9 and 13) are bifurcated from the fan flange on the engine into left- and right-hand kidney-shaped ducts having a relatively short arc length and a large wall separation distance. The full long duct with annular nozzle (fig. 10) and the full long duct with nearly annular nozzle (fig. 14) have an elongated kidney shape to reduce turning losses in the bifurcation section and to decrease the separation distance of the acoustic material from approximately 9 to 7 in. The full long annular duct configuration (fig. 15) essentially eliminates turning and was evaluated only as a reference of near-optimum design, since practical attainment would require engine and support strut structure redesign beyond the scope of this program. All concepts have five channels on each side to control turning losses, to provide additional duct channel surfaces for acoustic treatment, and to provide structural ties between duct walls.

In the comparative evaluation, drag changes were estimated from external nacelle losses, including the effects of friction, scrubbing, inlet, boattail, and strut interference. Internal fan duct losses included friction, turning, and nozzle performance. Weight changes for the various configurations were estimated on the basis of the use of the same materials and methods of fabrication. The trade between duct internal flow area and nacelle maximum diameter was studied by considering three duct flow areas at the nacelle maximum diameter. These areas provided for (1) a contraction from 828 in^2 at the fan exit to a flow area of 660 in^2, (2) a constant flow area for much of the duct length, and (3) an expansion from 828 in^2 at the fan exit to a maximum flow area of 900 in^2. In table II, the nacelle drag and weight effects for the three duct flow areas for each of the five design concepts may be compared. Utilizing the data in table II and assuming a constant payload and field length, the airplane performance was analyzed to determine the effect on airplane range. The changes in range as compared with the range of the baseline airplane are shown in figure 16 for the various flow areas considered. The full long, annular duct of figure 15, with 900-in^2 flow area, shows a range increase over the baseline configuration of approximately 25 n. mi. However, as previously stated, the full long annular duct is considered outside the scope of this program. Of the remaining design concepts, the full long duct, full annular nozzle (fig. 10), with 900-in^2 flow area, had the least predicted adverse effect on airplane range–slightly under 100 n. mi.

Duct selection.—In summary, the full long duct, full annular nozzle concept of figure 10, with a maximum flow area of 900 in^2, was considered the preferred concept respecting performance. Also, as mentioned previously, this design has definite acoustic attenuation advantages. including the smaller treatment separation in duct channels achieved by the elongated kidney design. Therefore, the full long annular nozzle concept was selected for design optimization in the boilerplate/prototype portion of the program.

MODEL TESTS

Material Skin Friction

The porous face skin of the acoustic lining provides a flow surface that is more rough than that provided by nonporous material. It was believed that the increased surface roughness along with other lining variables such as porosity, cell size, core depth, and core slant could affect the skin friction in the inlet and fan duct. Tests were run to compare the measured skin friction of various specimens of noise-attenuation material with that of a smooth flat plate.

The 12 specimens tested were typical of the acoustic linings being considered for use in the treated nacelle. Table III describes the test specimens. Figure 17 shows a typical fiberglass porous surface.

The average skin friction coefficient was calculated using Von Karman's integral momentum equation for incompressible flow in conjunction with the measured boundary layer (ref. 1). The test installation is shown in figure 18. Typical boundary layer profiles measured are shown in figure 19. Analysis of the test data indicated that the average skin friction coefficient of the panels tested is 36 percent greater than for the plexiglass plate at $R_e = 1.0 \times 10^6$ and 50 percent greater at $R_e = 5.0 \times 10^6$ (fig. 20). Differences in skin friction coefficients due to different porous skins or honeycomb core configurations could not be distinguished from test data.

Acoustic Ring Wake Survey

A test was conducted to measure the presure loss in the wake behind a two-dimensional model that simulated the outer acoustic ring of the treated inlet. The measured wake loss was used to estimate the loss in inlet total pressure recovery due to the acoustic rings.

The tests were conducted over a Mach number range of 0.1 to 0.4 in the Boeing 14.4- by 18.0-in. model low-speed wind tunnel. The full-scale model was mounted in the tunnel test section as shown in figure 21. Except for the treated surface, the model was fabricated of wood and had a maximum thickness of 0.65 in. with zero camber. A plan view of the model with all critical dimensions is shown in figure 22. The model was geometrically similar to

the outer ring except for the camber, which was eliminated because the mean line of the rings in the treated inlets was designed to be coincidental with the local inlet flow streamline.

Wake surveys were made at three stations downstream of the model's trailing edge during tests at three Mach numbers. The surveys, using a single traversing total pressure probe, indicate that the maximum total pressure coefficient $(P_{T_\infty} - P_{T_W})/q_\infty$ decreased with increasing distance from the model trailing edge, as shown in figure 23.

The momentum loss coefficient is plotted as a function of survey station for Mach numbers 0.2, 0.3, and 0.4 in figure 24. The average momentum loss coefficients decreased slightly with increase in distance from the model trailing edge and increased slightly with Mach number.

To estimate the effect the measured losses would have on the outer ring of the treated inlet, the momentum losses were changed to incremental losses in inlet pressure recovery as follows and plotted as a function of engine airflow in figure 25.

$$\frac{(P_{T_\infty} - P_{T_W})(A_M)}{q_\infty} \times \frac{q_\infty}{P_{T_\infty}} \times \frac{2\pi \text{rad}}{A_2} = \frac{(P_{T_\infty} - P_{T_W})}{P_{T_\infty}}$$

where:

P_{T_∞} = freestream total pressure, psi

P_{T_W} = total pressure measured in wake, psi

A_M = area per unit length of the model wake, $in^2/in.$

q_∞ = freestream dynamic pressure, psi

rad = radial location of outer ring center in the treated inlet, 20.6 in.

A_2 = engine fan face area, 1800 in^2

The tunnel was limited to Mach number = 0.4. The curve was therefore extrapolated using the momentum coefficient and the inlet flow velocity to obtain the average pressure recovery at takeoff and cruise. The estimated engine airflows for the treated nacelle at takeoff, cruise, and approach are noted on the curve. The estimated losses in pressure recovery, based on these airflows, are 0.00465, 0.00415, and 0.0019 for takeoff, cruise, and approach, respectively. In estimating the losses, the velocity gradients and streamline flow curvature that will be present in the inlet were not accounted for.

Treated Fan Duct

A 1/5-scale model of the selected fan duct configuration was constructed and tested to determine the internal performance and to locate regions of high pressure loss inside the duct. The tests were also intended to determine the accuracy of the estimates of internal duct pressure loss used in the conceptual studies. The model tests allowed a more flexible use of instrumentation and a greater range of operating conditions than are feasible during a full-scale engine test. This flexibility provided a highly detailed view of the internal flow and provided data to extrapolate the full-scale ground calibration results to cruise conditions.

The long duct model represented one-half of the boilerplate duct and was constructed so that it could be split apart for flow visualization. Acoustic material was not used in the model.

The model tests were conducted on the Boeing nozzle test rig, shown in figure 26, which measures thrust by mechanically balancing the moment created by the model thrust. Tests on a 1/5-scale Pratt & Whitney reference short duct were also run to provide correlation with available full-scale duct test data. The mass rate of flow through the model, required to determine the velocity coefficient, was determined by measuring the pressure differential across a calibrated flow nozzle between the plenum and experimental duct. The total pressure field at the exit plane of the experimental duct was measured with a 10-probe traversing rake. The relative performance of each channel of the duct was determined from these measurements. The rake probes were within 0.03 in. of the survey plane walls at all rake positions. Static pressures were measured on the inside and outside walls of each flow channel at five axial locations.

The total pressure field was surveyed at the exits of each of the four sections by successively removing sections, thereby providing an estimate of the total pressure loss of each duct section. The traverse test conditions were established by maintaining a constant duct inlet Mach number for the test. The flow visualization test was run by coating the inside of the duct with a mixture of oil and lampblack and rapidly establishing the cruise inlet pressure.

In evaluating the several fan duct configurations tested, where ducts of various lengths were compared, the entire duct loss (the pressure loss and nozzle expansion loss) was expressed as a velocity coefficient. This simplified the data reduction and provided a direct comparison of the performance of all the configurations. In figure 27, the measured velocity coefficients for the full long duct may be compared with those for the Pratt & Whitney reference short duct and those measured in previous 1/5-scale tests of the seven-eighths long duct (described in "Conceptual Studies"). As expected, the performance of the long duct was determined to be better than that of the seven-eighths long duct. The total pressure measurements indicated that the elongated kidney shape and reduced turning decreased the losses in the bifurcation section of the long duct to about half those in the seven-eights long duct model, as shown in figure 28. These results agreed with the estimates made during the conceptual studies.

To predict the full-scale performance of the 1/5-scale model ducts, the effects of Reynolds number, acoustic treatment, and scrubbing drag were estimated. When fan duct performance was related to the total nacelle performance, the scrubbing drag produced by the baseline duct was considered as a thrust loss. Since the scrubbing drag is directly related to the fan duct pressure ratio, the performance effect was included in the fan duct velocity coefficient and fan duct gross thrust coefficient. The predicted full-scale performances of the full long and seven-eighths long ducts are compared with the performance of the Boeing baseline short duct in figure 29. The prediction for baseline short duct performance is based on previous 1/10-scale model tests. From these data, the thrust of the long duct was predicted to be approximately 2.0 percent greater at takeoff and 3.5 percent greater at cruise conditions than that of the baseline duct.

Flow visualization tests and pressure data indicated flow separation at the top and bottom of the entrance to the duct. This separation was probably due largely to the leading edges of the splitters tripping the duct inlet laminar boundary layer. Since the entrance flow to a full-scale duct is turbulent, it was not certain that the model flow separation would appear in full-scale tests. The model data also indicated severe turning and misdirected flow near and at the nozzle of the duct. Since the flow in this section is constantly accelerating, there was no indication of separation or large total pressure losses.

Results of the model tests were examined to define a practical means of evaluating the fan duct performance during the full-scale ground and flight tests. Static pressure taps were more easily installed in a model than the full-scale engine and, as the model data showed, provided sufficient data to indicate the duct flow quality. Fifty static pressures were recorded during the model tests. Static taps were included at similar locations in the boilerplate and flightworthy designs. The ratio of static to total pressure at the duct entrance is plotted for various duct stations for each flow channel in figure 30. The measured static pressure values correlate well with values predicted from one-dimensional theory. The differences in pressures at the downstream end of the bifurcation section (duct station [Sta 135]) and at the end of the duct for the various channels (fig. 30) are directly related to the total pressure losses measured at approximately the same stations (fig. 28). The flow separation near the inlets of the extreme channels, indicated by the flow visualization, is also apparent from the low static pressures at station 135 (fig. 30). Based on the model test results, it was determined that the wall static data provided a sufficiently accurate description of the internal flow quality. Differences between the model and full-scale measurements due to the different boundary layers (and therefore flow areas) will appear, but there should be no changes in the static trends unless the flow field has changed.

Nacelle Wind Tunnel Tests

A transonic wind tunnel test was conducted to investigate the high-speed external aerodynamic characteristics of the modified nacelle. A 0.068-scale half-model with internal nacelle flow was used to simulate the nacelle, strut, and wing geometry, as illustrated in figure 31. Three configurations were tested: (1) a long duct nacelle, (2) the baseline short

duct, and (3) the clean wing with nacelles and struts removed. The long duct model of the modified nacelle represented the external contours of a full-scale nacelle with the following characteristics: full long duct, annular fan nozzle coplanar with the primary exit, kidney-shaped 900-in^2 internal flow area for the fan air, sonic inlet (eight-segment contracting wall), 49-in. inlet length from highlight to engine face, and an NACA 1 series external inlet contour.

The test was conducted in the Boeing transonic wind tunnel facilities. Test parameters included a range of Mach numbers from 0.65 to 0.9 and angles of attack from -2.0° to +6.0°.

Significant results of the test are summarized in figure 32. The data presented include the total external drag of four nacelles plus the nacelle struts. The drag values have been corrected for the tare drag of the internal nacelle flow. Drag adjustments have also been made to correct the inlet velocity ratio to a full-scale cruise condition. For the drag comparison in figure 32, the performance of the clean wing configuration at Mach number 0.65 has been shifted to zero to serve as a drag reference level. The modified nacelle configuration is noted to have a lower drag level than the short duct at Mach number 0.65, but the drag increases more rapidly with Mach number.

Figure 33 illustrates the development of full-scale aerodynamic performance from the wind tunnel data. The external performance of the nacelle is defined so as to include only the external contour from the inlet highlight to the fan exit. That drag attributed to the remainder of the nacelle (i.e., those areas scrubbed by the fan efflux) is excluded from the aerodynamic drag and is considered a thrust loss. Therefore, for the baseline short duct the drag of the aft cowl must be estimated for the wind tunnel configuration. This aft cowl drag is then subtracted from the total (aft + fan) nacelle drag, as shown in figure 33a, to give the resulting unmodified nacelle performance. No adjustment is required for the modified long duct nacelle since the fan efflux exit is coplanar with the primary nozzle. First-order corrections for Reynolds number have then been made to the wind tunnel data to give the estimated full-scale results, shown in figure 33b. It will be noted that the zero reference baseline for the full-scale data is the drag coefficient for the complete airplane less nacelles and struts.

Figure 33 gives the development of full-scale drag data at a lift coefficient of 0.4, whereas figure 34 gives similarly deduced drag data for a range of lift coefficients.

As noted earlier, this wind tunnel test was conducted on a full long duct nacelle with an inlet geometry representative of an adjustable sonic inlet. Pertinent to an external drag analysis, the only geometrical differences between this model and the flightworthy treated nacelle were their respective highlight diameters and a 4-in. increase in inlet length. The several highlight diameters are summarized as follows (full-scale dimensions):

	Highlight diameter, in.
Current 707 baseline nacelle	48.5
Treated nacelle (as flight tested)	50.0
Wind tunnel model	47.5

According to the drag estimation methods currently used by The Boeing Company, the geometrical differences between model and flight test nacelles would lead to an increment of 0.0001 full-scale drag coefficient over that predicted directly from the wind tunnel tests. Adding this increment to those given in figure 34 at $C_L = 0.4$ and at Mach numbers 0.80 and 0.83 indicates respective total drag coefficient increments of 0.0004 and 0.00055 due to the nacelle modifications. These increments are approximately 1.8 percent and 2.5 percent of total airplane cruise drag. It will be noted that this estimate does not include an allowance for full-scale excrescence drag.

Lift and pitching moment changes were also studied during the model tests. In general, these changes were found to be small and of little significance.

BOILERPLATE/PROTOTYPE, TREATED FAN DUCT

Design

The full long, full annular nozzle duct concept selected for full-scale boilerplate/prototype design consists of three basic components (see figs. 10 and 36). The forward, or bifurcation, duct component divides the annular exit from the fan into a left- and right-hand kidney-shaped half duct. This division is required to accommodate the engine support strut, the constant-speed alternator drive, and nacelle ground clearance. The second component is the wrap cowl duct, which consists of a left- and right-hand half duct. These duct halves are essentially of constant area and kidney shape. The nozzle duct makes up the third component. The forward section of the nozzle duct is called the thrust reverser reserve section. It represents that portion of the fan duct which in a production design could incorporate a fan thrust reverser. This would be an alternate design to a fan thrust reverser located in the bifurcation duct as is standard on the 707 airplane. The aft section of the nozzle duct provides the transition from the two half ducts to the full annular shape. This section terminates essentially coplanar with the primary nozzle. In a production design, this aft section would translate aft during primary jet thrust reverser operation. The boilerplate duct was designed to simulate as closely as practicable the contemplated flight design (see vol. IV).

Aerodynamic.—The detail development of fan duct contours that would hold internal aerodynamic losses to a minimum with the configuration selected required that the duct be fitted around the engine and accessories to give the smallest nacelle diameter; that turning in the bifurcation duct and fore portion of wrap cowl be kept to a minimum; that expansion from fan exit area of 828 in^2 to the 900-in^2 constant area section preclude unacceptable local diffusion; and that the constant area section be as long a length as the space available between engine and external nacelle contour would allow. For the aft external contour, a radius of approximately six times the nacelle diameter was selected. These constraints required the duct to be proportioned in cross-section area, as shown in figure 35.

Internal contours were obtained by the use of a mathematical transformation of three-dimensional duct curvature into a plane. See figures 36 and 37 for the resulting contours. To keep the turning losses reasonable and to decrease the possibility of flow separation, the radii of curvature in the flow direction were made greater than the channel height. The diffusion through the bifurcation section is equivalent to that in a conical diffuser with a wall angle of about 1.1°, and is about the same as the growth in the boundary layer displacement thickness. Where practicable, the diffusion was accomplished with a linear area progression. The constant area section is approximately 48 in. long. It retains the same cross section as the exit of the bifurcation section for the entire length. The nozzle transition section is about 86 in. long. The transition design was obtained by fairing smooth lines in a manner that gave only a slight amount of curvature to the internal contours in the flow direction. To facilitate the fabrication of the boilerplate duct, curvature of the nozzle transition was approximated with a series of straight line segments.

Structural.—The complete boilerplate duct was designed to satisfy a design ultimate differential pressure of 40 psi. Because of the limited intended use and compound shape of the bifurcation duct, it was designed to be constructed of glass-fabric-base epoxy resin laminate. Duct walls and the channel splitters are an integrally bonded assembly. The forward flange is bolted to the engine fan exit flange, and the aft flange utilizes a compression-type mechanical seal in mating with the wrap cowl duct.

The wrap cowl duct, which encloses the accessory section of the engine, was designed to permit access for engine maintenance. The fore and aft ends of the cowl were inclined planes (see fig. 36) to simulate a contemplated production configuration wherein the wrap cowl duct halves would swing from a vertical hinge located at the forward end. However, for the ground test the wrap cowl duct halves were bolted to the test stand structure that simulates the airplane nacelle strut. Acoustic requirements dictated that the full length of wrap cowl duct walls and channel splitters be acoustically treated, as described previously (fig. 12). For this purpose, polyimide-fiberglass sandwich material, which has good acoustic and structural properties, was used (see vol. II for more detailed information). To gain design and construction experience with the structural capabilities of polyimide, it was decided to construct the boilerplate wrap cowls completely of this material. The polyimide-sandwich wrap cowl duct walls and splitters are joined together by through bolts contained in the splitters to form the final assembly. Detail design of the polyimide-fiberglass sandwich components is covered in volumes II and IV. The inside surface of the inner wall is protected from engine heat by a foil/fiberglass insulation blanket.

Fabrication

To ensure proper duct-to-engine clearances and to determine necessary engine tubing changes, a clearance mockup was constructed around the 707 airplane JT3D engine mockup stand (fig. 38).

The boilerplate duct was constructed without the need for special tooling except for the polyimide-fiberglass acoustic/structural panels. Typical formed metal tooling for the polyimide-sandwich layup and curing are shown in figures 39 and 40. To minimize tool construction, the acoustic side porous laminates and the nonporous sandwich closure laminates were formed on the same fixtures.

Figure 41 shows the completed epoxy fiberglass bifurcation duct, which was formed on a water-soluble mold conforming to the duct inside mold lines.

Since the polyimide-fiberglass wrap cowl duct was fabricated in manner similar to the flightworthy article, reference should be made to volume IV. Construction is illustrated in figures 42 and 43.

The essentially all-metal nozzle duct is pictured under assembly in figures 41 and 44, and the completed boilerplate duct is shown in figures 45 and 46.

Test

The boilerplate treated long duct was installed and tested on a JT3D-3B engine at the Boeing Tulalip Test Facility (figs. 47 and 48). The test configuration included the Pratt & Whitney reference inlet and the 707 airplane primary nozzle. A baseline configuration, the 707 airplane short fan duct and primary nozzle with the Pratt & Whitney bellmouth inlet, was also tested. Acoustic test configurations used an inlet noise directionalizer to minimize the possibility of inlet radiated noise affecting the duct radiated noise measurements.

The basic engine parameters measured were the engine thrust and fuel consumption, compressor speeds, turbine and compressor pressure ratios, and turbine and fan discharge temperatures. To monitor engine operation, these measurements were compared with those of the Pratt & Whitney reference configuration run in a previous test program. To evaluate duct performance, they were compared with those of the baseline configuration.

Static and total pressures were measured inside and at the exit of the boilerplate duct to provide data for evaluating the internal performance of the full-scale duct. The purpose of the exit pressure measurement was to determine the individual loss of each duct flow channel and to provide an average total duct loss. The average total duct loss was then compared with that determined by the thrust measurements. The internal pressure measurements were intended to show the axial distribution of loss in each flow channel.

Acoustic measurements were made in the far field, using microphones located on a 200-ft radius in the horizontal plane through the engine centerline and on a 75-ft radius in the vertical plane (fig. 49). Full-scale acoustic evaluation of the treated duct was obtained by comparing the noise radiated from the boilerplate duct with that radiated from the baseline short duct.

The test site environmental conditions were recorded during each run so that the acoustic and engine data could be corrected to standard day conditions. Environmental parameters recorded were atmospheric pressure and temperature, relative humidity, wind velocity, and wind direction. General weather conditions, such as rain, fog and overcast, were noted.

Propulsion and aerodynamic performance tests were conducted with 13 test points between idle and takeoff. The test points were defined in terms of low-pressure compressor rotor speed, and each condition was held for 3 min before recording data to ensure engine stability. Acoustic data were recorded for 1 min after a 4-min stabilization period at each of seven test points. Each test condition was run three times and the data were averaged.

Acoustic performance.—Far-field acoustic data were analyzed into preferred 1/3-octave bandwidths, with the analysis system providing the average sound pressure level over 6 to 8 sec of data. For each engine power setting, the resulting sets of data were arithmetically averaged. In addition, narrowband analysis was used to resolve spectral components, and SPL versus time analyses were used to study data variability. With the engine set at approach thrust, typical SPL variations during a 1-min data sample are shown in figure 50 for both the baseline and boilerplate treated fan ducts. Also shown are the instantaneous maximum and minimum levels recorded during the three 1-min data samples for this particular engine condition.

Acoustic spectral data recorded in the horizontal plane were affected by the ground plane, and the effect was most noticeable in measured spectra as a dip in the frequency range of 500 to 800 Hz. Comparison of horizontal and vertical plane data, given in figure 51, indicates that both sound pressure reinforcement and cancellation were present due to the interaction of direct and reflected sound waves. Figure 52 shows this acoustic wave interference phenomenon based on simple plane reflection theory. However, the changing nature of both ground surface and atmospheric conditions and the extended noise source characteristics of the engine are such that the problem is extremely complex. At this time, only an indication of the presence of such effects may be made.

Comparison of acoustic data from previous JT3D ground tests with in-flight data for a 707 airplane showed that better agreement was obtained in the 1- to 10-kHz frequency range using data from the horizontal plane. For this reason, horizontal plane results have been used for the determination of PNL values. Where spectra are presented, samples from both planes of measurement are shown. It was observed that 1/3-octave band level reductions achieved by installation of the long treated ducts were similar when determined from either horizontal or vertical plane measurement.

Data from the short duct baseline configuration were compared with short duct data obtained previously. Comparison of the data, shown in figures 53 and 54, provides information on the repeatability of data from the test facility over a 6-mo time period. It also shows the variable nature of the effects from the ground plane. The interference phenomenon is more noticeable in the later test results. Vertical plane data from both periods show good agreement.

At a static thrust equivalent to a typical in-flight thrust during landing approach, the sound pressure level of the 1/3-octave bands containing the fan blade passage frequency was reduced by approximately 20 dB. For these same conditions, the SPL of the bands containing the second harmonic of the fan blade passage frequencies was reduced by 15 to 17 dB. In frequency bands above 5000 Hz, turbine-generated noise (see App. C, vol. II) was found to be present and the reduction in fan noise at these frequencies was therefore effectively limited. Comparative spectra at the angle of maximum fan noise for baseline short untreated and boilerplate full-length treated fan ducts are shown in figure 53. It can be seen that at frequencies below 1000 Hz, where primary and secondary jet noise predominates, sound pressure levels were lower by 3 to 5 dB for the full-length ducts. However, it was found that at microphone locations toward the point of maximum jet noise, about 140° from the inlet, the jet noise levels for both baseline short and boilerplate long duct configurations were similar. This change in directivity characteristics of jet noise is attributed to the coplanar nozzle arrangement of the long ducts. Correlation with in-flight data was made to determine whether the same changes in directivity were present (see vol. IV).

Comparative spectra at maximum gross thrust are shown in figure 54. As at lower thrusts, the strong fan noise components in the 1- to 10-kHz frequency range have been virtually eliminated, but due to the higher noise levels of the primary and secondary jet, the maximum measured reduction is limited.

Sound pressure level radiation patterns of the 1/3-octave band containing the fan blade frequencies are shown for approach and takeoff thrust in figure 55. The peak SPL's in this critical frequency band are shown for both baseline and boilerplate fan ducts in figure 56 as a function of gross engine thrust. It was found that a substantially constant reduction—20 to 22 dB—in the fan blade passage frequency band SPL was achieved up to a gross static thrust of approximately 13 000 lb. At higher thrusts the predominance of the jet noise spectra effectively limits the SPL reduction that can be measured.

One-third octave bandwidth analysis does not provide the spectral resolution required to identify the true attenuation of the discrete fan-generated noise components. Narrowband analysis examples, which are shown in figure 57, enable the physical attenuations of these discrete components to be more accurately identified.

During engine operation, the fan blade passage frequencies are between 2 and 3.8 kHz. The corresponding range of frequencies for the second harmonic of these components is, therefore, 4 to 7.6 kHz. The attenuation of these components may be used to develop an attenuation spectrum in the frequency range of 2 to 7.6 kHz. This experimentally determined attenuation spectrum shows good agreement when compared with the design target spectrum, as given in figure 58.

Narrowband analysis also revealed a discrete frequency component at approximately 4 kHz. The source of this component, which was in evidence only at lower thrust conditions, has not yet been identified. This component does not, however, increase the 1/3-octave band levels by any significant amount.

No measureable changes in sound pressure levels in the 2- to 6-kHz frequency range were recorded in the far field with a blanking cover installed over the last 30 in. of acoustic treatment in the ducts. It was concluded that the initial 69 in. of acoustic treatment attenuated fan noise to a level equal to or below the noise levels set by other sources.

Efforts were made to identify these noise sources and thereby establish whether similar levels would exist with the flightworthy nacelle. Three additional tests were performed with the boilerplate duct configuration modified as outlined below.

- Acoustical insulation was added to cover the exterior of the forward end of the test configuration (bellmouth, fan case, and bifurcation section). This insulation was made to simulate the fan cowl of the flightworthy design, which could possibly reduce noise transmission.

- Acoustical insulation was added to cover the exterior of the thrust reverser reserve section of the nozzle duct, which was a possible source of noise transmission.

- The duct nozzle splitters were locally altered at the exit plane. The purpose of this change was to effectively eliminate aerodynamic separation at this point (caused by the abrupt change in splitter surface contour) and thus eliminate a possible source of broadband noise. Flightworthy hardware was designed to avoid this problem.

Results from these additional tests showed no change in measured noise levels. The broadband noise levels are attributed to primary and secondary discharge flow. The narrowband spectra in figure 57 shows discrete components at fan blade passage frequencies. As the magnitude of these components did not change when treatment length was reduced or when sections of the configuration were acoustically wrapped, they are attributed to inadequate noise suppression at the forward end of the test configuration.

Although the treated inlet, with possibly better inlet noise suppression than the directionalizer, may eliminate the discrete components at fan blade passage frequencies, the effect on 1/3-octave band levels would be small. The spectral component at 4 kHz, the source of which has not been identified, is expected to be present in the flightworthy configuration. It was concluded that noise levels similar to those measured during tests of the boilerplate treated fan ducts will also be measured during static testing of the flightworthy hardware.

As a preliminary indication of the in-flight, acoustic performance of full-length treated fan ducts, polar far-field acoustic data were extrapolated to a line 200 ft from and parallel to the engine centerline. At each point corresponding to an angular microphone location on this sideline, the PNL was determined from the extrapolated 1/3-octave band levels. A comparison between the boilerplate and baseline fan duct noise levels, using data corrected to a 200-ft sideline, is shown in figure 59. As an approximation, it may be assumed that the noise level of one engine at 200 ft is representative of that of four engines during a 400-ft altitude level flyover (SPL varies as the inverse ratio of distance squared). This assumption is valid, since errors from atmospheric absorption corrections are minimal due to the fact that the instantaneous PNLM occurs at a point close to the overhead position (approximately 110° to the inlet centerline).

The predicted mean reductions in PNLM during a 400-ft-altitude level flyover are shown in figure 60. The mean reduction at approach thrust is 12 to 13 PNdB. At thrusts below those normally used during flight operations, PNL reductions are progressively limited by the increasing predominance of noise components other than fan discrete tones. At higher thrusts, the increasing levels of primary jet noise are reflected in decreasing PNL reductions. At takeoff thrust, a 5- to 6-PNdB reduction is predicted. Although data showed that with duct treatment the design target attenuation spectrum had been achieved, the predicted PNL reductions at approach thrust did not show the 14 to 15 PNdB anticipated. It was concluded that the cumulative effect of noise from other sources constituted a noise floor that effectively limited the PNL reductions. An additional 1- to 2-PNdB reduction was estimated through reduction of these other noise sources with a flightworthy nacelle. As stated, the attenuation characteristics of the duct treatment were equal to the design requirements for meeting the noise reduction objective. The duct treatment configuration of the boilerplate ducts was, therefore, considered suitable for installation in the flightworthy hardware.

Propulsion performance.—The boilerplate duct exit area was adjusted to correspond to the operating condition specified by previous tests of the Pratt & Whitney reference configuration. The operating condition is defined in terms of the fan pressure ratio as a function of fan speed. The fan exit distortion was less than 5 percent at the takeoff condition when the boilerplate duct was installed. This is considerably less distortion than that of the baseline configuration (fig. 61). The distortion of the total pressure field at the fan exit is a measure of the distribution of the duct loss and is a primary consideration in mating a duct to the engine. Pratt & Whitney specifies a maximum total distortion of 14 percent to prevent excessive stress on the fan blades.

As shown by figure 62, the thrust developed by the JT3D-3B engine with the boilerplate ducts was found to be 1 percent greater than that with the baseline ducts (approximately 200 lb at takeoff), while the specific fuel consumption was measured to be 1 percent less (fig. 63). Since the fan thrust under static conditions is approximately half the total thrust, the performance of the boilerplate duct was 2 percent better than that of the baseline duct. This result confirmed the performance predicted by the model test, reported in this volume, up to the takeoff pressure ratio of the engine.

The pressure field at the duct exit was measured by traversing the exit plane over a 180° arc with a rake containing static and total pressure probes. Internal wall static pressures were recorded at five axial locations, and total pressures were recorded near the forward end of the duct. The circumferential distribution of the duct total pressure loss is shown in figure 64. The average pressure at the exit of each of the five duct channels is shown as a function of inlet pressure in figure 65. The pressure data indicate an unexpected high-pressure loss in the next to the bottom flow channel. The cause of this loss, which apparently occurs in the aft section of the duct, is not known. A rapid increase in pressure loss occurs in the bottom two channels as inlet pressure is increased.

The internal static pressure trends show good agreement with the model data except in the bottom channel, where the static pressure in the nozzle does not decrease as expected (fig. 66). The boilerplate data indicate an increase in the outside wall static pressure near the exit of the bottom channel. The cause of this pressure increase was not established. The boilerplate duct static pressure values agreed to within 2 percent of the corrected model data. The model data were corrected to the measured full-scale dynamic pressure, and the effects of full-scale skin friction (Reynolds number and acoustic material) were estimated. The pressures in the top channel are higher and those in the channel next to the bottom are lower than expected. The higher statics in the top channel could be explained if the indicated model flow separation at the inlet of the channel (and resultant large pressure loss) were laminar. The low static pressure in the next to the bottom channel correlates with the low total pressure recovery at the exit measured by the traversing rake. The static pressures measured by the traversing rake indicated a distorted flow field at the bottom of the duct, with the exit pressure of the bottom channel approximately 0.5 psi greater than that of the channel next to the bottom.

CONCLUDING REMARKS

Conceptual studies of treated inlet and fan duct configurations, and the model and full-scale boilerplate testing related thereto, led to the following conclusions.

- The fan duct treatment achieved the target attenuation spectrum with a maximum reduction of 30 dB in the fan blade passage frequency range of 2200 to 4000 Hz. However, only 12- to 13-PNdB reduction was evident at approach thrust, which was short of the 15-PNdB objective. It was concluded that the cumulative effect of noise from other sources during the boilerplate ground tests produced a noise floor limiting further total engine PNL reduction. An additional 1- to 2-PNdB reduction was estimated through reduction of this background noise in the flightworthy nacelle. Therefore, the boilerplate configuration was judged suitable for flightworthy development where a complete nacelle design and a treated inlet in lieu of a directionalizer would reduce the noise floor.

- Ground tests of the boilerplate treated long duct indicated that a noise reduction of 5 to 6 PNdB will result at takeoff thrust.

- Inasmuch as the contribution of inlet noise to total perceived noise is 5 PNdB lower than fan exhaust noise, it is necessary to reduce forward radiated noise by only 10 PNdB to meet the total target of 15 PNdB.

- From nacelle wind tunnel tests, it is indicated that the total airplane cruise drag for the treated-nacelle airplane will increase 1.8 percent at Mach 0.80 and 2.5 percent at Mach 0.83 with respect to the baseline airplane.

- Data from model tests forecast a 3.5-percent thrust improvement in cruise for the boilerplate treated long duct with respect to the baseline short duct.

- Full-scale testing of the boilerplate treated long duct showed 2 percent greater takeoff thrust than for the baseline short duct, confirming predicted performance.

- Total fan exit distortion was less than 5 percent at takeoff for the boilerplate treated long duct in contrast to measured distortion of over 11 percent for the baseline short duct.

- Tests with 30 in. of acoustic treatment in the nozzle duct blanked off demonstrated that the initial 69 in. of treatment in the wrap cowl duct was sufficient to attenuate fan noise to a level equal to or below the noise levels set by other sources.

- Of the several inlet concepts studied, the two-treated-ring configuration with untreated struts provided the noise reduction necessary to satisfy the program objective, with the least pressure recovery loss and the least weight penalty.

- Of the many fan duct concepts evaluated, the selected full long, full annular coplanar nozzle design showed the greatest ability to meet the 15-PNdB fan exhaust noise attenuation goal and exhibited the least range penalty.

The Boeing Company
Commercial Airplane Group
Seattle, Washington, September 1969

REFERENCE

1. Schlichting, Hermann: Boundary Layer Theory. McGraw-Hill Book Co., Inc., New York, 1960.

TABLE I.—INLET DESIGN TRADE STUDY RESULTS

Concept (a)	Treatment required, ft^2	Cruise pressure recovery loss, percent	Weight increase, lb (b)	Length increase, in. (b)
1	84	1.2	93	9
2	113	1.3	134	9
3	119	1.5	143	9
4	157	1.7	201	16

[a]See figure 3 for description of inlet concepts.

[b]Referenced to Boeing 707-320B/C airplane existing inlet.

TABLE II.—DUCT DESIGN TRADE STUDY RESULTS

Duct configuration	Duct flow area, in^2	Nacelle drag at M = 0.8 and 35 000-ft altitude, lb/nacelle			Nacelle weight increase, lb/nacelle (a)
		Internal drag, lb	External drag, lb	Total drag, lb	
Full long, annular duct (fig. 15)	660	208	257	465	711
	828	169	274	443	726
	900	129	279	408	733
Full long duct, full annular nozzle (fig. 10)	660	248	280	528	638
	828	209	290	499	660
	900	177	296	473	670
Full long duct, nearly annular nozzle (fig. 14)	660	259	276	535	622
	828	231	290	521	644
	900	206	295	501	654
Seven-eighths long duct, nearly annular nozzle (fig. 13)	660	244	300	544	577
	828	223	314	537	599
	900	198	320	518	609
Seven-eighths long duct kidney nozzle (fig. 9)	660	244	297	541	575
	828	223	310	533	597
	900	197	316	513	609

[a]With respect to the existing Boeing 707-320B/C airplane short fan duct nacelle (baseline).

TABLE III.–SKIN FRICTION TEST SPECIMENS

Porous layer description			Honeycomb core description		
Material	Porosity, rayls (cgs)	Orientation of weave with respect to flow, deg	Slant, deg	Depth, in.	Cell size, in.
Woven fiberglass laminate	30	45	0	1/2	3/8
Semiwoven stainless steel fiber	30	90	0	1/2	3/8
Woven fiberglass laminate	30	90	0	1/4	3/8
Woven fiberglass laminate	30	90	0	1/2	1/8
Woven fiberglass laminate	30	90	0	1/2	1/2
Woven fiberglass laminate	30	90	0	1	3/8
Woven fiberglass laminate	30	45	30	1/4	1/8
Woven fiberglass laminate	30	45	30	1/4	1/8
Woven fiberglass laminate	30	90	60	1/4	1/8
Woven fiberglass laminate	18	45	0	1/2	3/8
Woven fiberglass laminate	3	90	0	1/2	3/8
Woven fiberglass laminate	25	90	0.5-in.-thick solid core		
Plexiglass	–	–	0.5-in.-thick sheet		

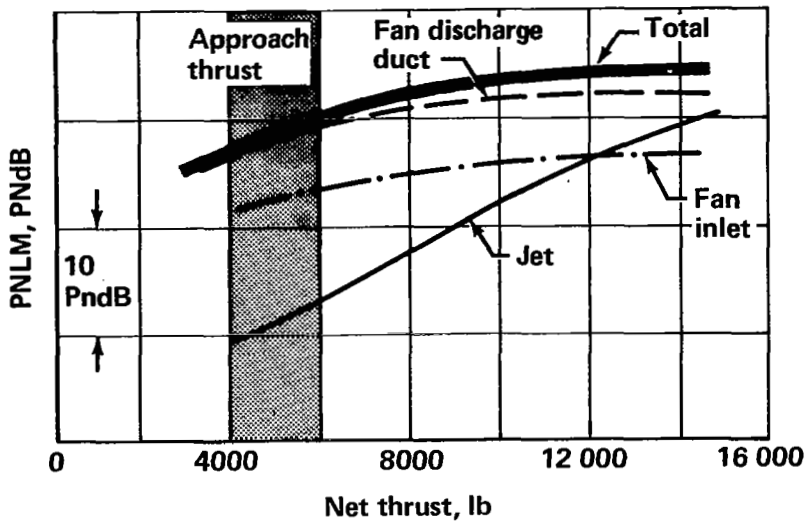

FIGURE 1.—TURBOFAN NOISE COMPONENTS DURING LOW-ALTITUDE FLYOVER

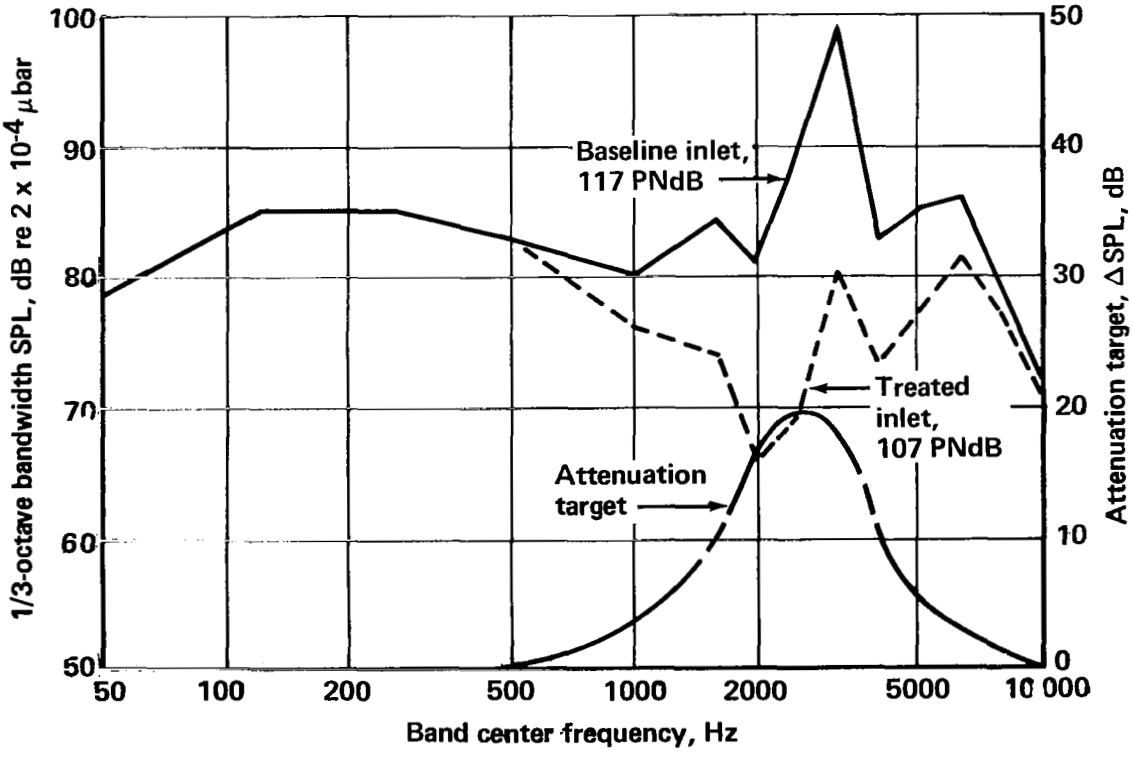

FIGURE 2.—INLET NOISE ATTENUATION TARGET

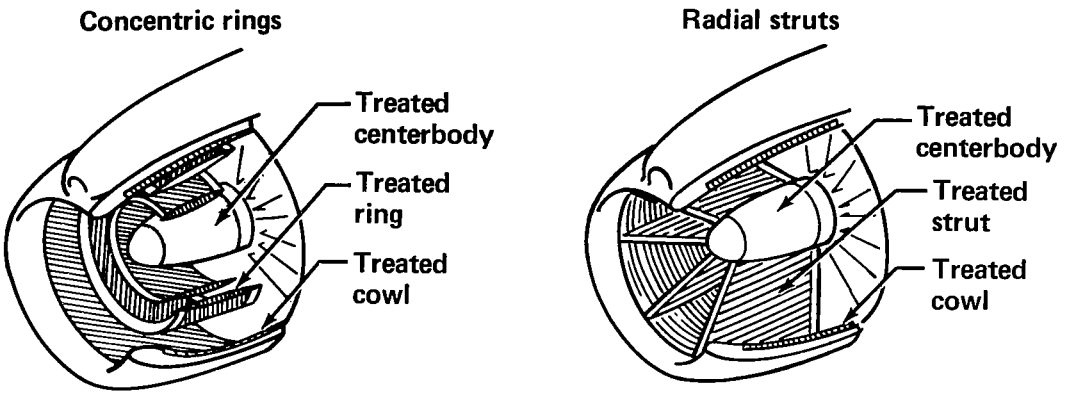

Concept 1 = 8 untreated struts + 2 treated rings
Concept 2 = 8 treated struts + 2 treated rings
Concept 3 = 12 treated struts + 1 treated ring
Concept 4 = 12 treated struts

All concepts have treated cowl and centerbody.
See table I for evaluation results.

FIGURE 3.—INLET CONCEPTS

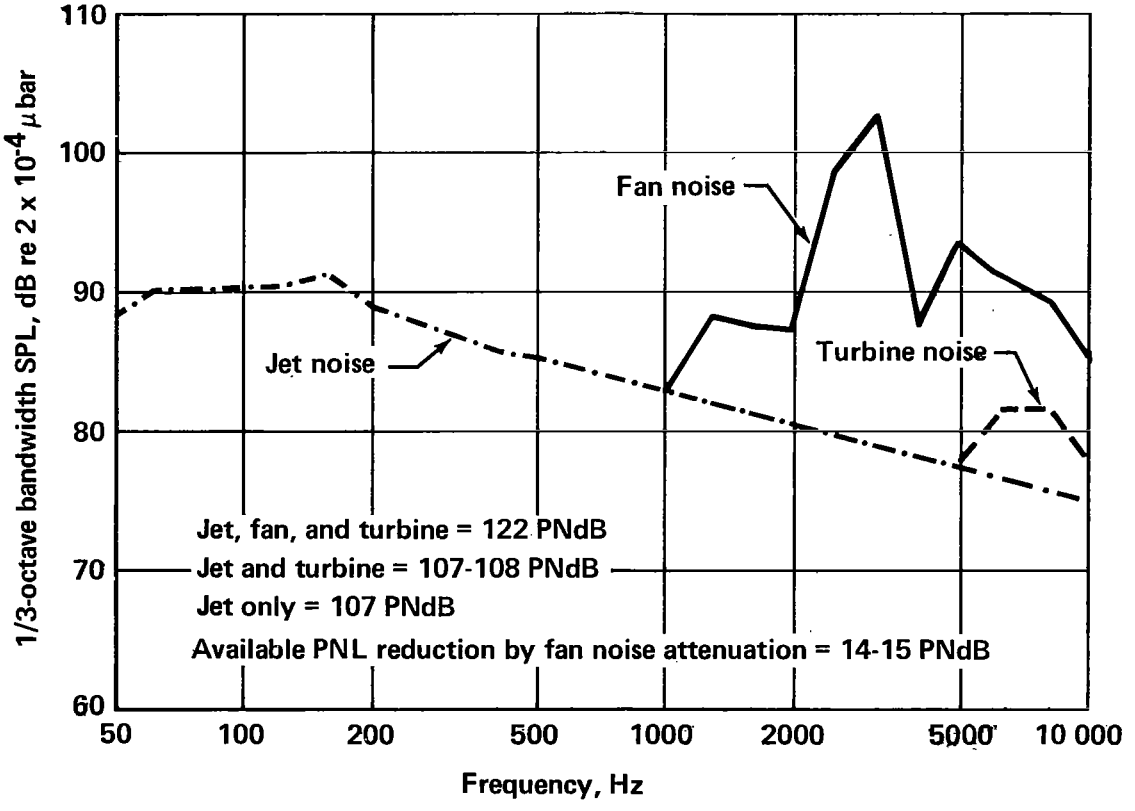

FIGURE 4.—TYPICAL NOISE SPECTRA AT APPROACH THRUST

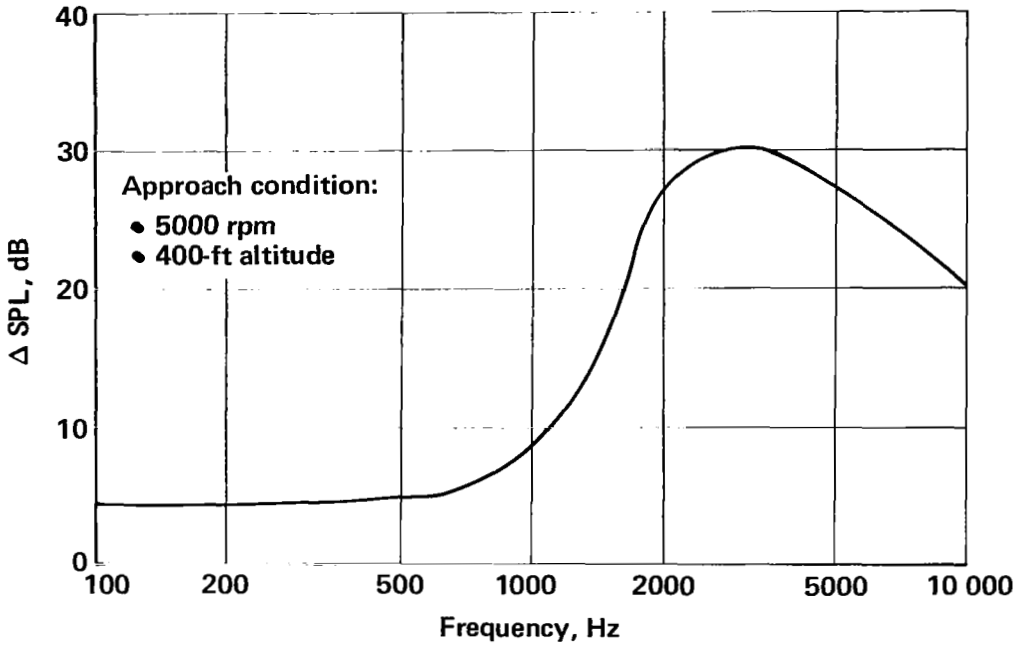

FIGURE 5.—FAN DUCT ATTENUATION TARGET

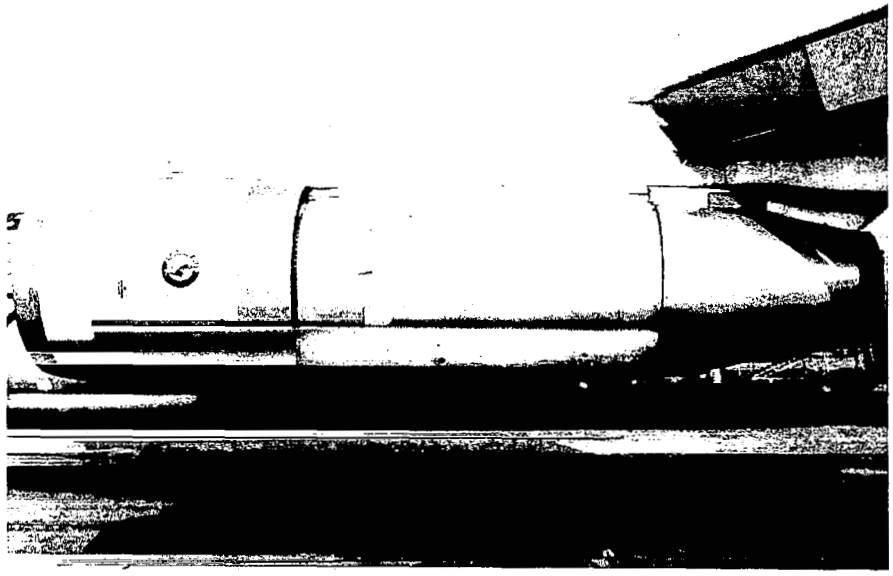

FIGURE 6.—707-320B/C PRODUCTION NACELLE

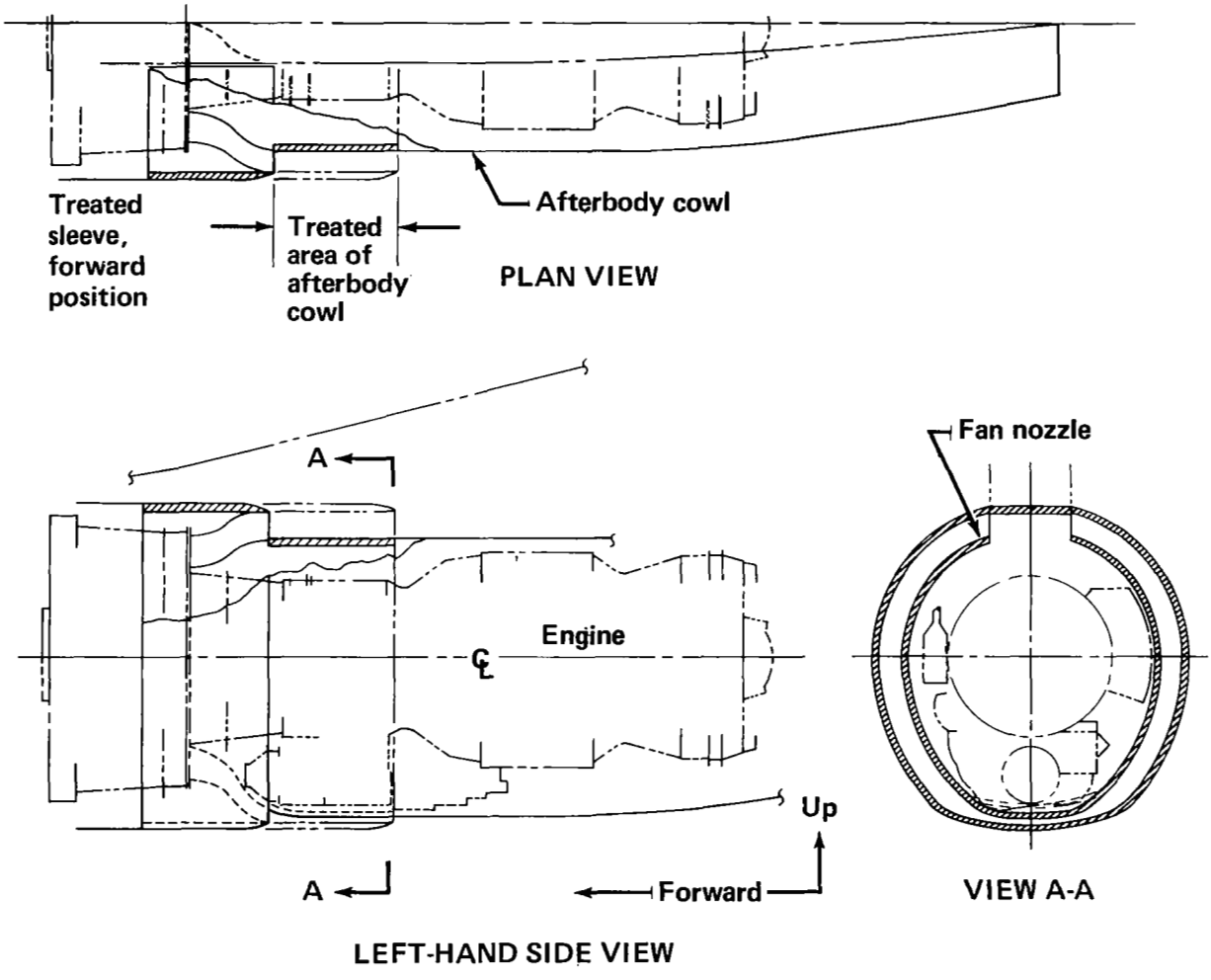

FIGURE 7.–SHORT DUCT WITH SLIDING SLEEVE

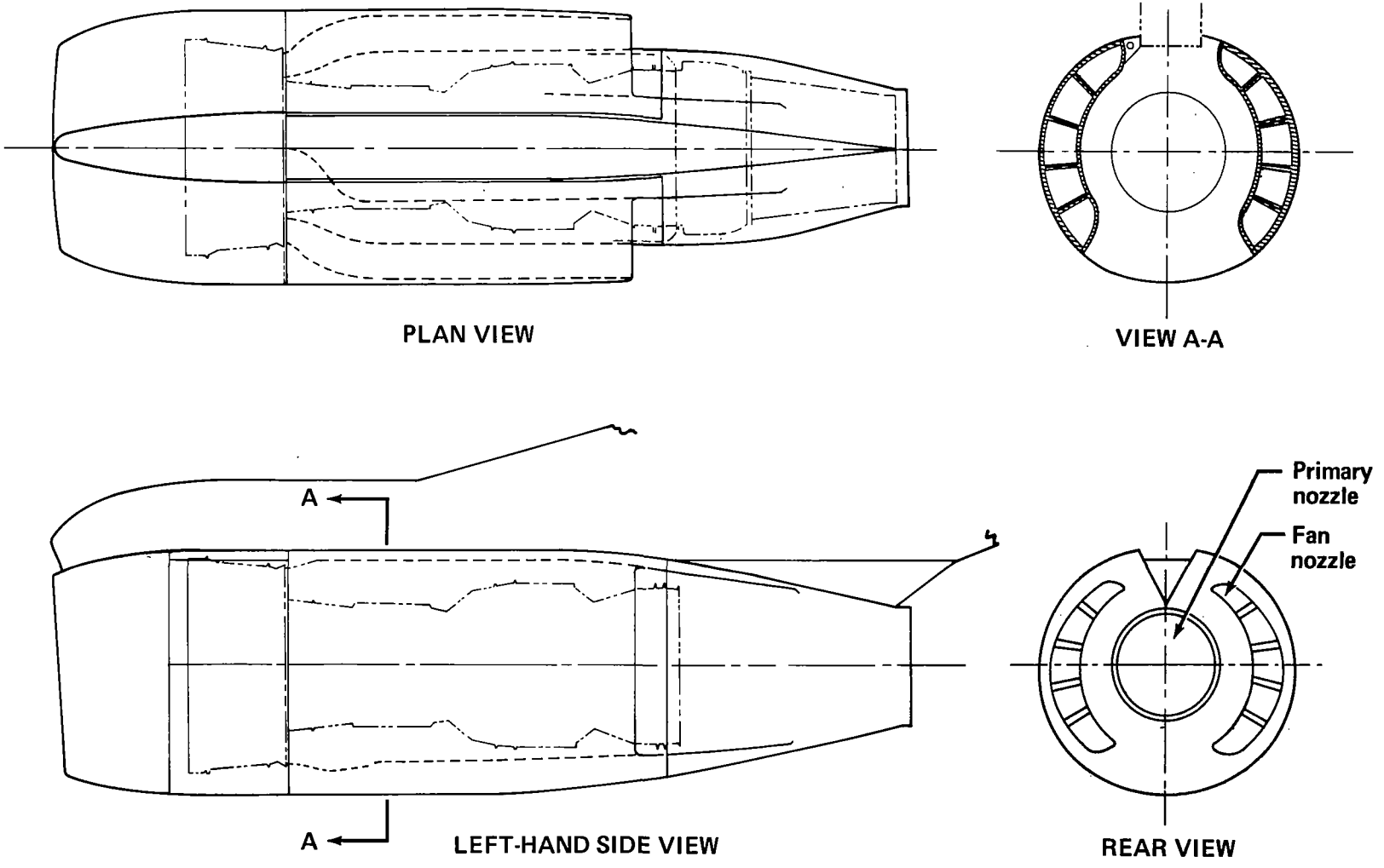

FIGURE 8.—THREE-QUARTERS LONG DUCT

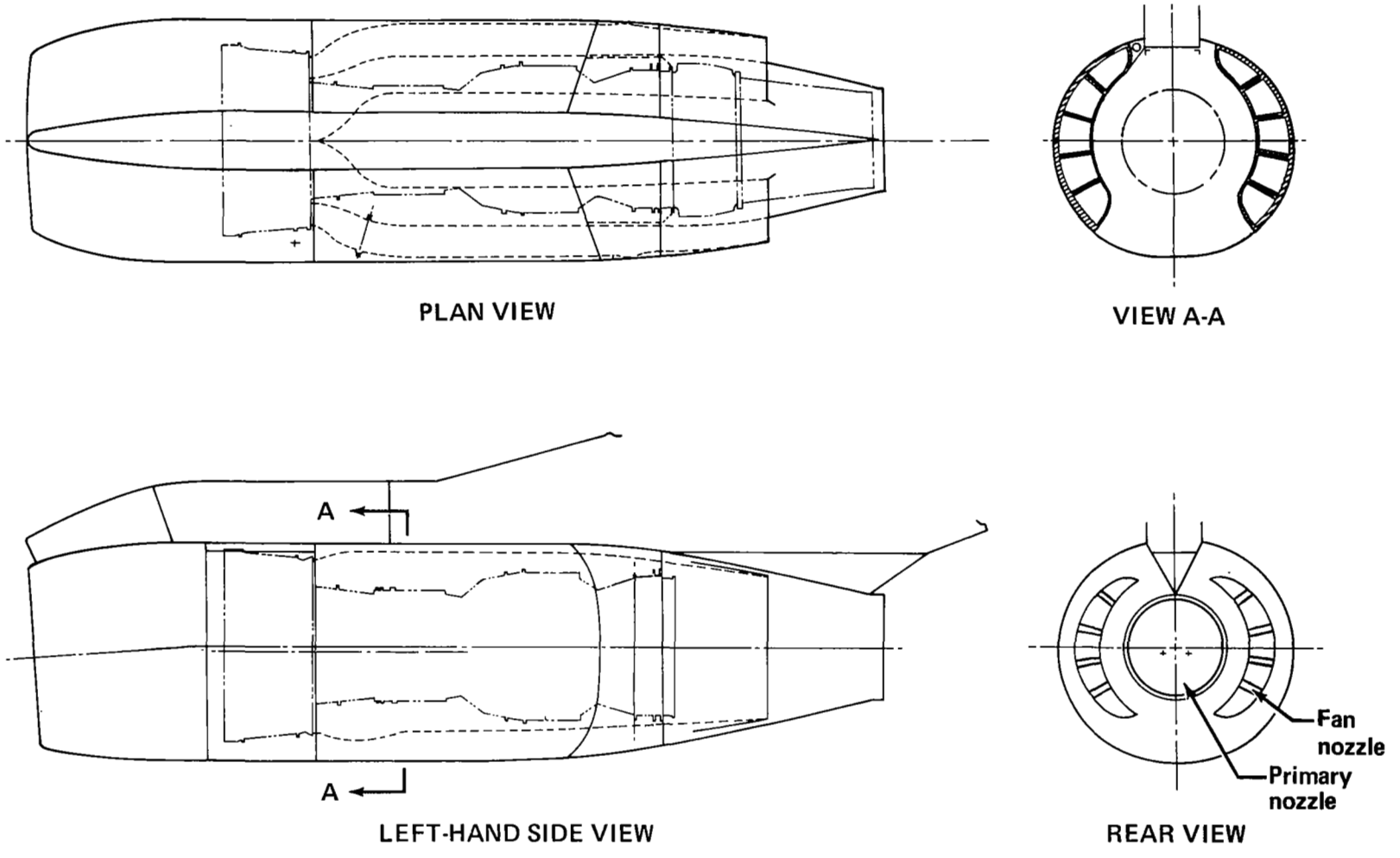

FIGURE 9.—SEVEN-EIGHTHS LONG DUCT, KIDNEY NOZZLE

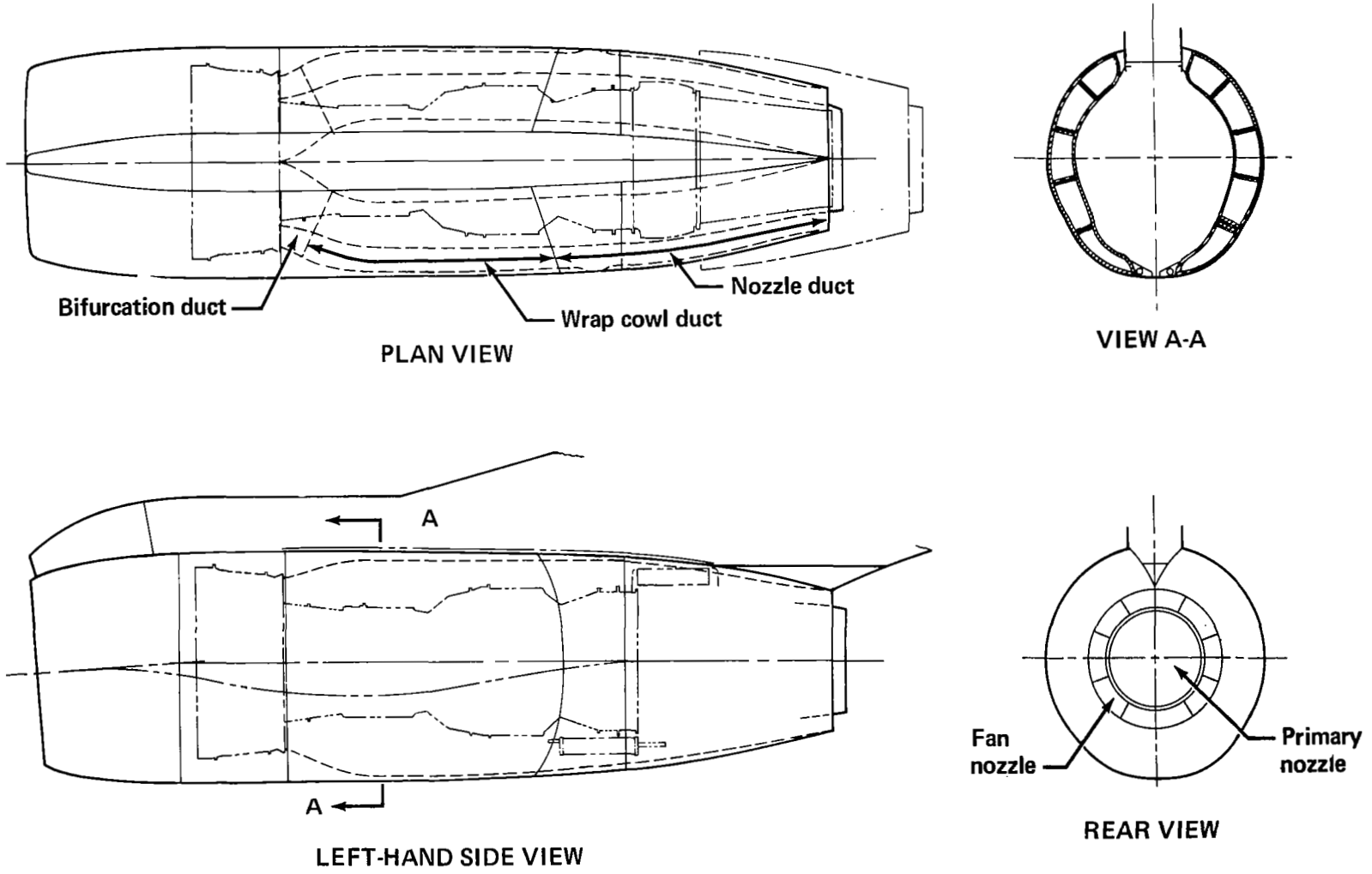

FIGURE 10.–FULL LONG DUCT, FULL ANNULAR NOZZLE

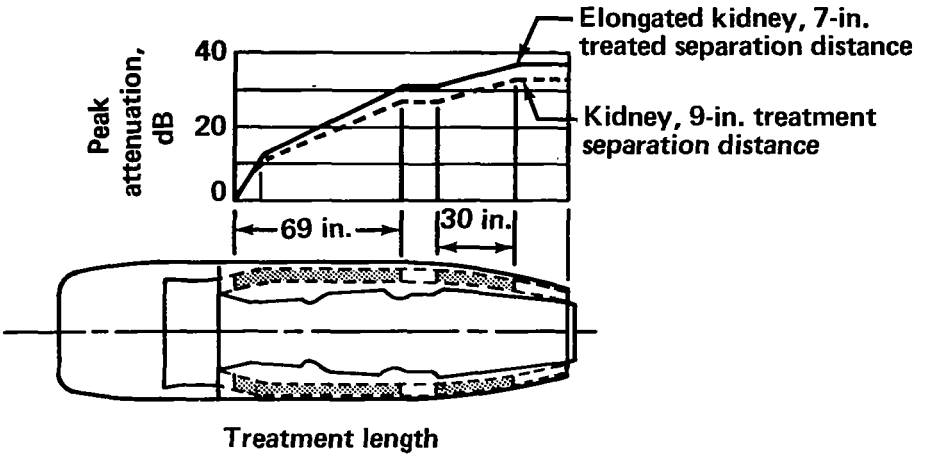

FIGURE 11.—VARIATION OF ATTENUATION WITH LINING LENGTH

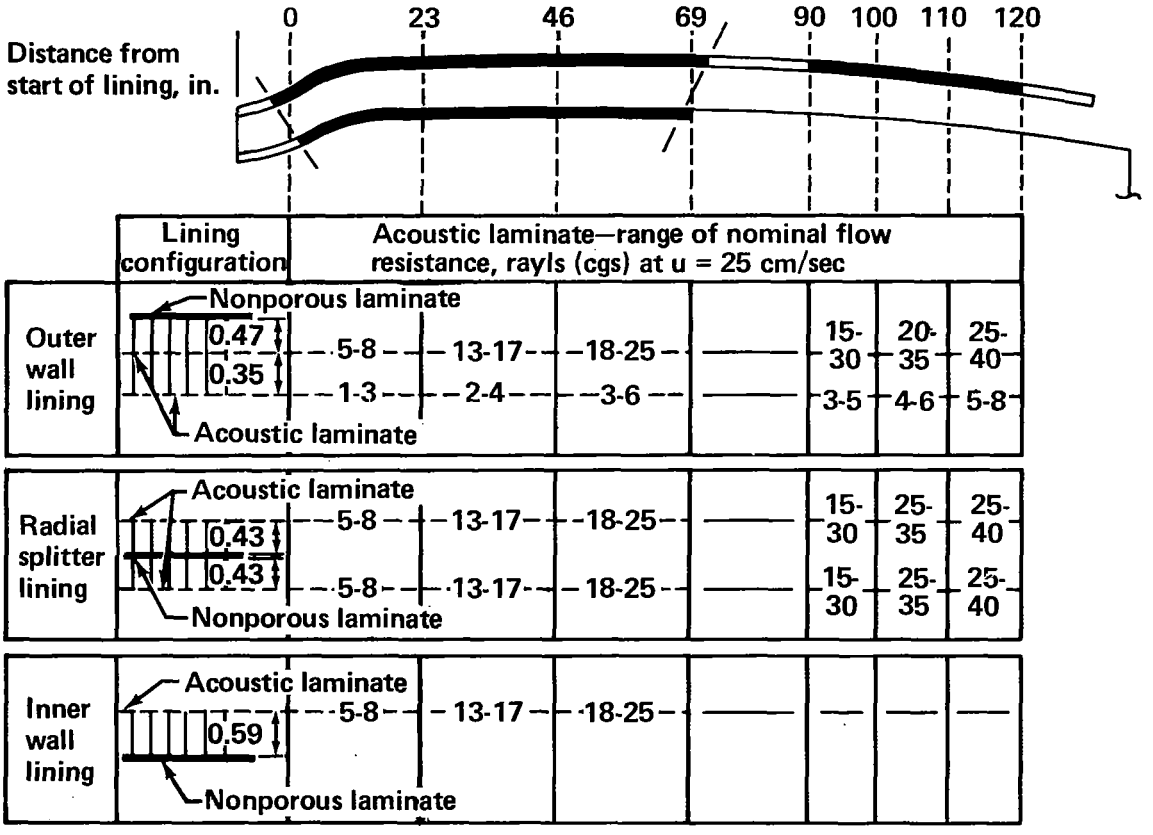

FIGURE 12.—NOMINAL FLOW RESISTANCE FOR BOILERPLATE/PROTOTYPE FAN DUCT

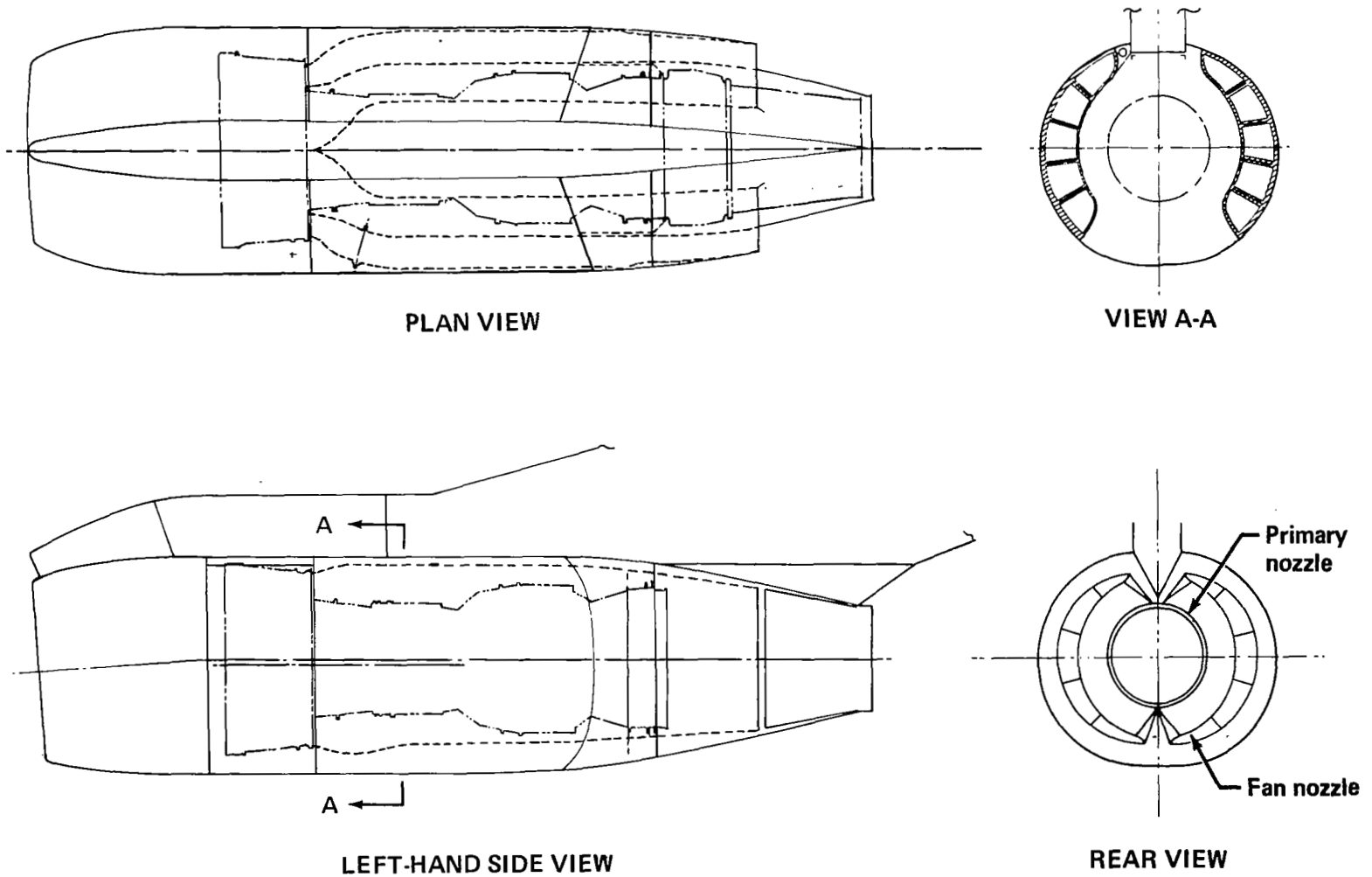

FIGURE 13.–SEVEN-EIGHTHS LONG DUCT, NEARLY ANNULAR NOZZLE

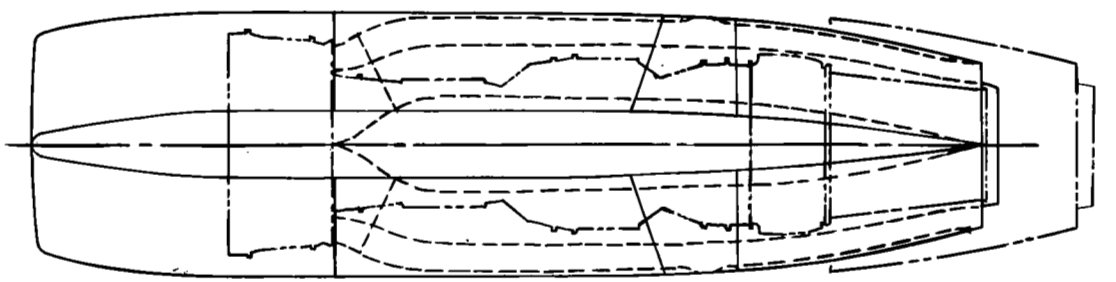

PLAN VIEW

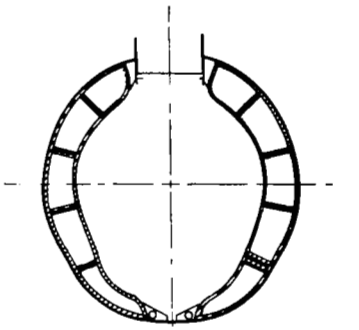

VIEW A-A

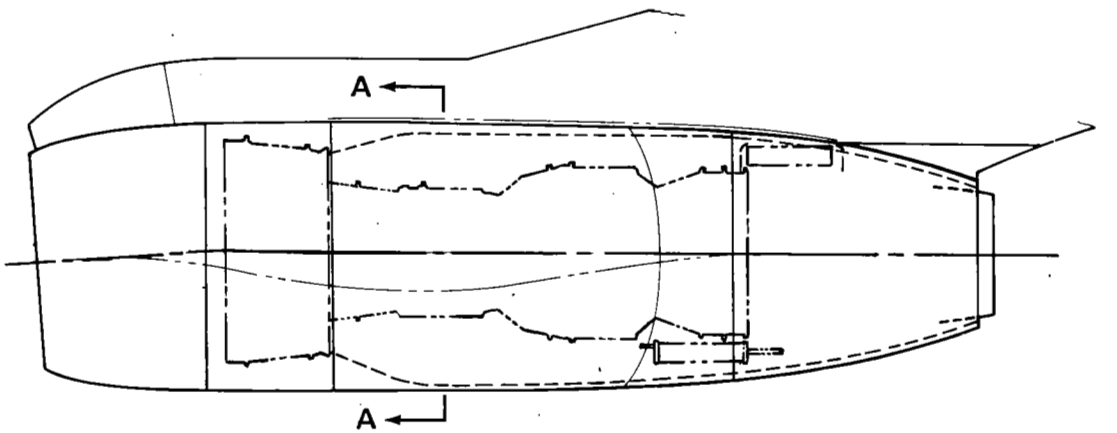

LEFT-HAND SIDE VIEW

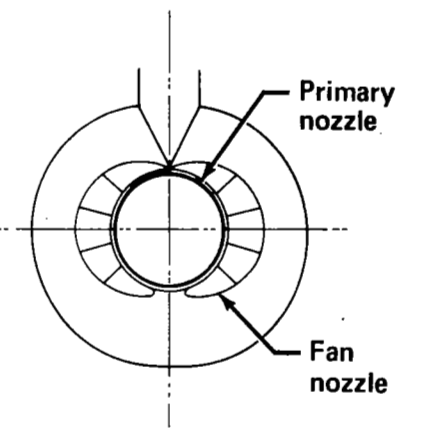

REAR VIEW

FIGURE 14.–FULL LONG DUCT, NEARLY ANNULAR NOZZLE

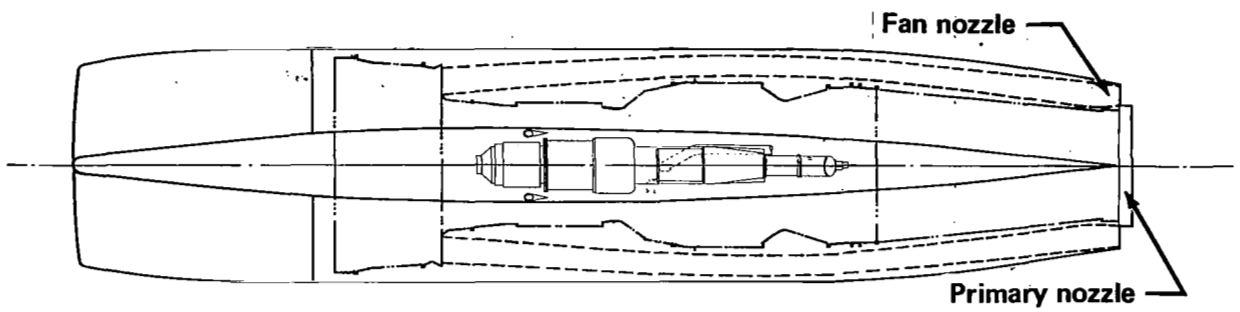

PLAN VIEW

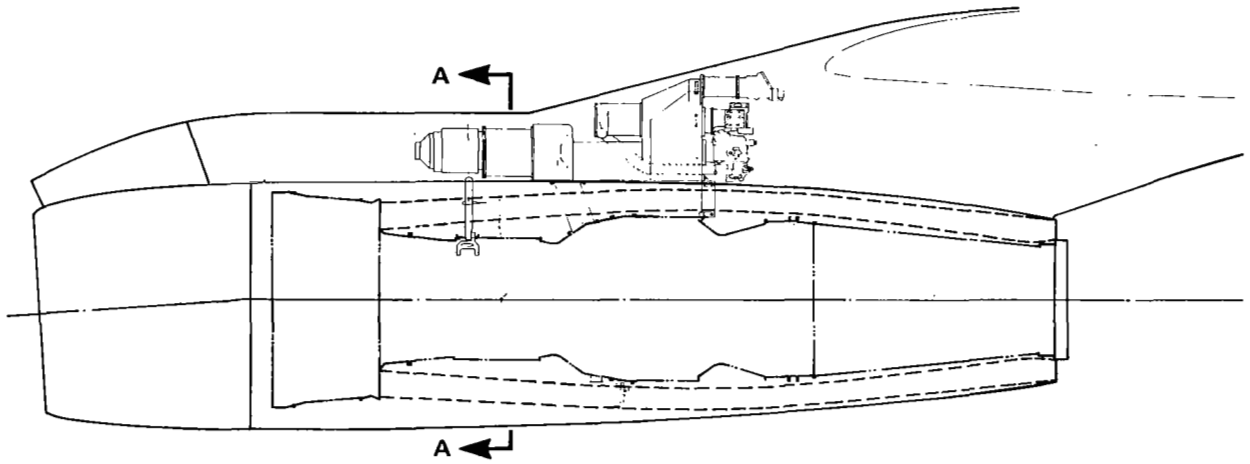

LEFT-HAND SIDE VIEW

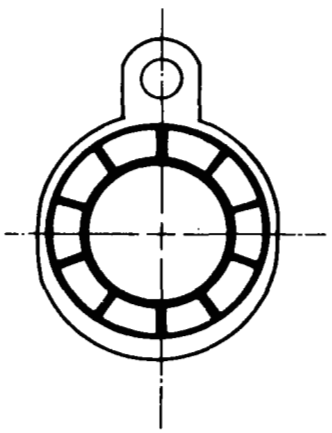

VIEW A-A

FIGURE 15.—FULL LONG, ANNULAR DUCT

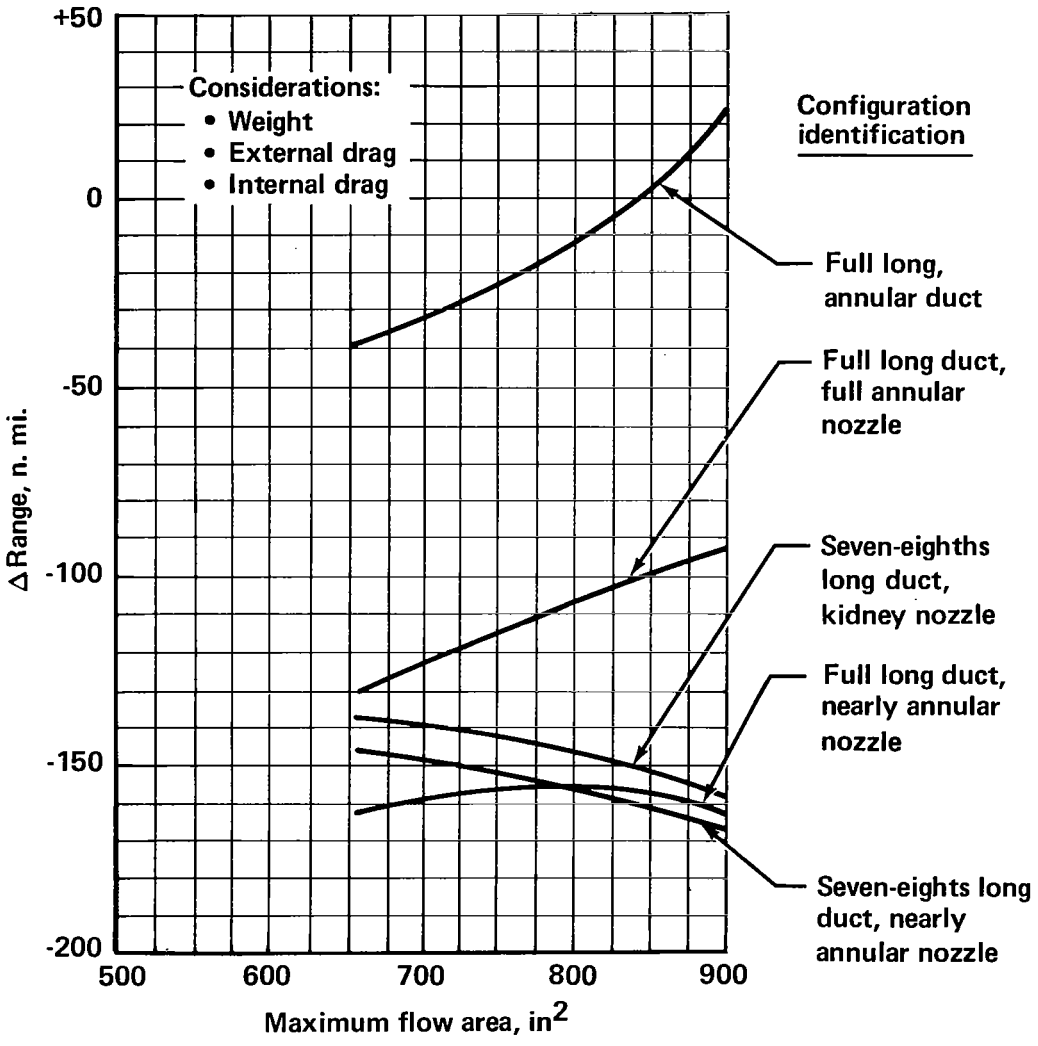

FIGURE 16.—DUCT DESIGN TRADE STUDY, AIRPLANE RANGE PENALTY

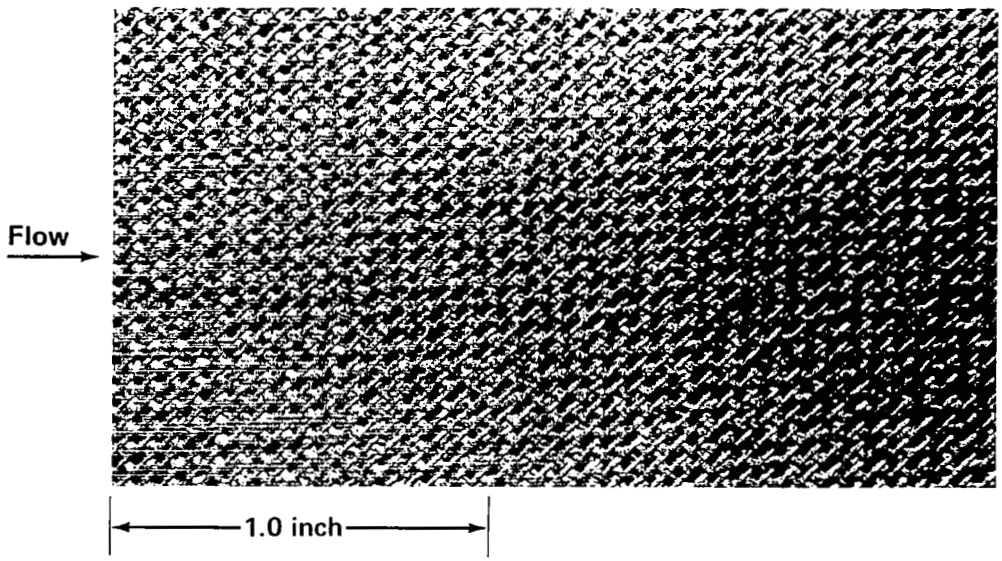

FIGURE 17.–30-RAYL (CGS) WOVEN FIBERGLASS LAMINATE TEST SPECIMEN

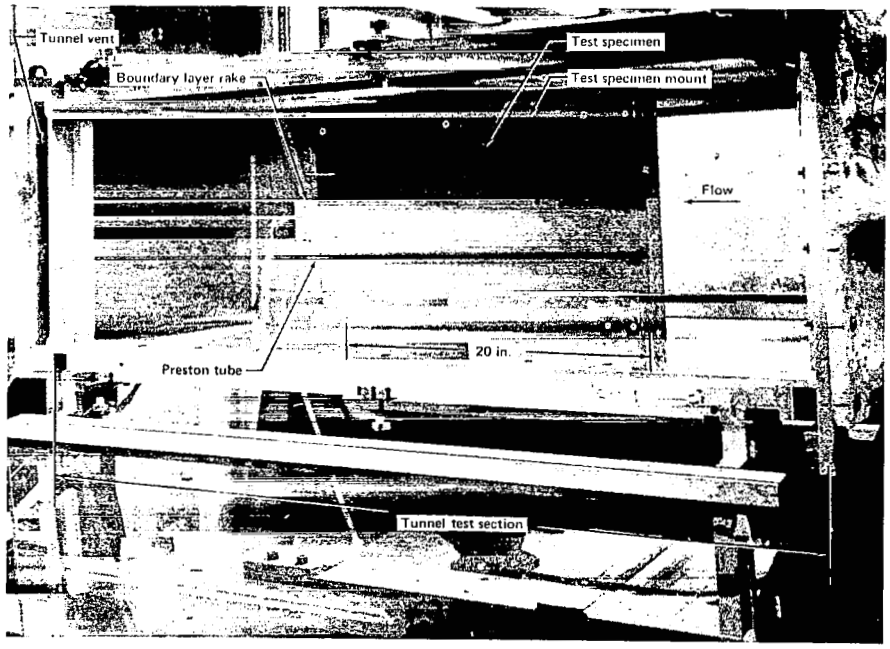

FIGURE 18.–INSTALLED TEST SPECIMEN AND BOUNDARY LAYER RAKE

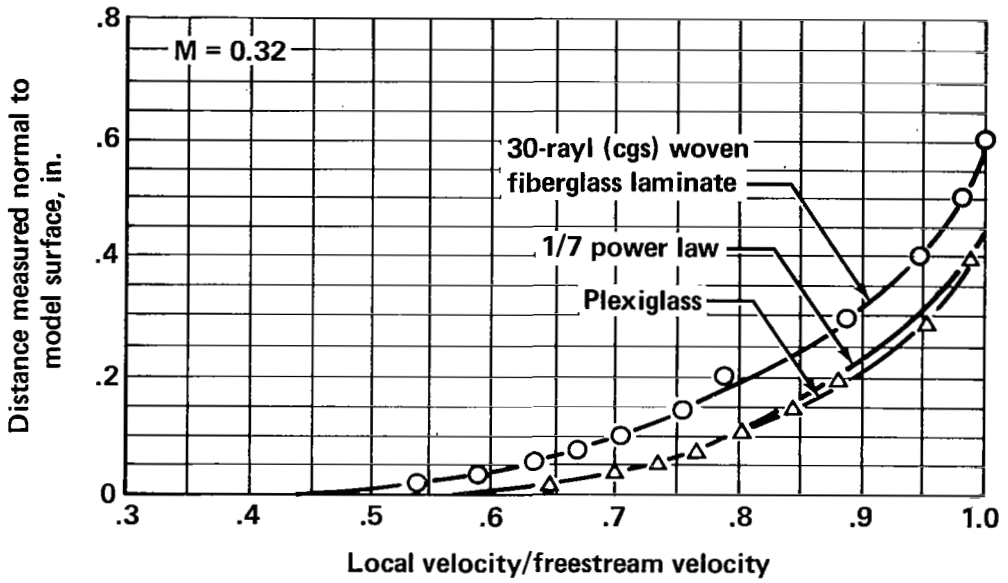

FIGURE 19.–BOUNDARY LAYER VELOCITY PROFILES

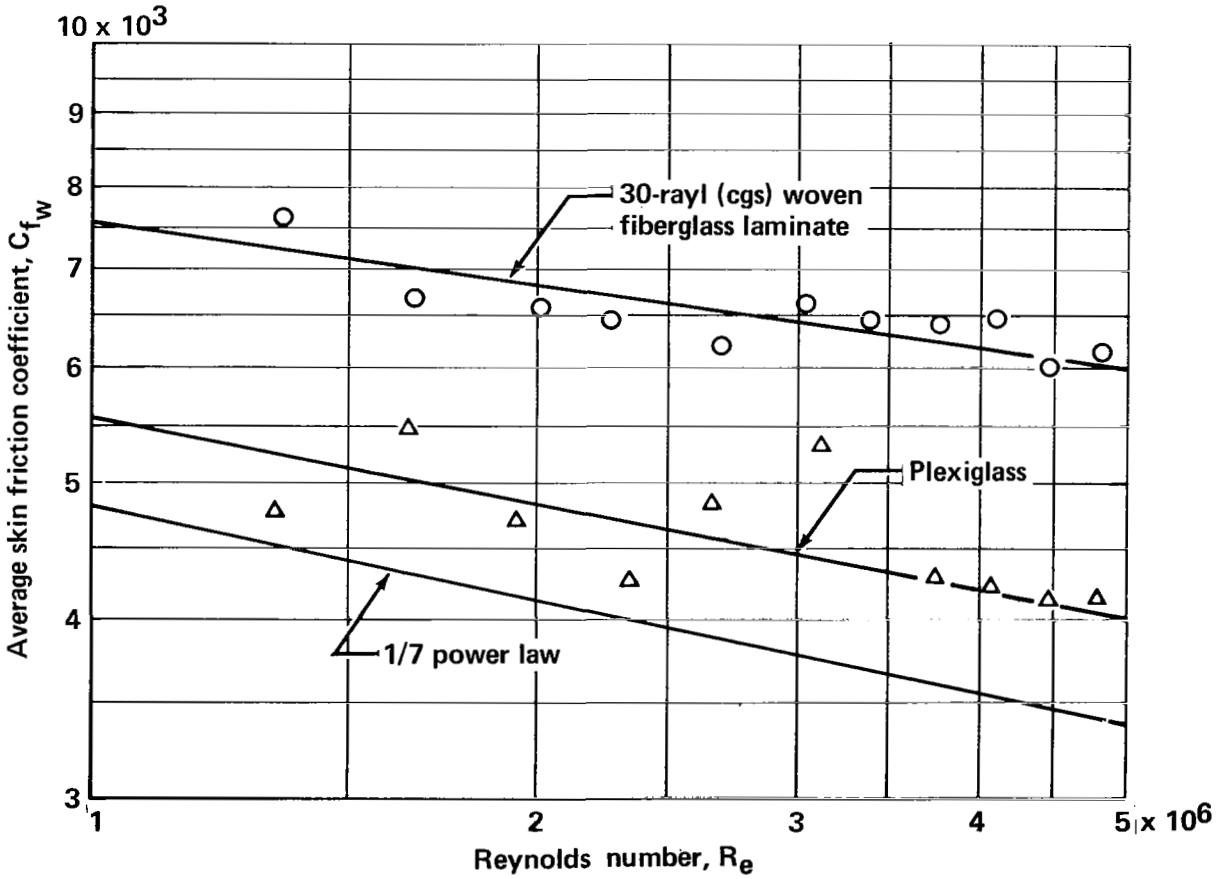

FIGURE 20.–AVERAGE SKIN FRICTION COEFFICIENT FOR 30-RAYL (CGS) WOVEN FIBERGLASS LAMINATE AND PLEXIGLASS PLATE

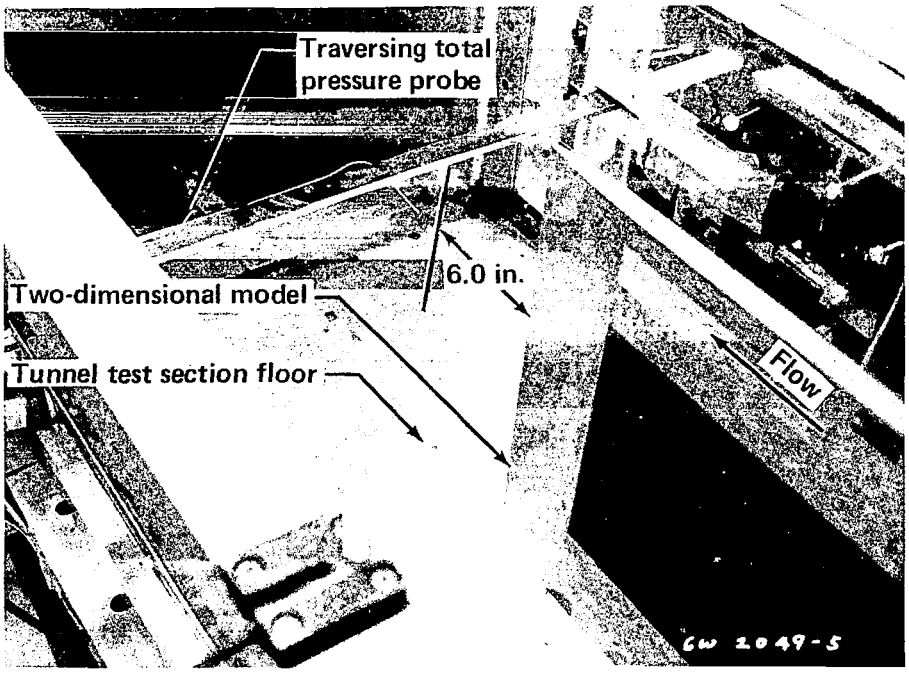

FIGURE 21.–SIMULATED INLET RING MODEL INSTALLED IN TUNNEL

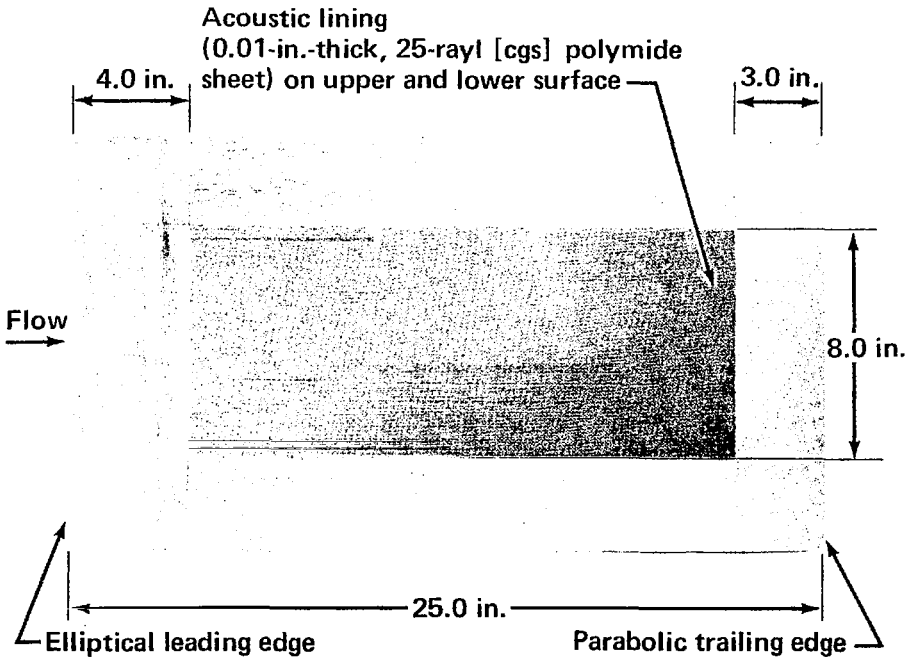

FIGURE 22.–PLAN VIEW OF SIMULATED INLET RING MODEL

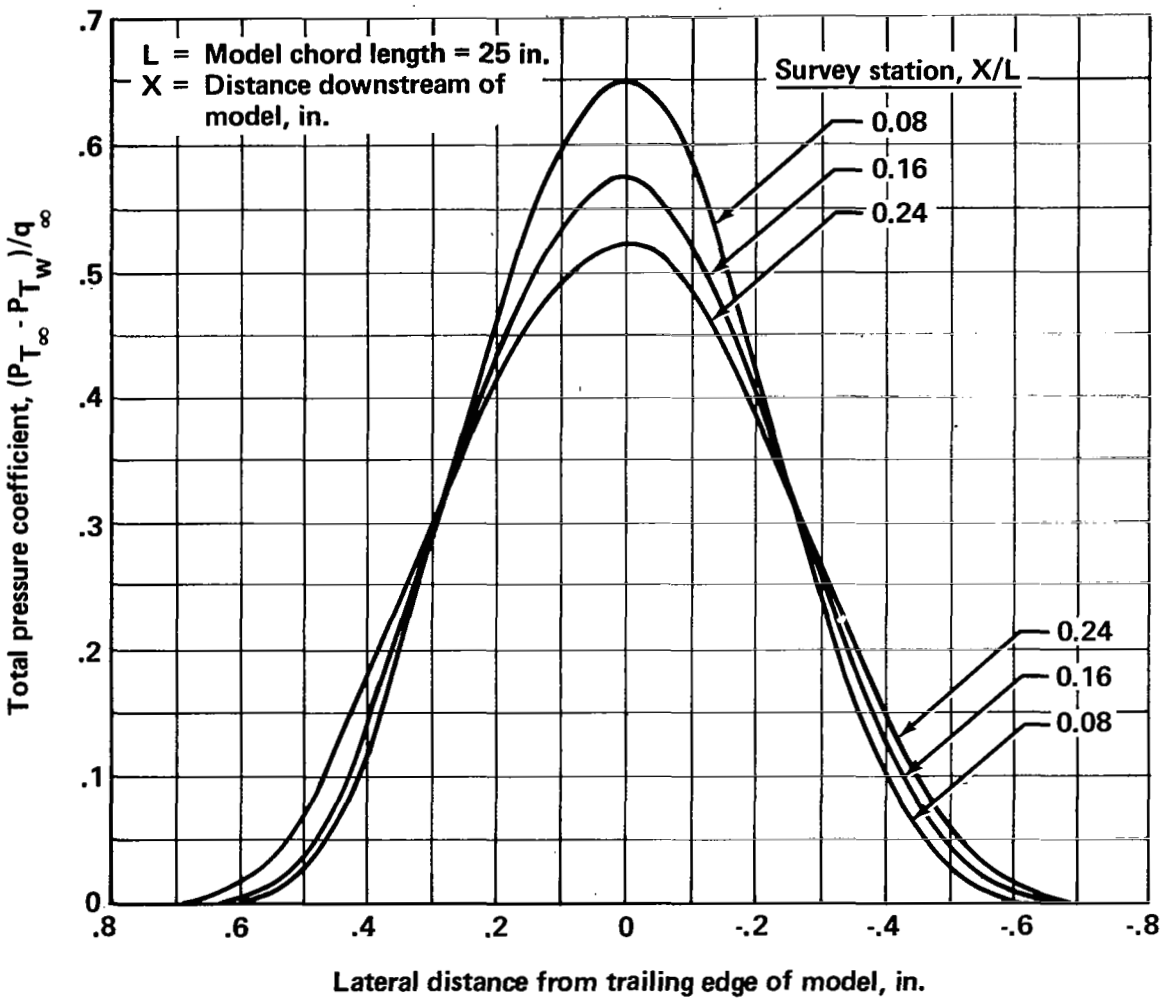

FIGURE 23.–SIMULATED INLET RING WAKE SHAPES

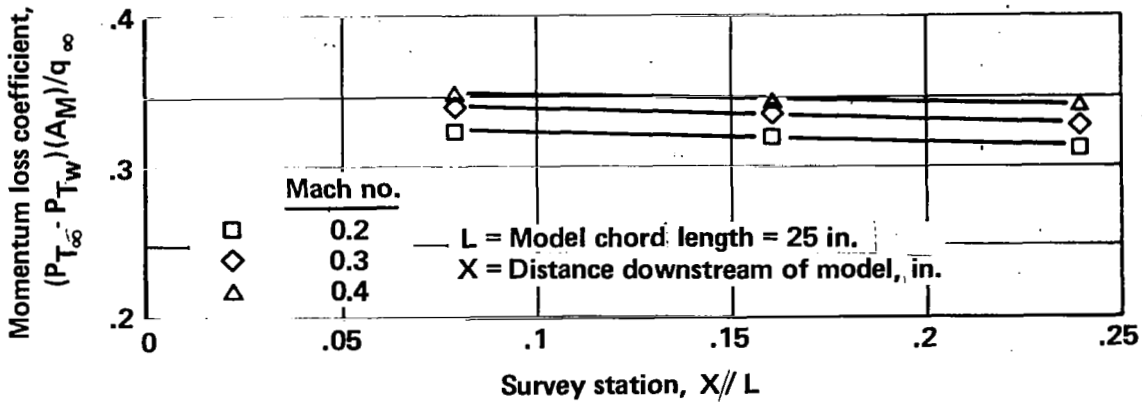

FIGURE 24.–EFFECT OF MACH NUMBER AND WAKE SURVEY STATION ON AVERAGE MOMENTUM LOSS

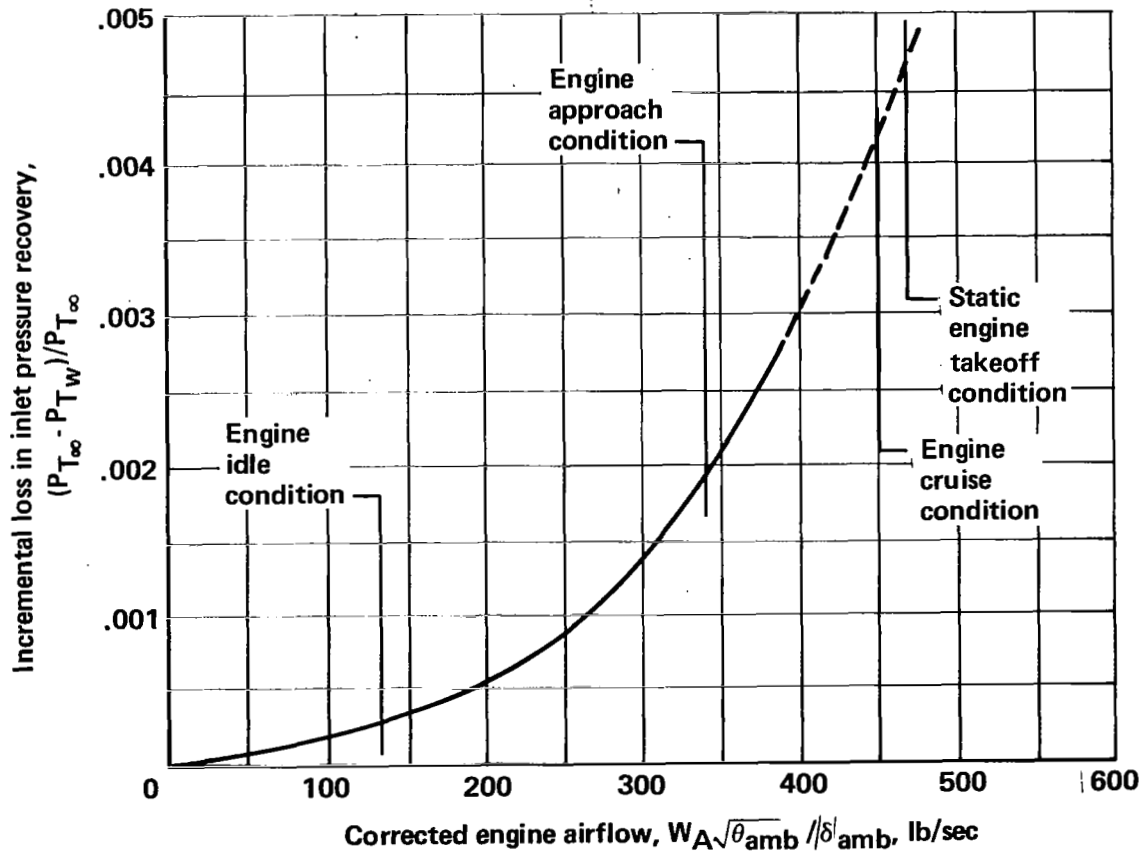

FIGURE 25.–EFFECT OF ENGINE AIRFLOW ON INCREMENTAL LOSS IN INLET PRESSURE RECOVERY DUE TO THE OUTER RING

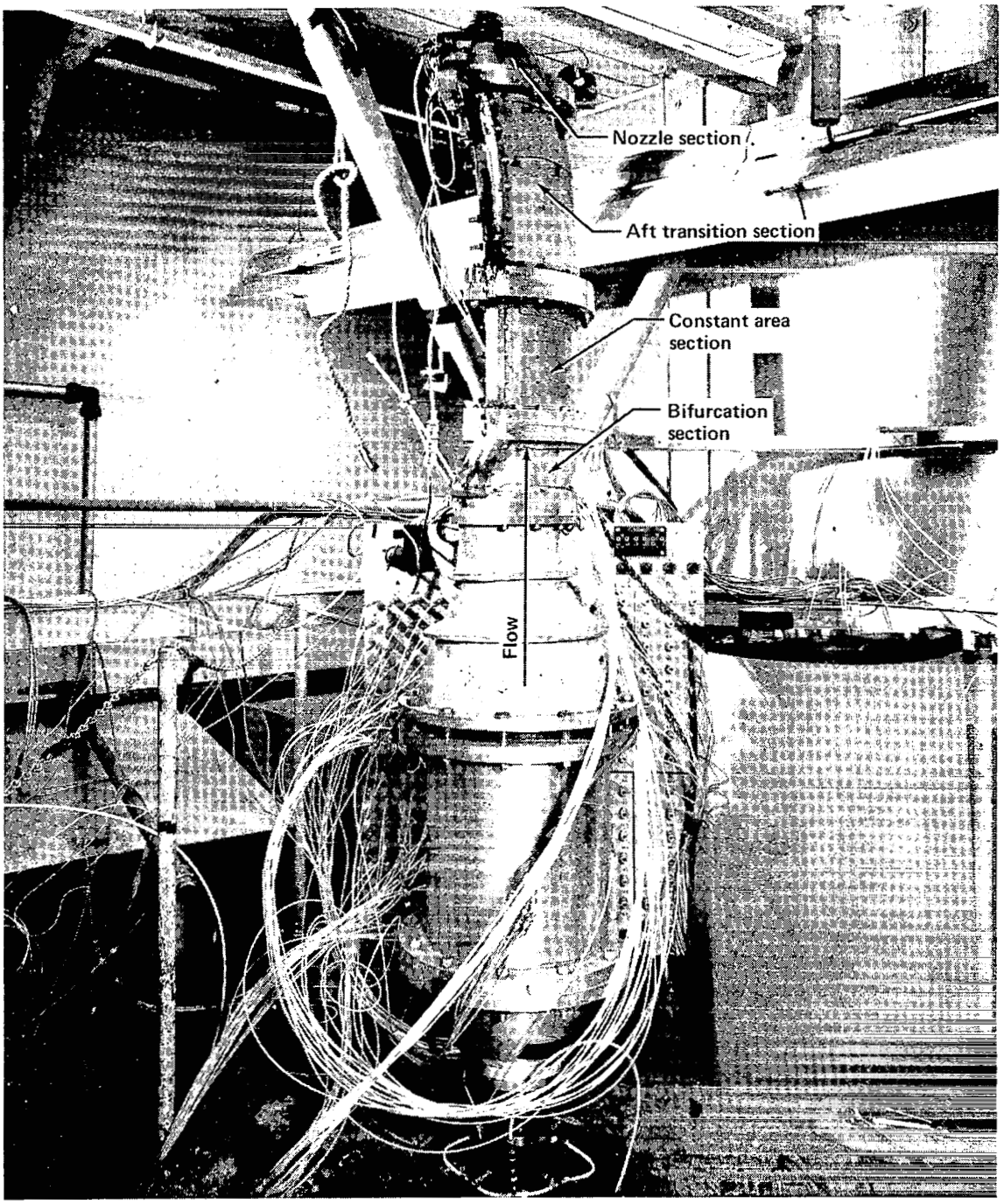

FIGURE 26.–900-SQUARE-INCH LONG DUCT MODEL INSTALLED ON DUAL NOZZLE RIG

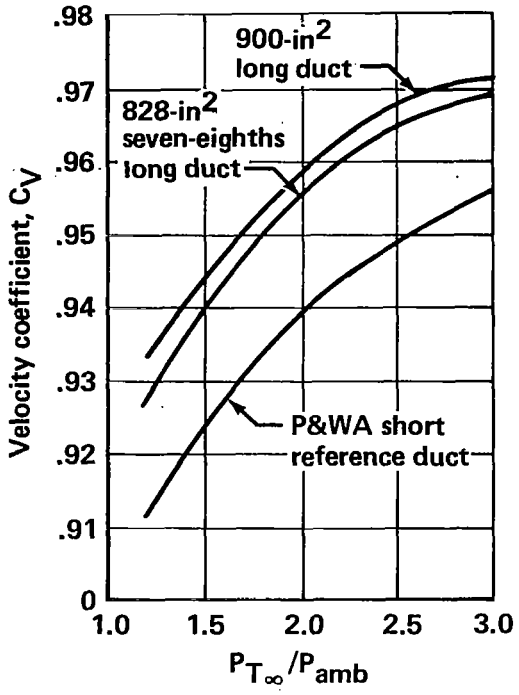

FIGURE 27.–VELOCITY COEFFICIENTS, 1/5-SCALE MODEL TESTS

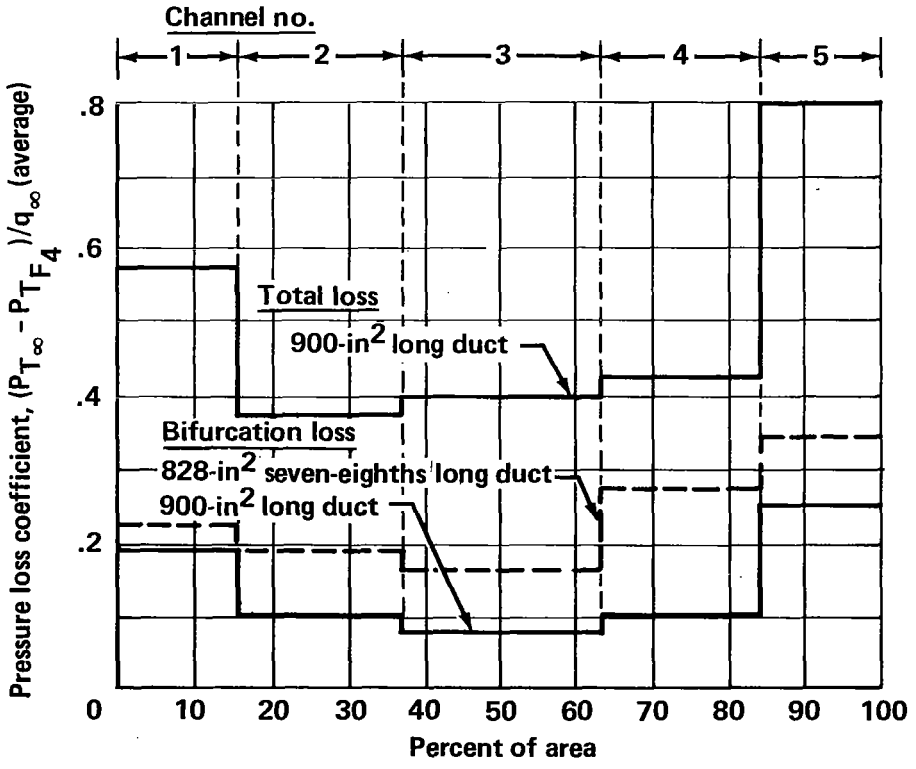

FIGURE 28.–MODEL DUCT PRESSURE LOSSES

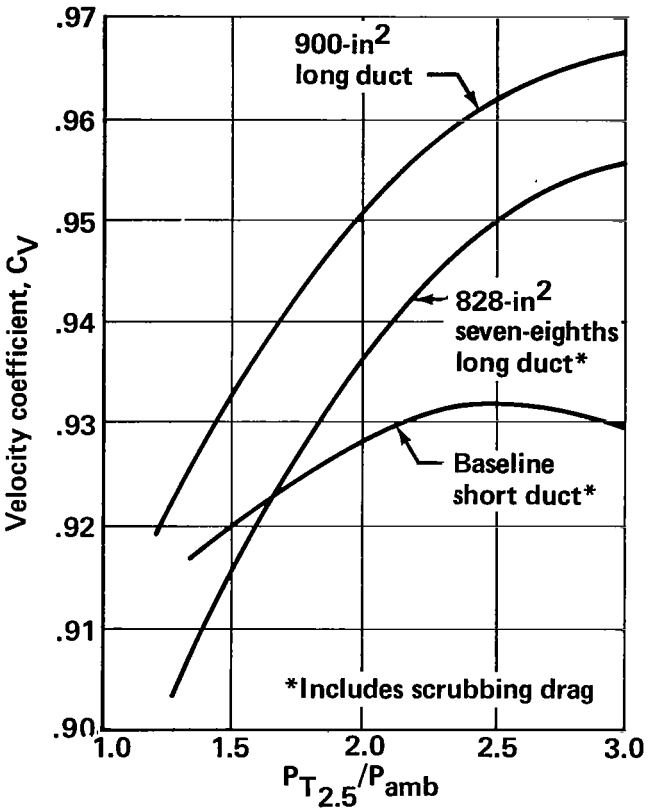

FIGURE 29.–PREDICTED FULL-SCALE DUCT PERFORMANCE

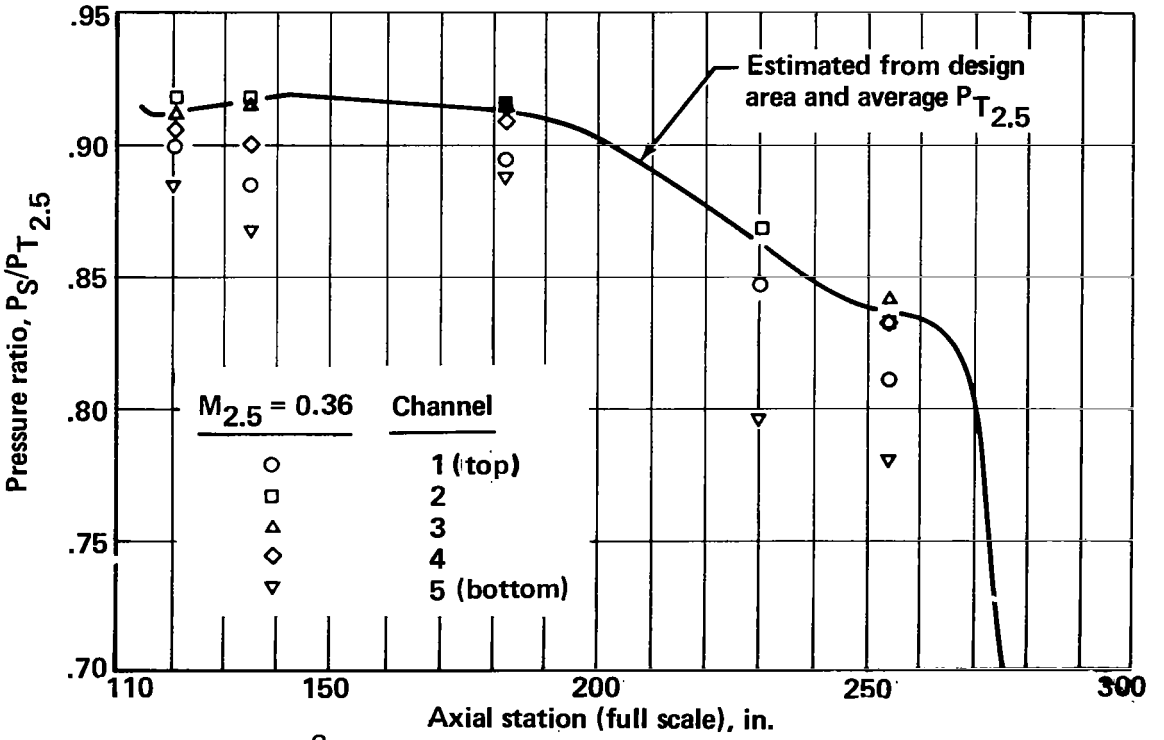

FIGURE 30.–900-IN^2 LONG DUCT, 1/5-SCALE MODEL STATIC PRESSURE DATA

FIGURE 31.—WIND TUNNEL INSTALLATION OF LONG DUCT NACELLE

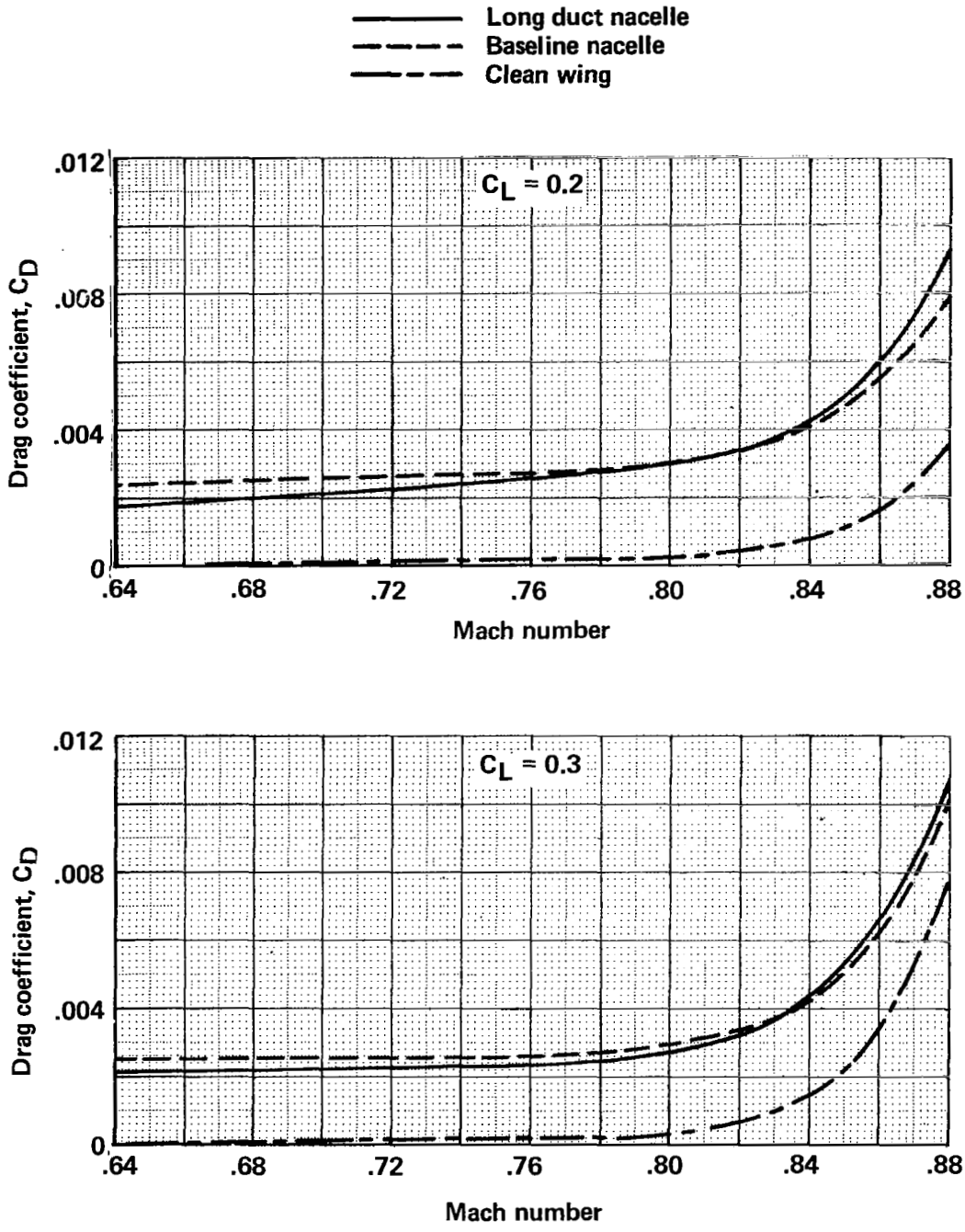

FIGURE 32.—NACELLE DRAG CHARACTERISTICS, MODEL TEST DATA

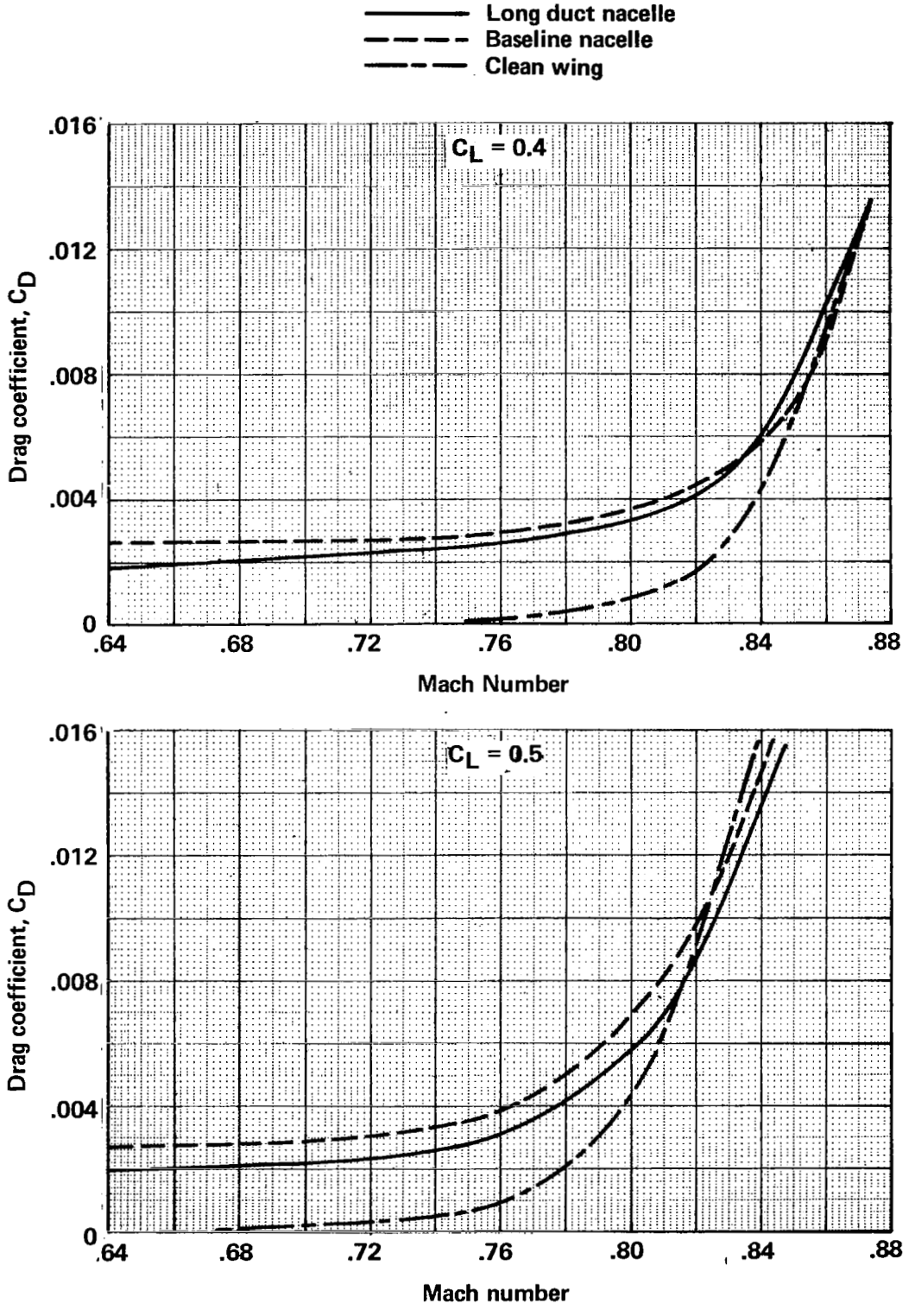

FIGURE 32.–NACELLE DRAG CHARACTERISTICS, MODEL TEST DATA–Concluded

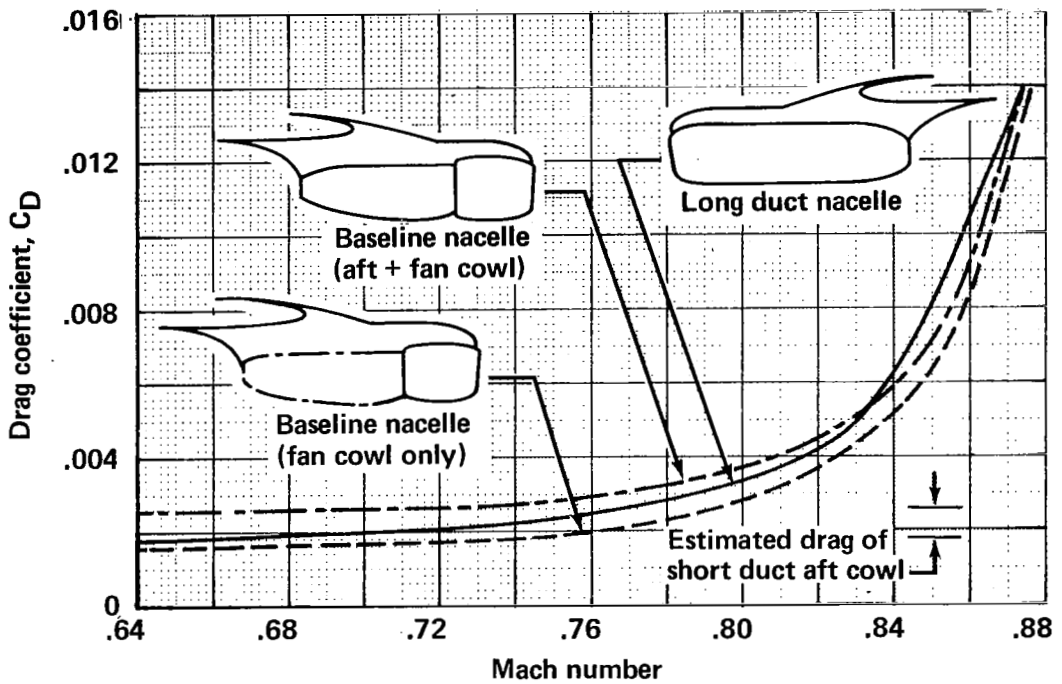

(a) NACELLE DRAG, MODEL TEST DATA

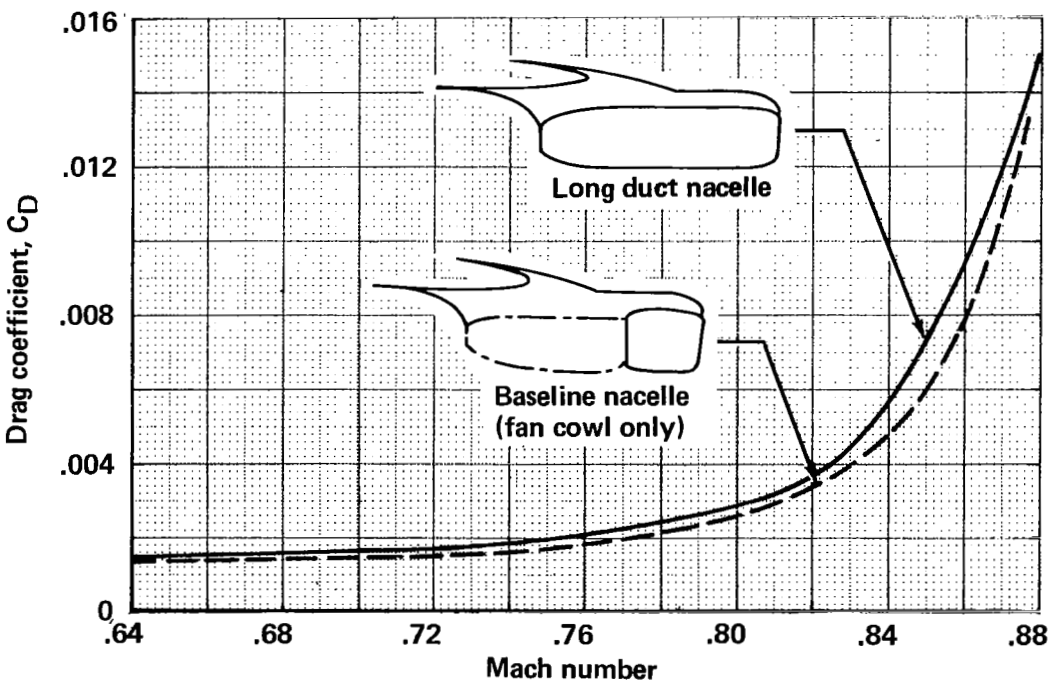

(b) PREDICTED FULL-SCALE NACELLE DRAG

FIGURE 33.–NACELLE DRAG DEVELOPMENT FOR $C_L = 0.4$

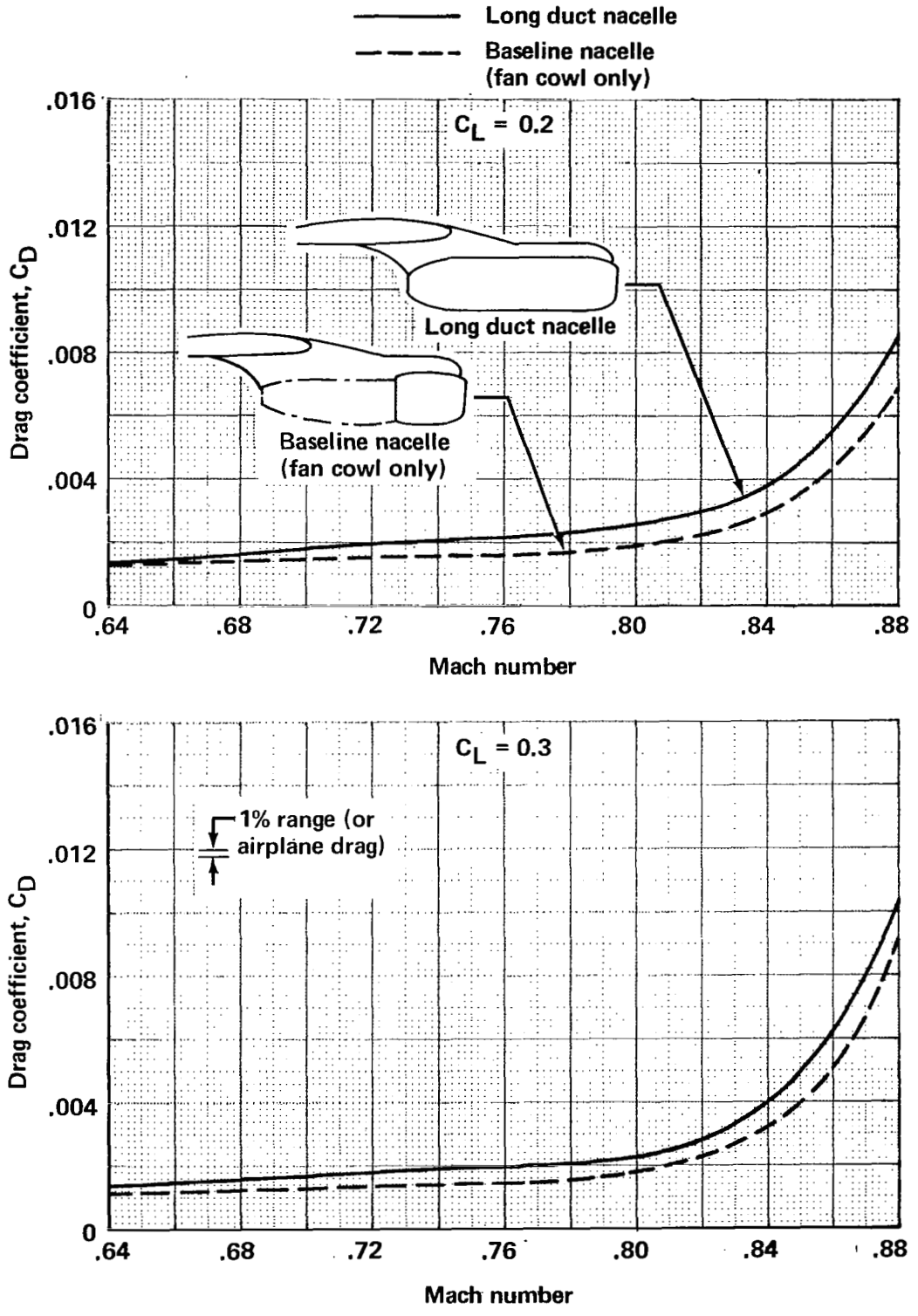

FIGURE 34.–COMPARISON BETWEEN LONG DUCT AND BASELINE NACELLE, PREDICTED FULL-SCALE DRAG

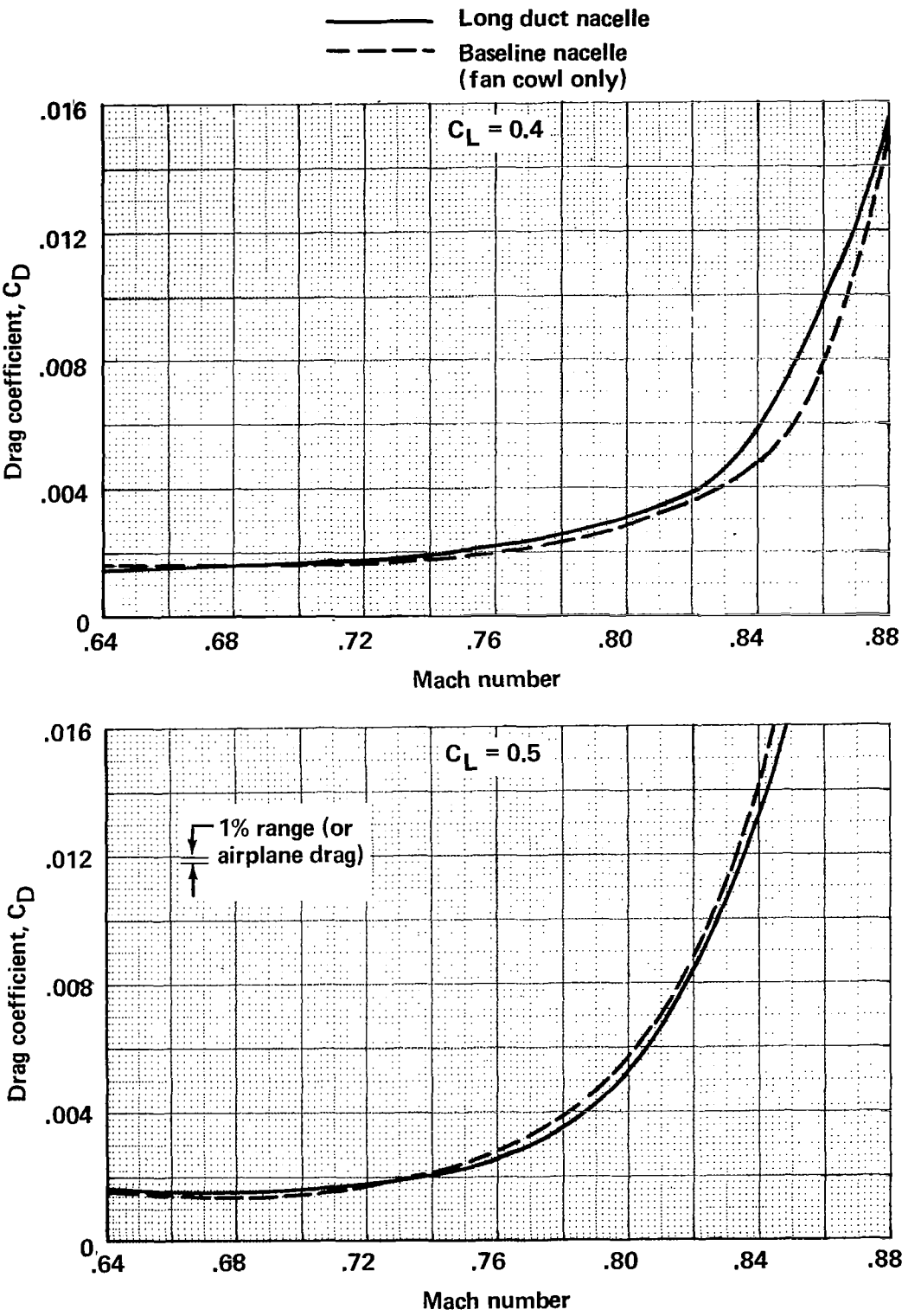

FIGURE 34.—COMPARISON BETWEEN LONG DUCT AND BASELINE NACELLE, PREDICTED FULL-SCALE DRAG—Concluded

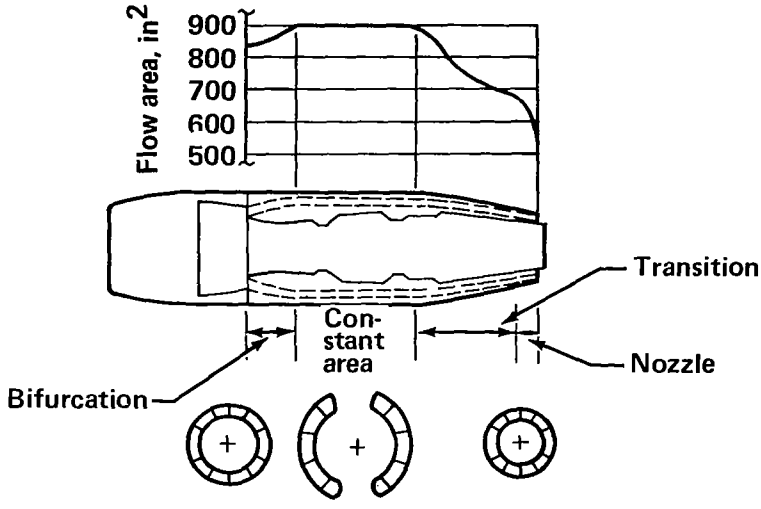

FIGURE 35.—SELECTED DUCT CONFIGURATION FLOW AREA DISTRIBUTION

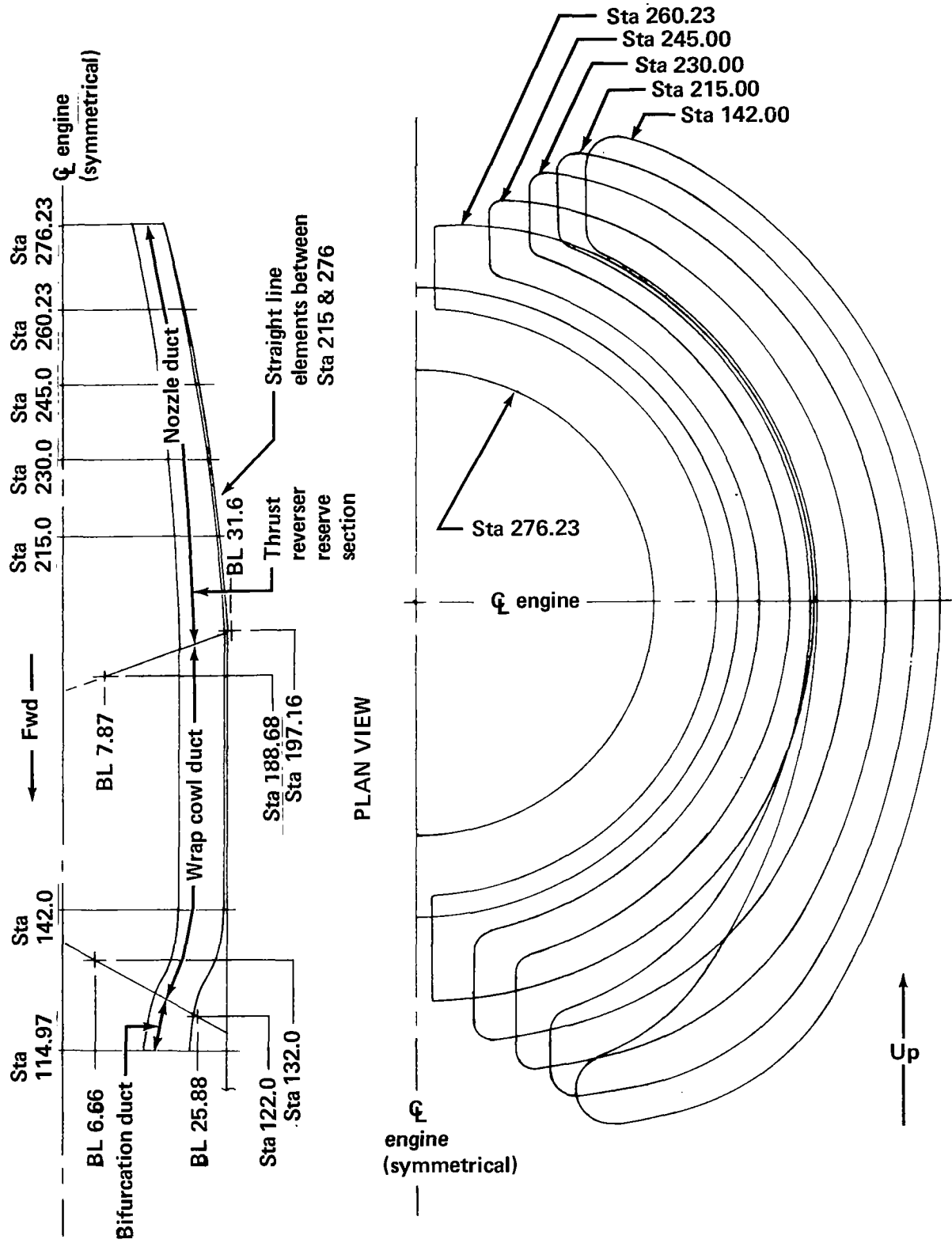

FIGURE 36.—BOILERPLATE INTERNAL DUCT LINES AFT OF STATION 142.00

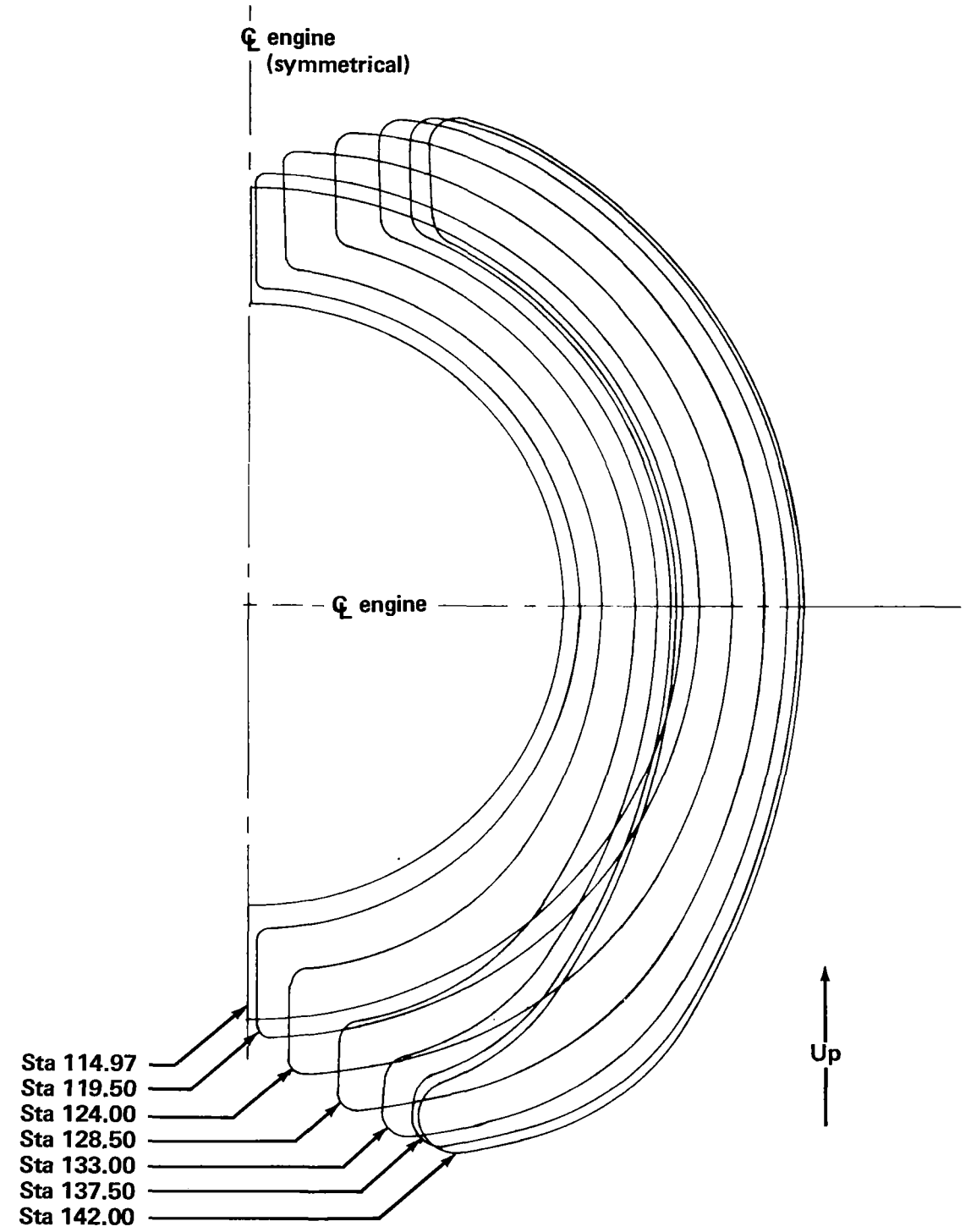

FIGURE 37.—BOILERPLATE INTERNAL DUCT LINES FORWARD OF STATION 142.00

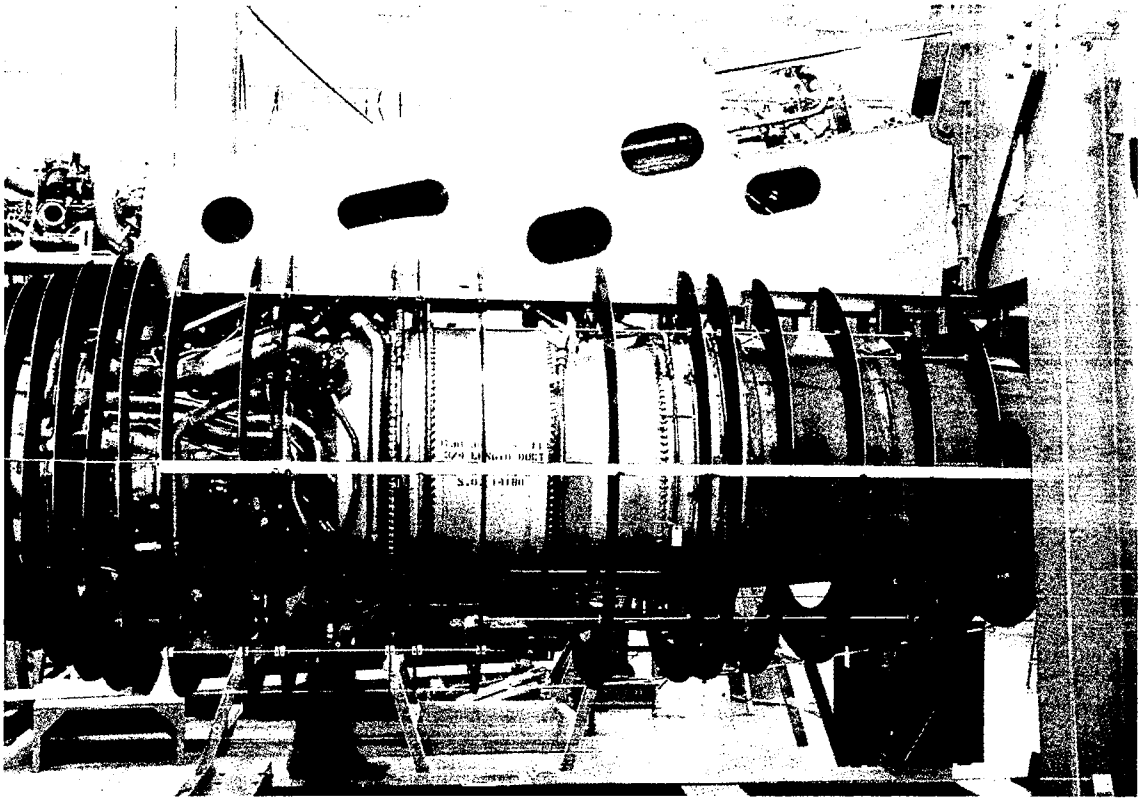

FIGURE 38.—DUCT-TO-ENGINE CLEARANCE MOCKUP

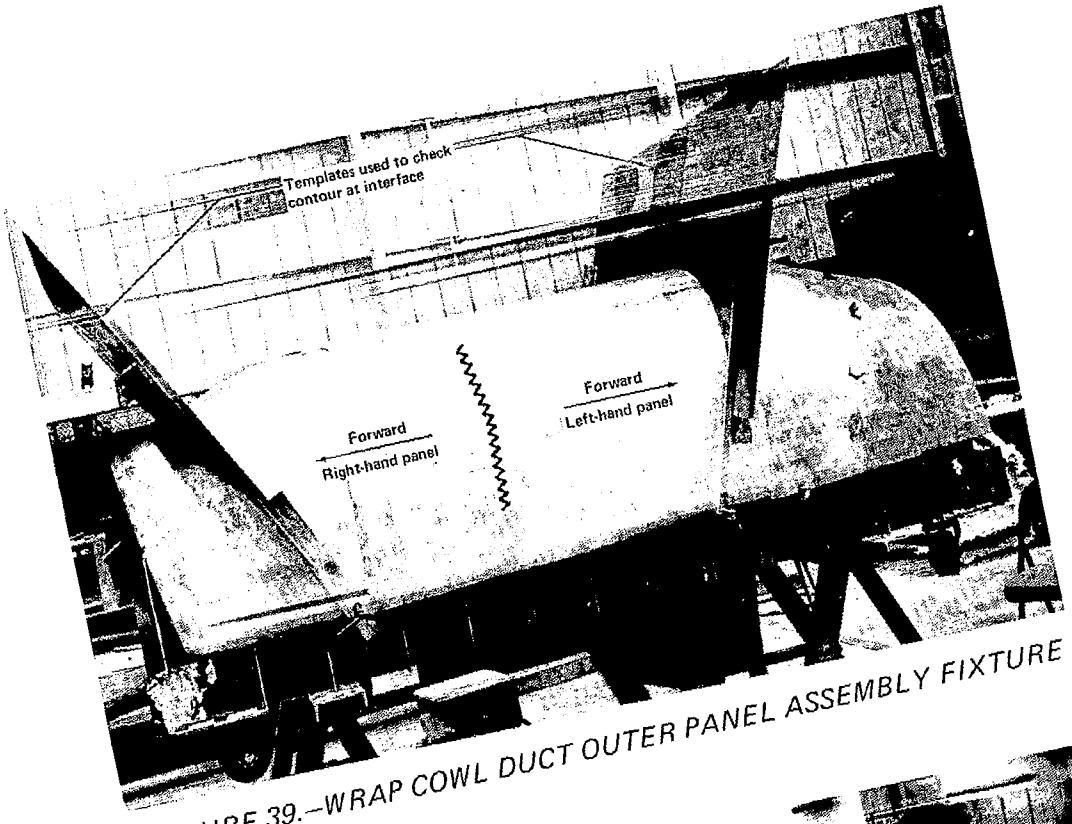

FIGURE 39.–WRAP COWL DUCT OUTER PANEL ASSEMBLY FIXTURE

DUCT POLYIMIDE INSERT PANEL LAYUP

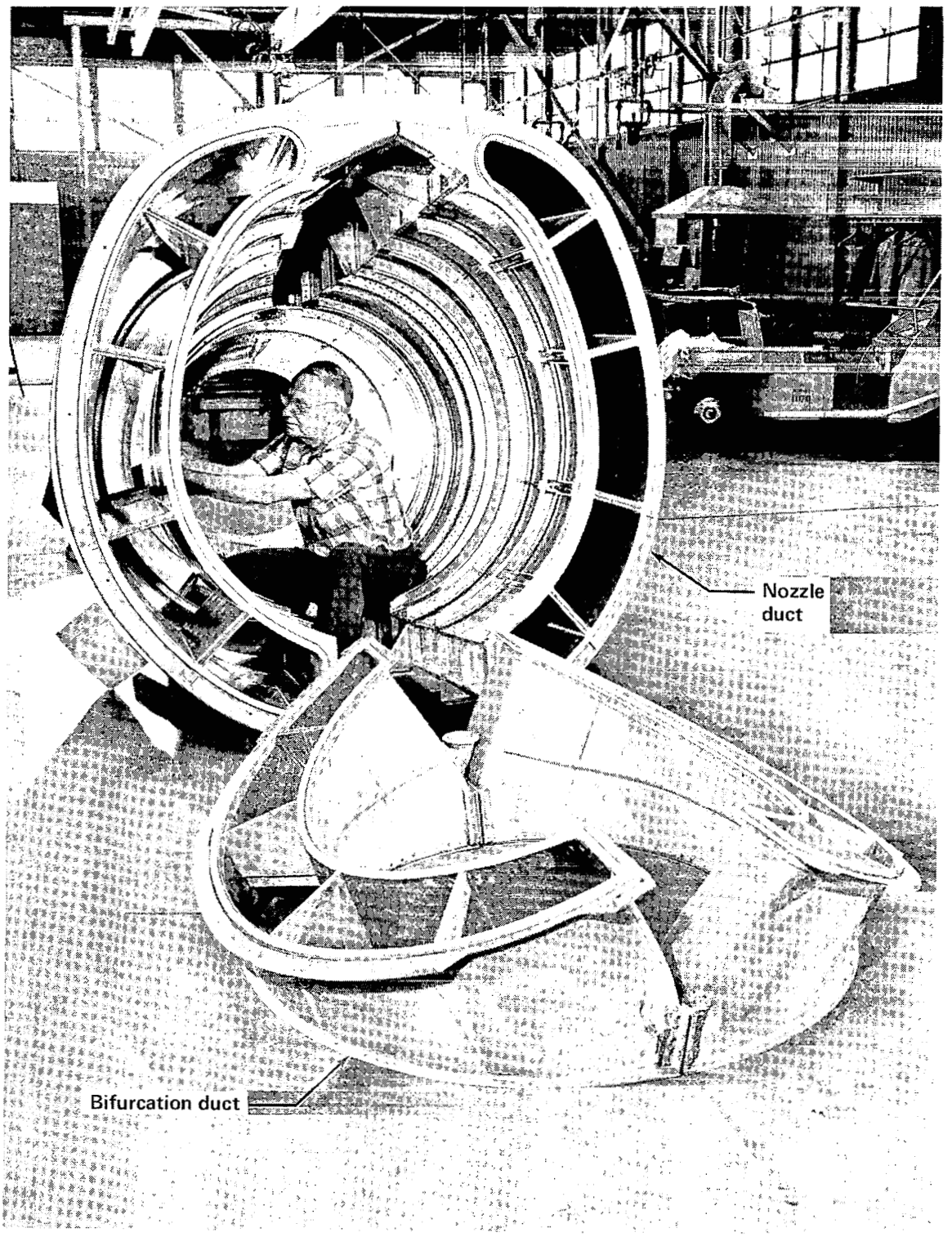

FIGURE 41.–NOZZLE AND BIFURCATION DUCTS

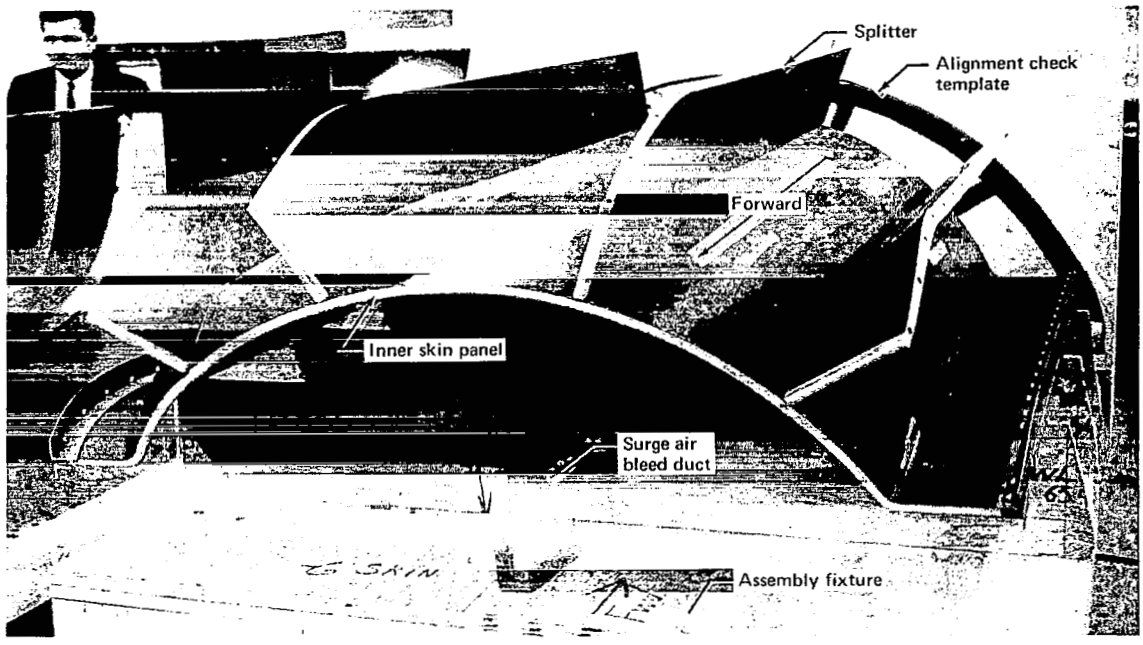

FIGURE 42.—WRAP COWL DUCT POLYIMIDE SPLITTER AND INNER PANEL ASSEMBLY

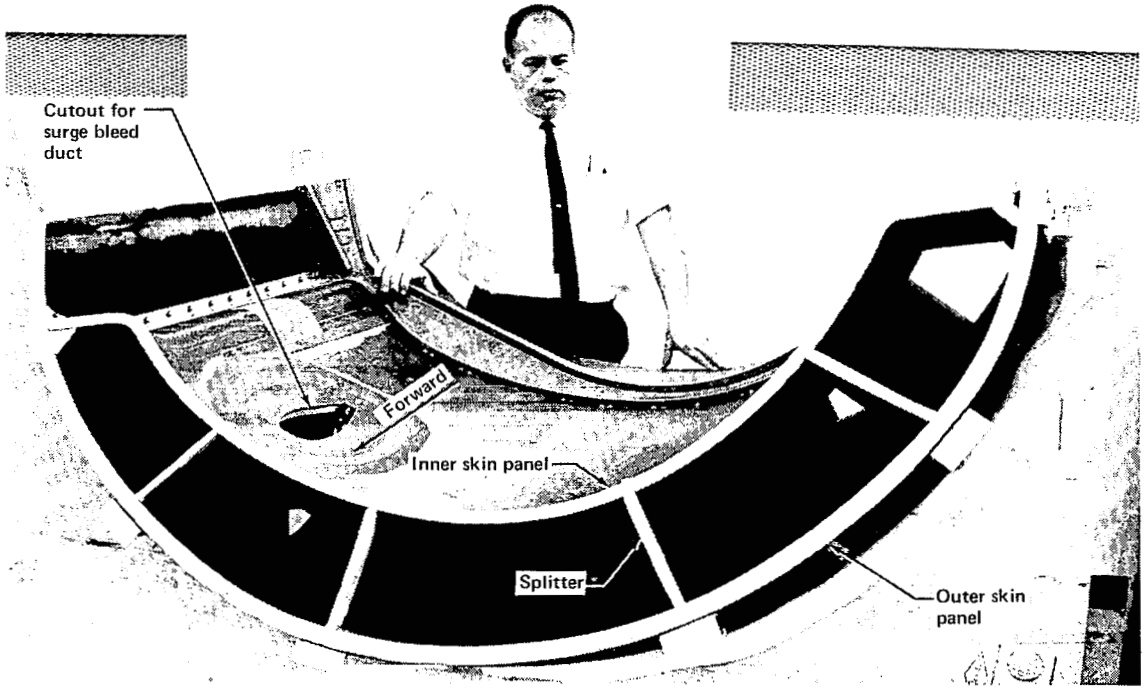

FIGURE 43.—WRAP COWL DUCT POLYIMIDE ASSEMBLY

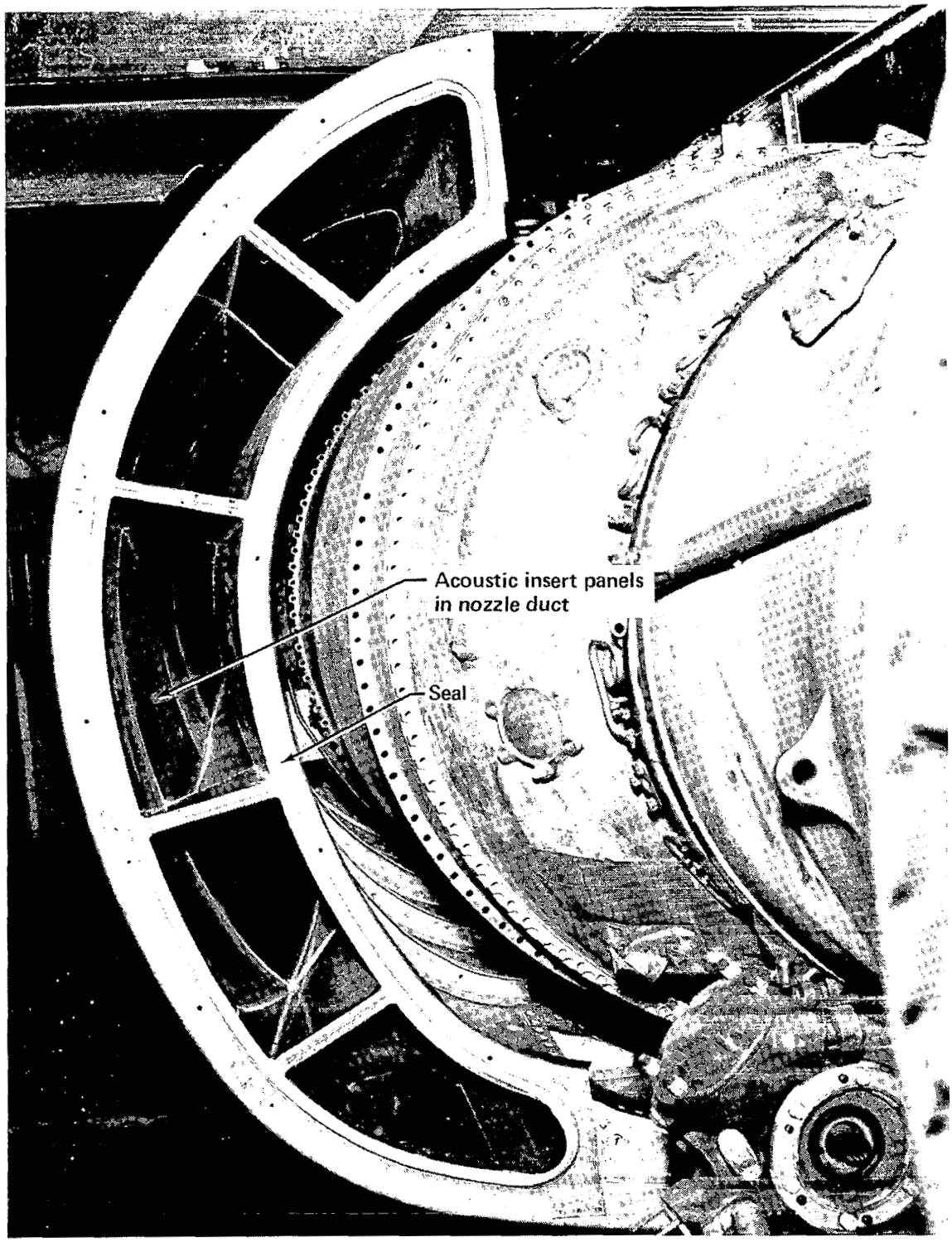

FIGURE 44.—BOILERPLATE NOZZLE DUCT INSTALLATION

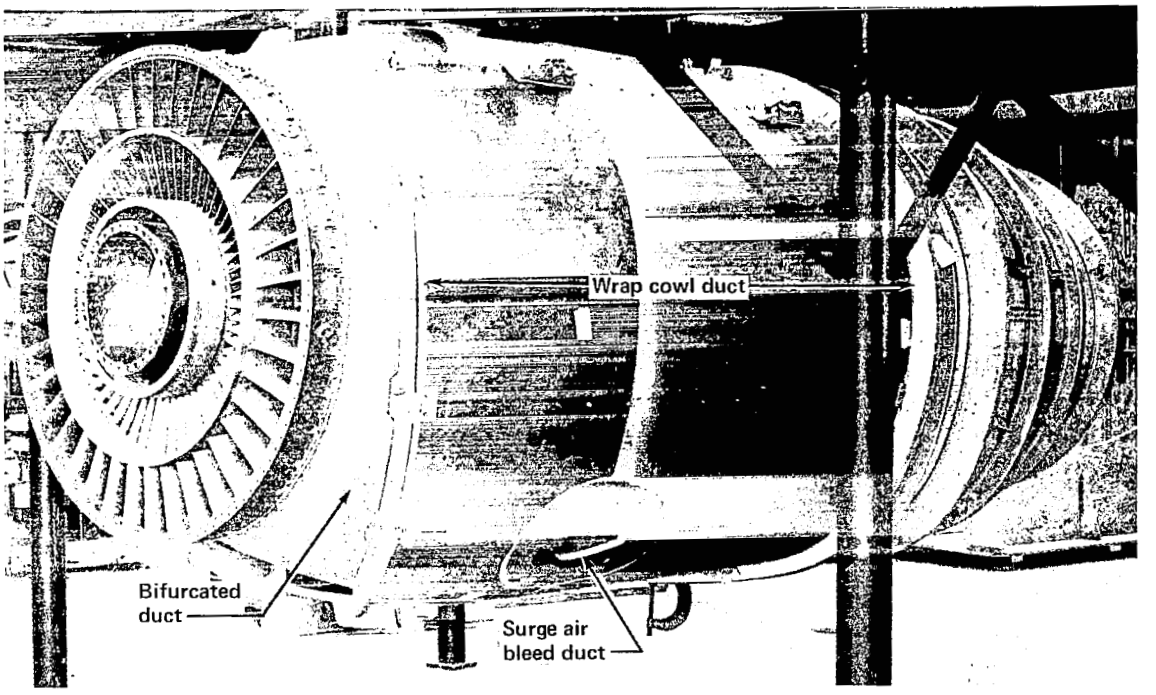

FIGURE 45.—BOILERPLATE DUCT INSTALLATION, FRONT QUARTER VIEW

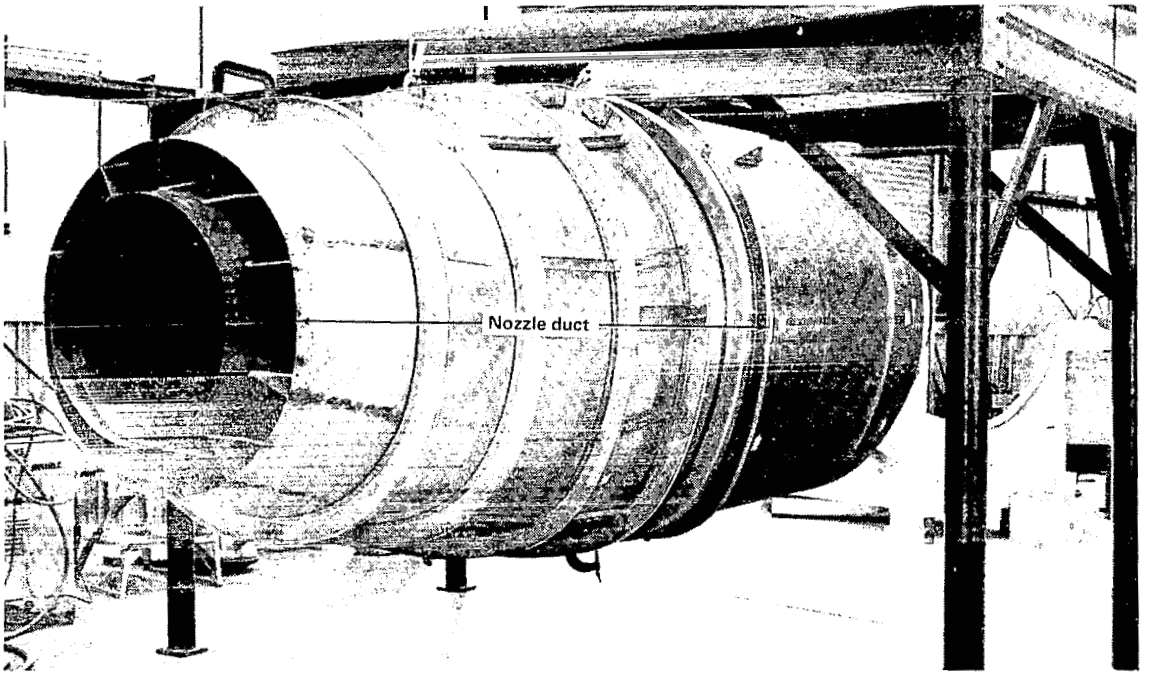

FIGURE 46.—BOILERPLATE DUCT INSTALLATION, REAR QUARTER VIEW

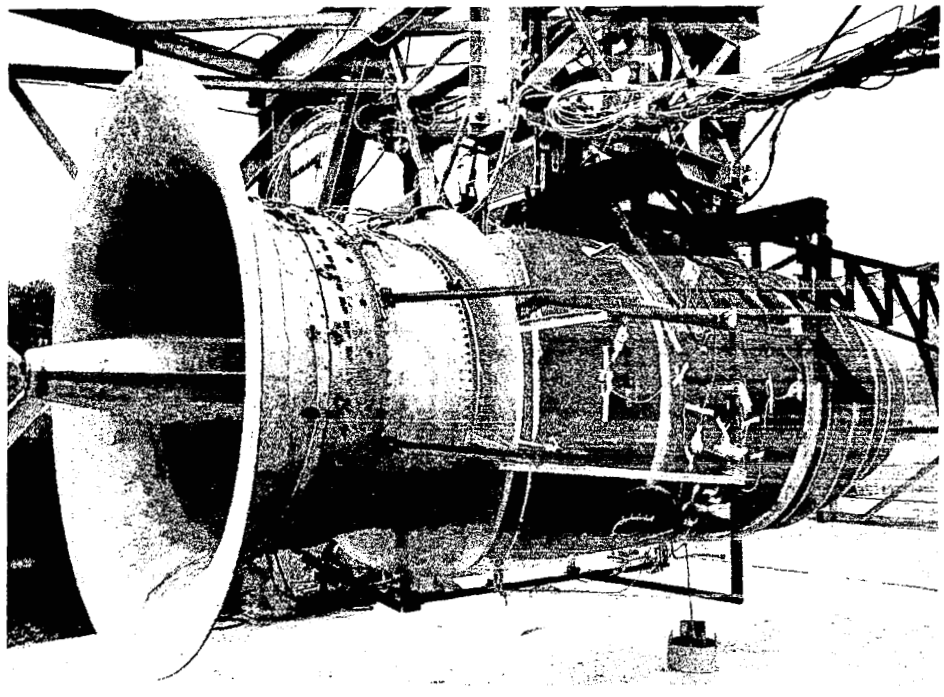

FIGURE 47.–BOILERPLATE DUCT INSTALLATION ON ENGINE TEST RIG

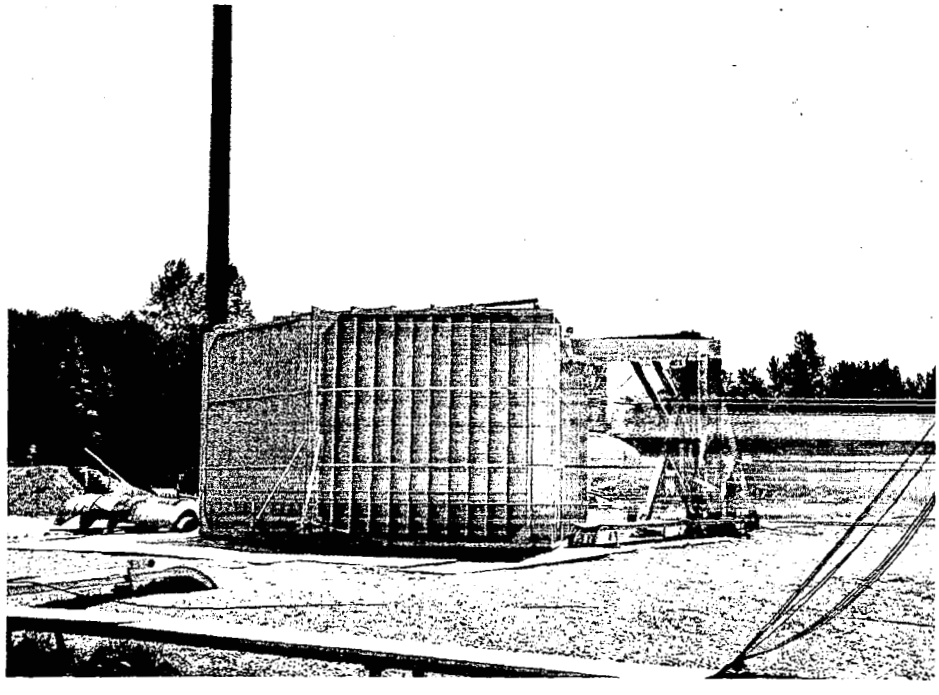

FIGURE 48.–TEST SITE AND INLET NOISE DIRECTIONALIZER

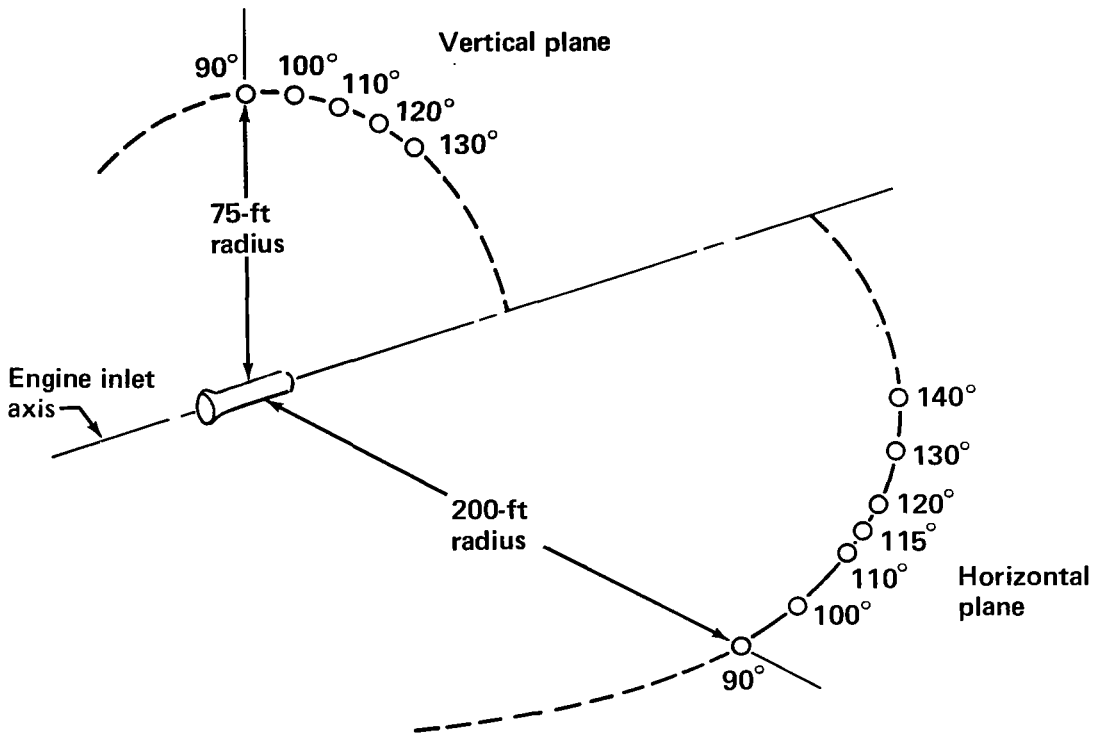

FIGURE 49.—MICROPHONE LOCATIONS

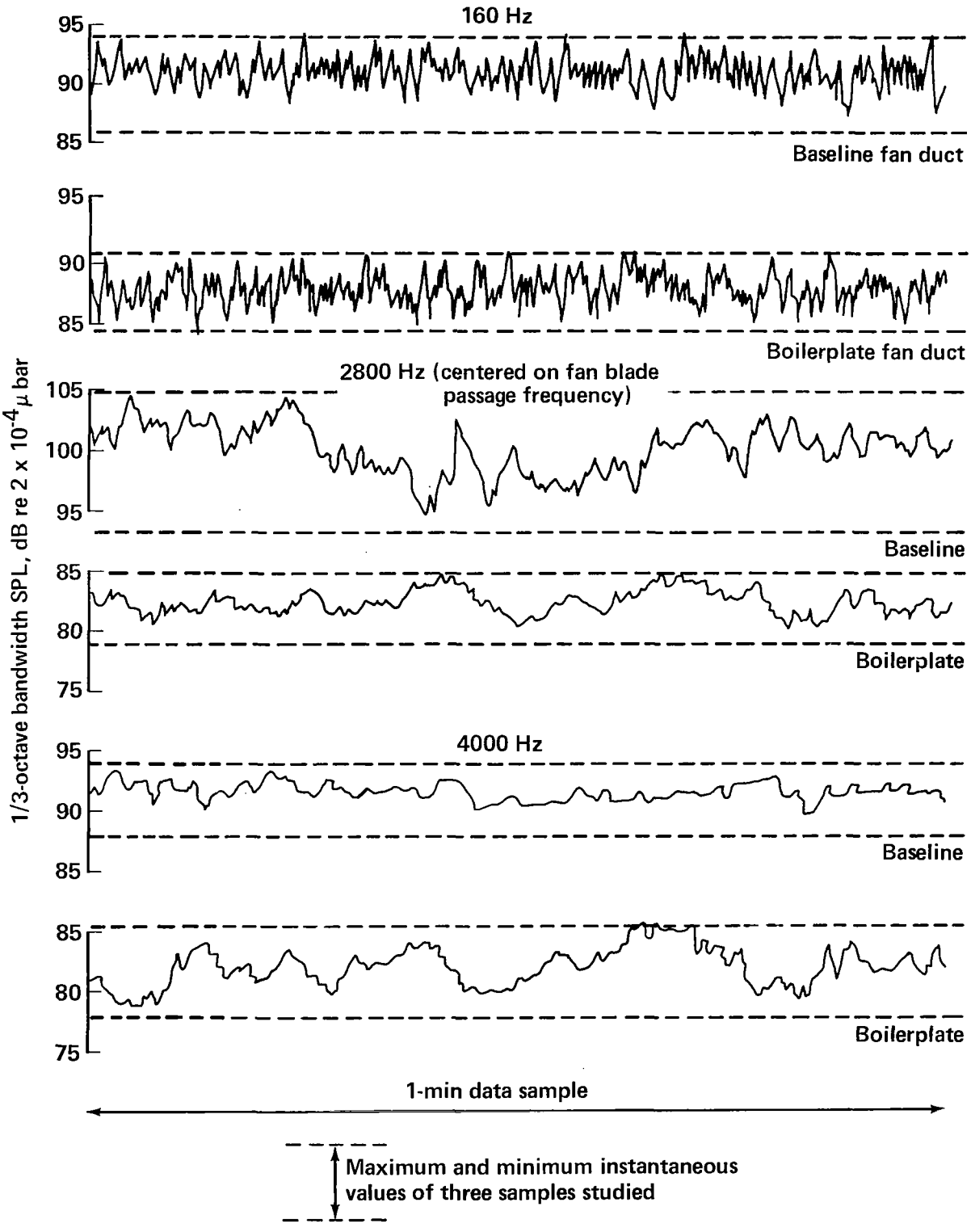

FIGURE 50.—TYPICAL SPL VARIATIONS AS A FUNCTION OF TIME, APPROACH THRUST

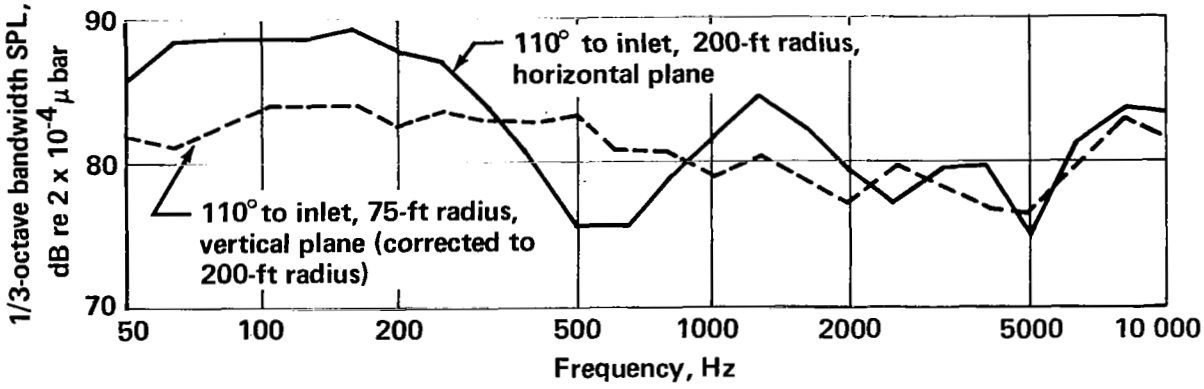

(a) COMPARISON OF HORIZONTAL AND VERTICAL PLANE DATA

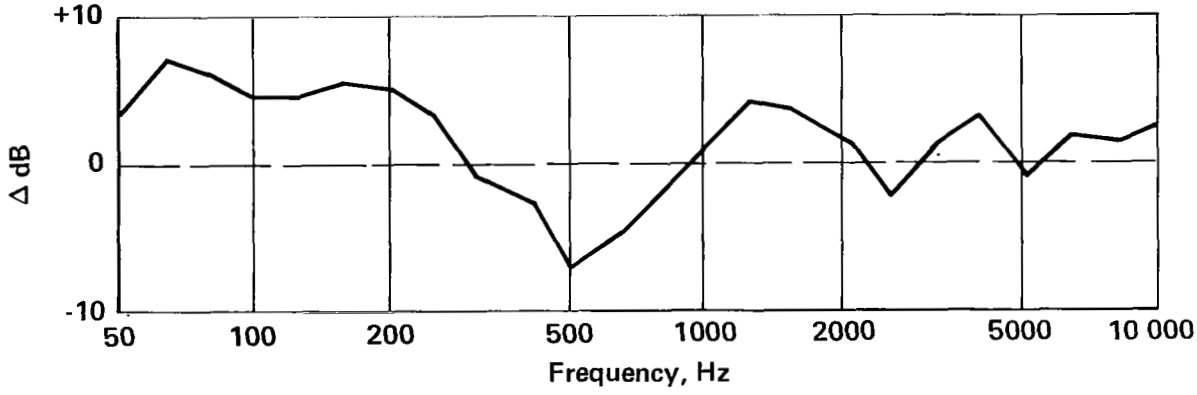

(b) DIFFERENCE BETWEEN HORIZONTAL AND VERTICAL PLANE DATA

FIGURE 51.–COMPARISON OF HORIZONTAL AND VERTICAL PLANE DATA

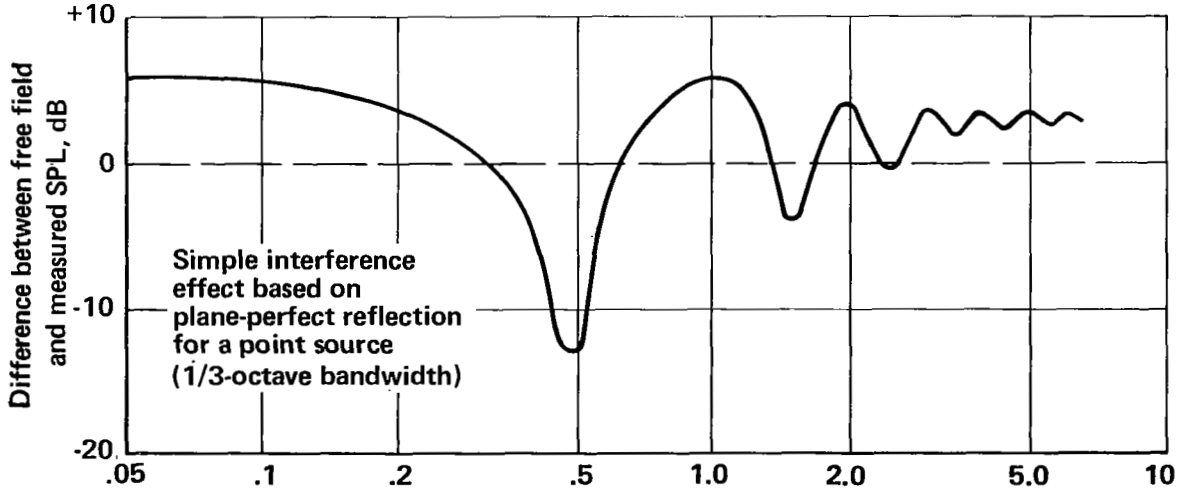

FIGURE 52.–ACOUSTIC WAVE INTERFERENCE EFFECT ON MEASUREMENTS MADE CLOSE TO A REFLECTING PLANE

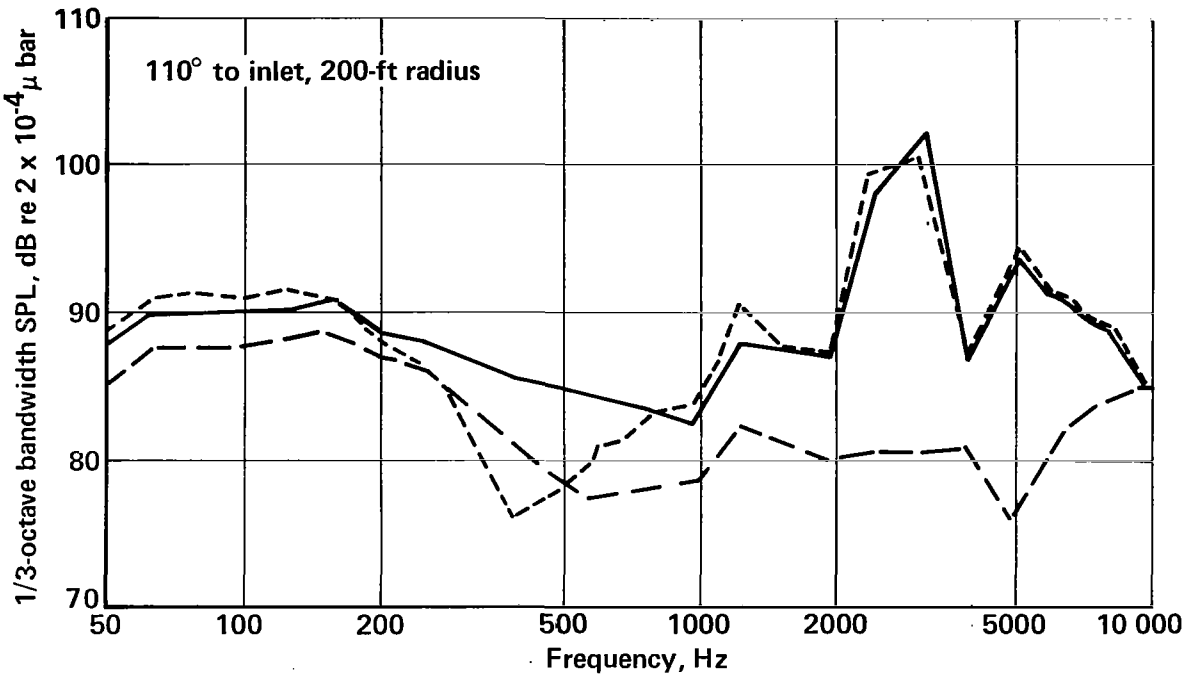

(a) HORIZONTAL PLANE

Baseline fan ducts—April 1968
Baseline fan ducts—October 1968
Boilerplate fan ducts

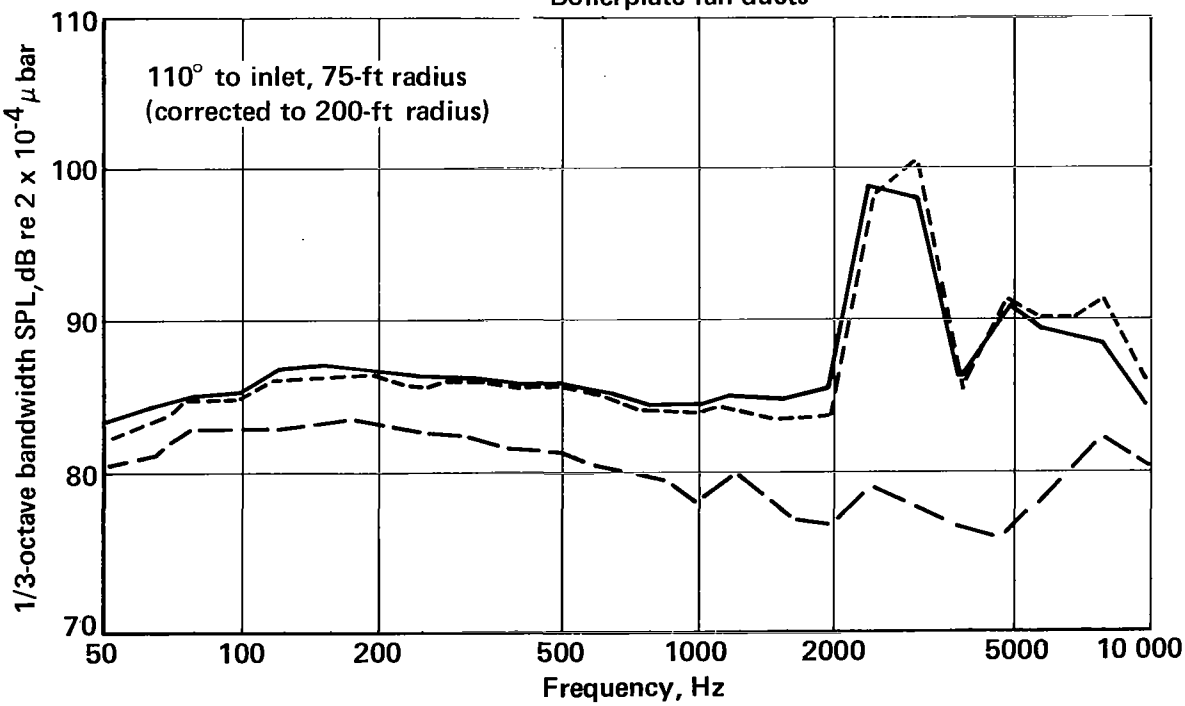

(b) VERTICAL PLANE

FIGURE 53.—COMPARISON OF SPECTRA AT ANGLE OF MAXIMUM FAN NOISE AT APPROACH THRUST

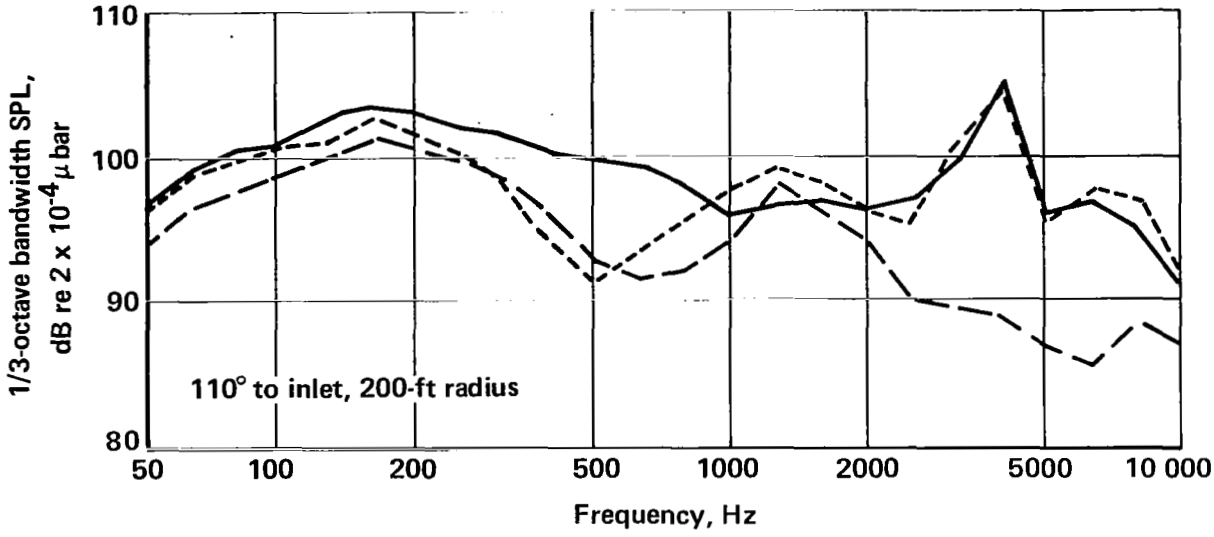

(a) HORIZONTAL PLANE

Baseline fan ducts—April 1968
Baseline fan ducts—October 1968
Boilerplate fan ducts

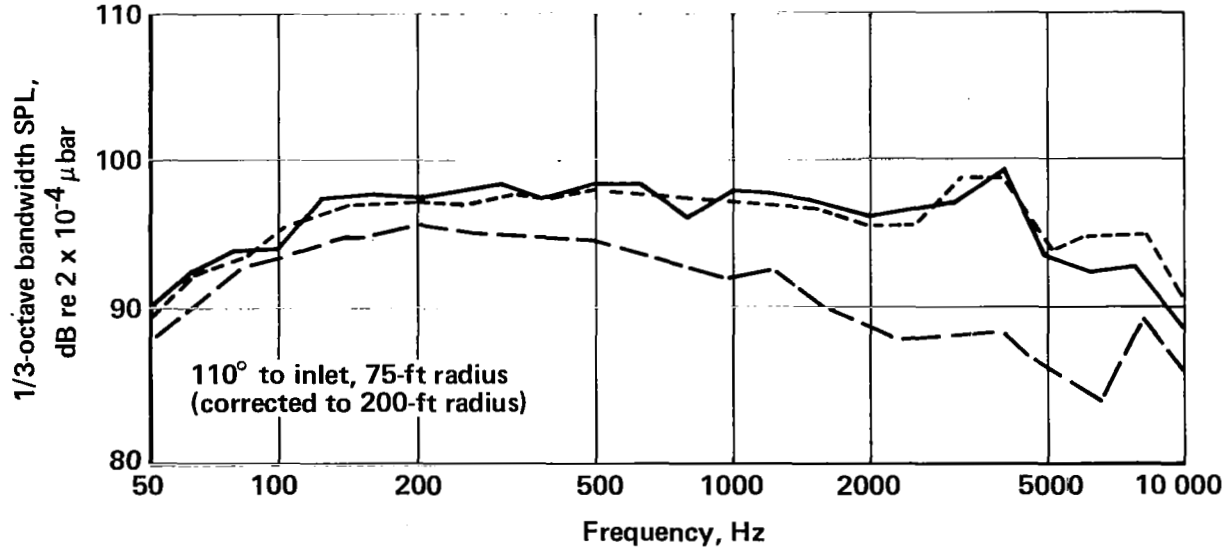

(b) VERTICAL PLANE

FIGURE 54.—COMPARISON OF SPECTRA AT ANGLE OF MAXIMUM FAN NOISE AT TAKEOFF THRUST

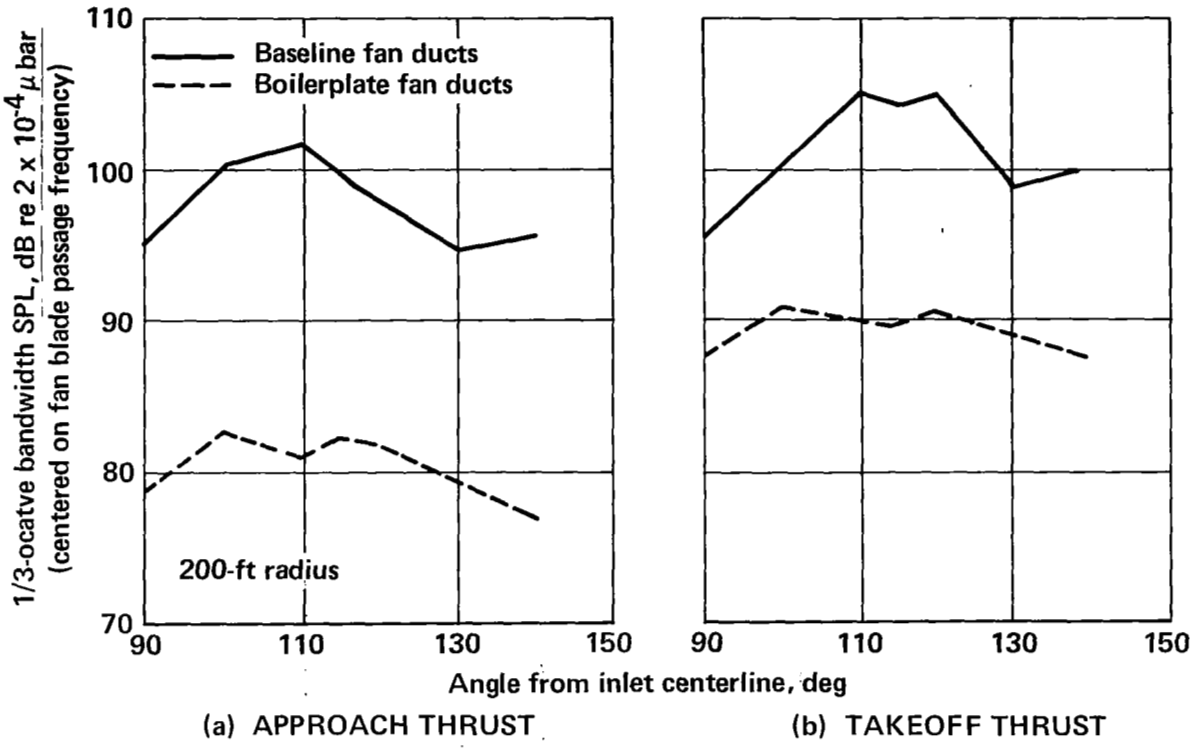

FIGURE 55.–FAN DUCT NOISE RADIATION PATTERNS

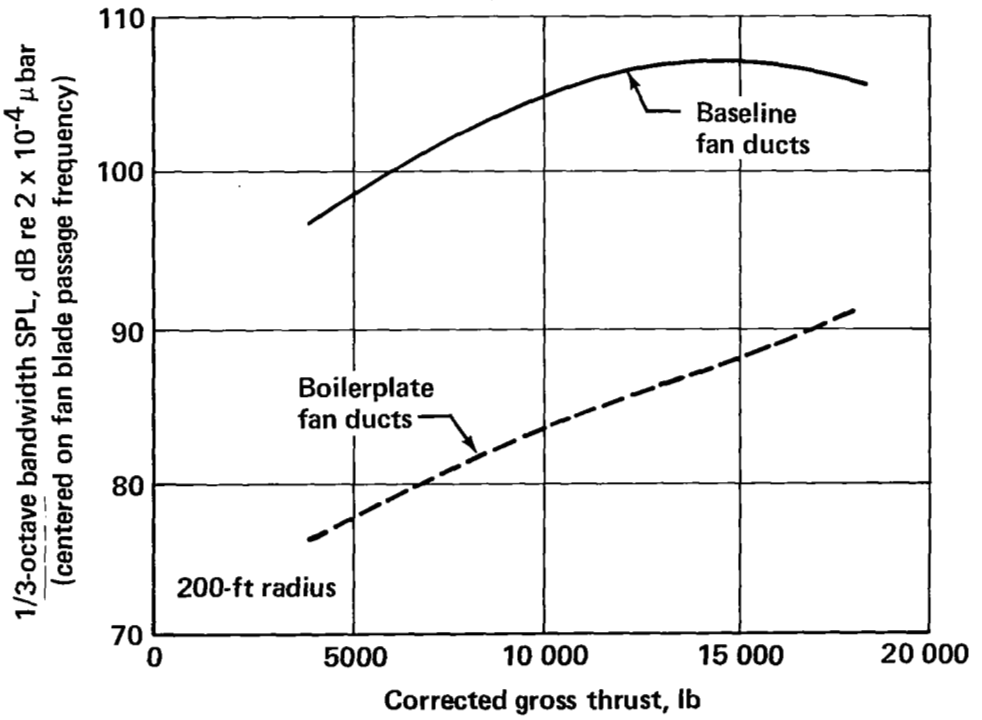

FIGURE 56.–MAXIMUM NOISE LEVELS OF DUCT-RADIATED FAN NOISE

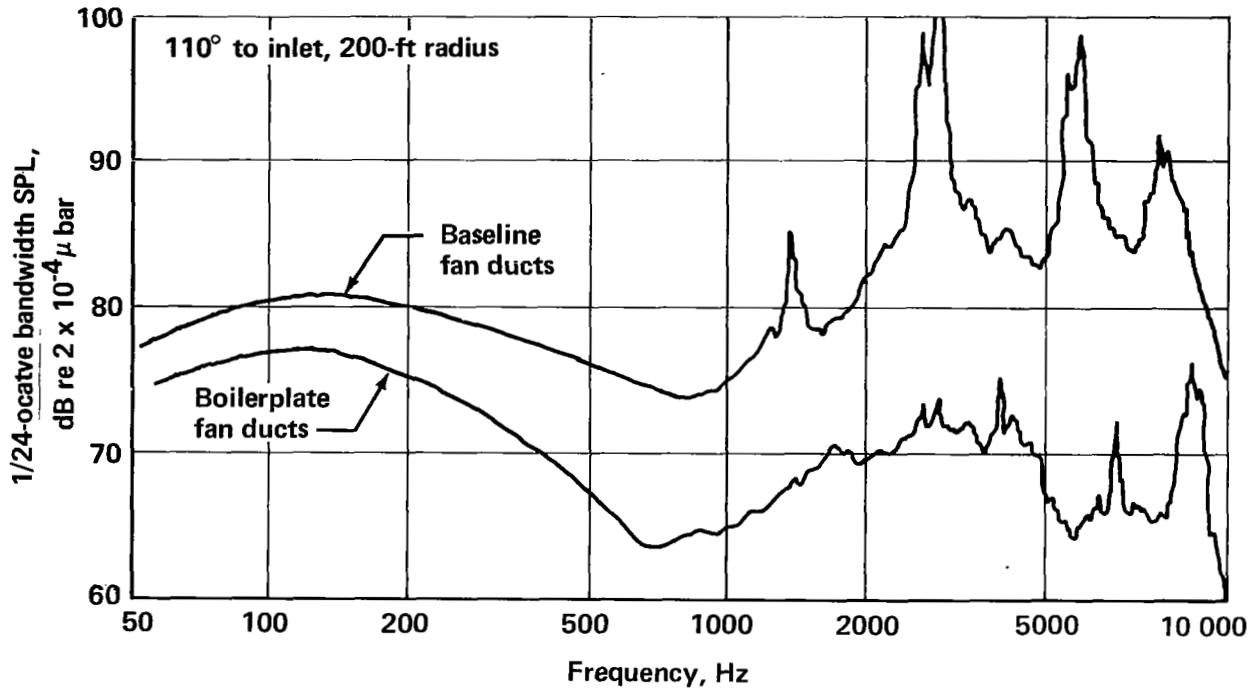

(a) HORZONTAL PLANE

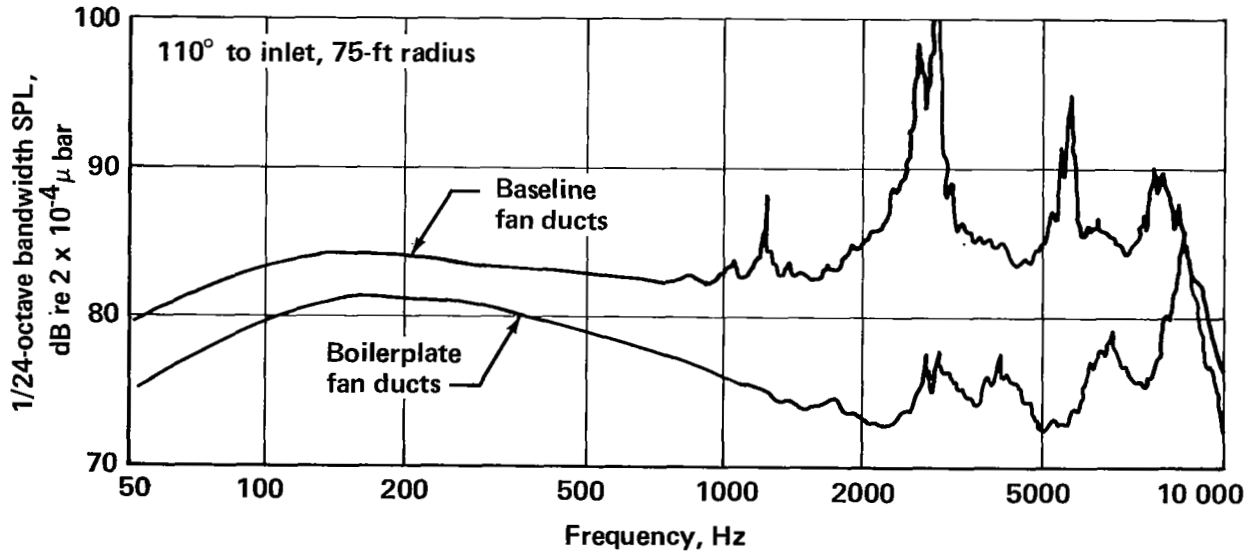

(b) VERTICAL PLANE

FIGURE 57.—TYPICAL NARROWBAND DUCT NOISE SPECTRA AT APPROACH THRUST

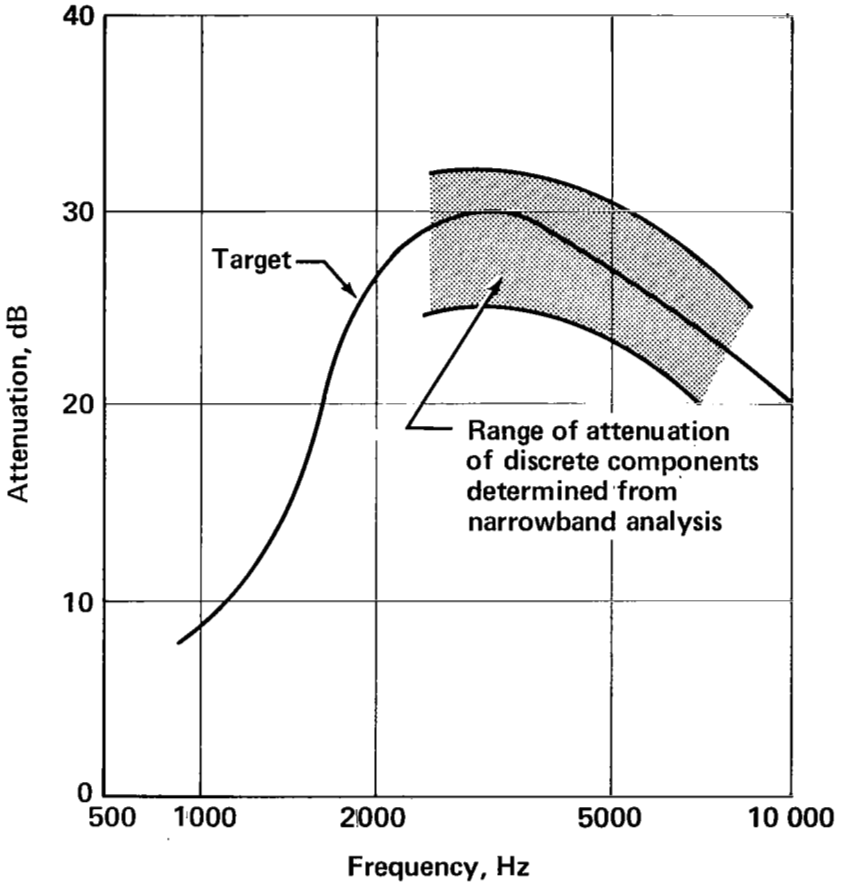

FIGURE 58.—TARGET AND MEASURED FAN DUCT ATTENUATIONS

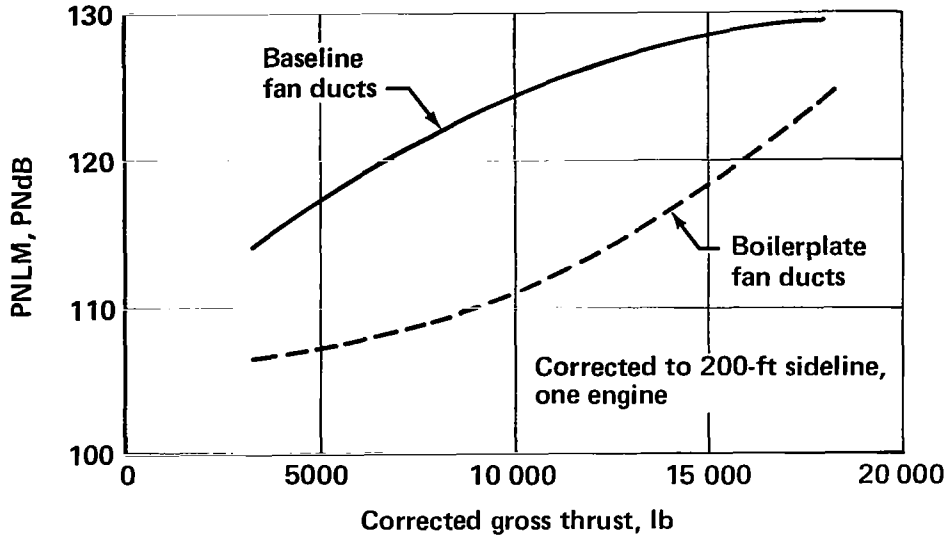

FIGURE 59.–COMPARISON OF MAXIMUM PERCEIVED NOISE LEVELS

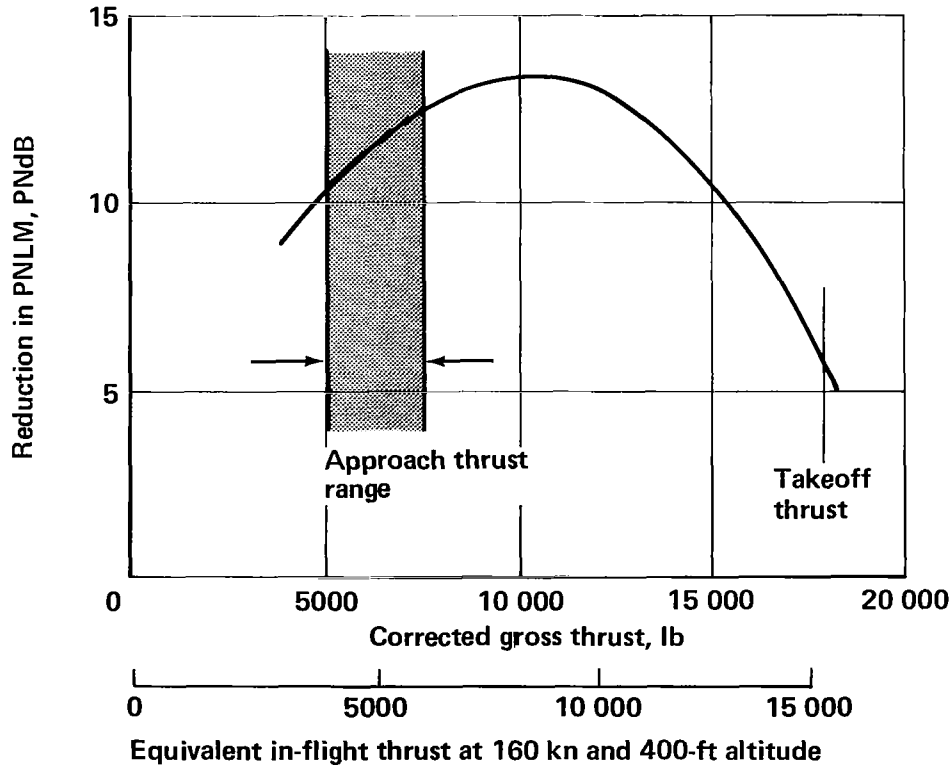

FIGURE 60.–PREDICTED REDUCTION OF MAXIMUM PERCEIVED NOISE LEVEL

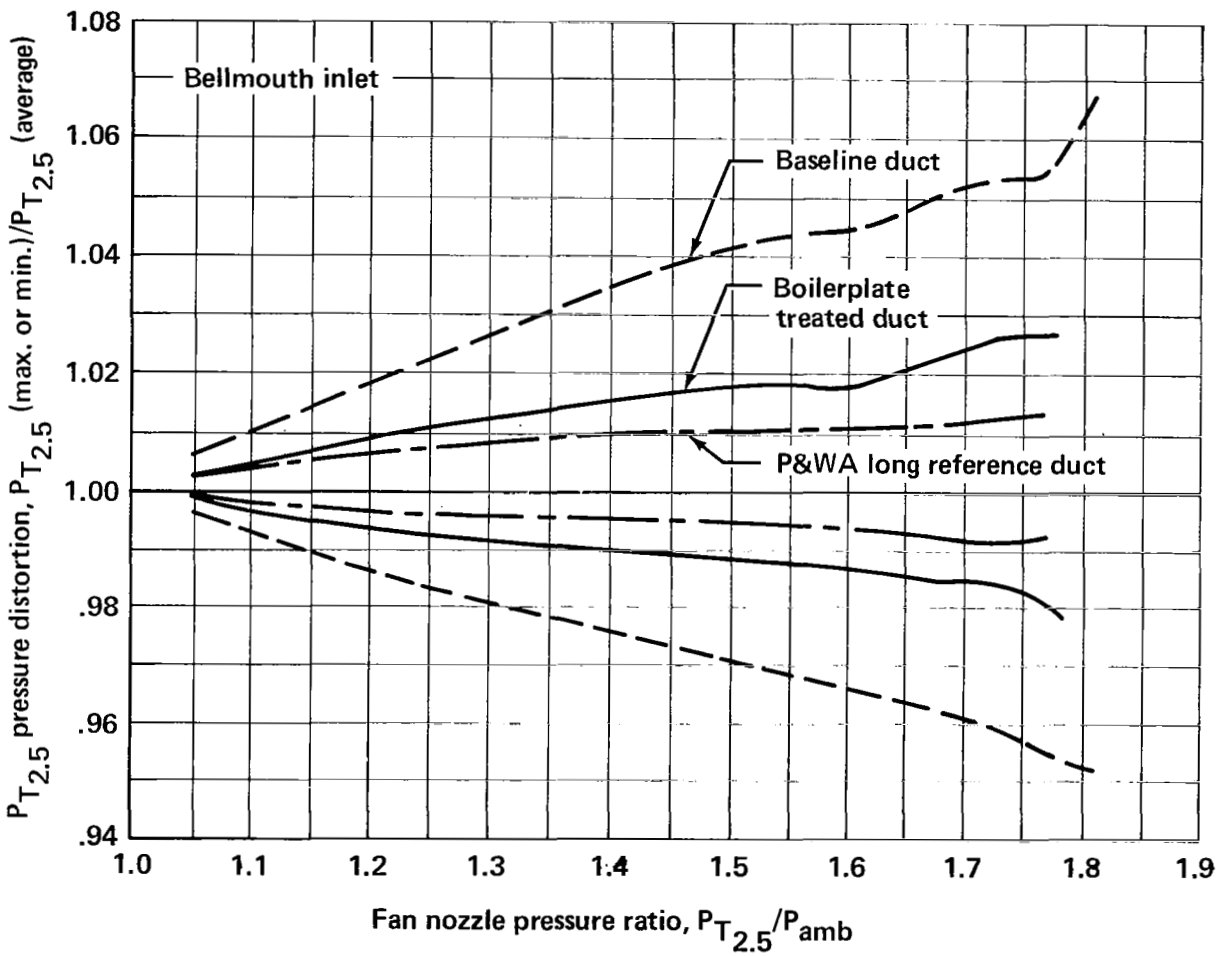

FIGURE 61.—FAN EXIT DISTORTION LIMITS

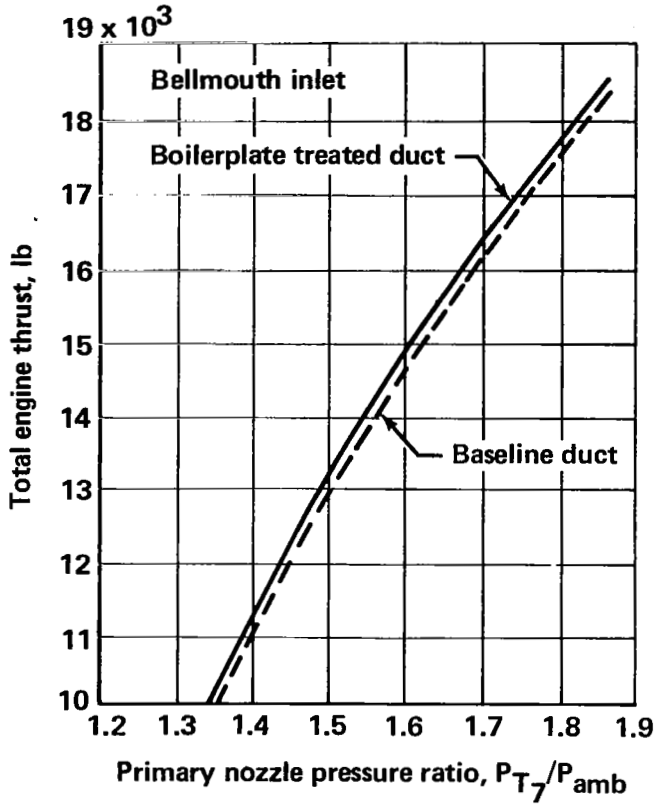

FIGURE 62.—TOTAL ENGINE THRUST COMPARISON

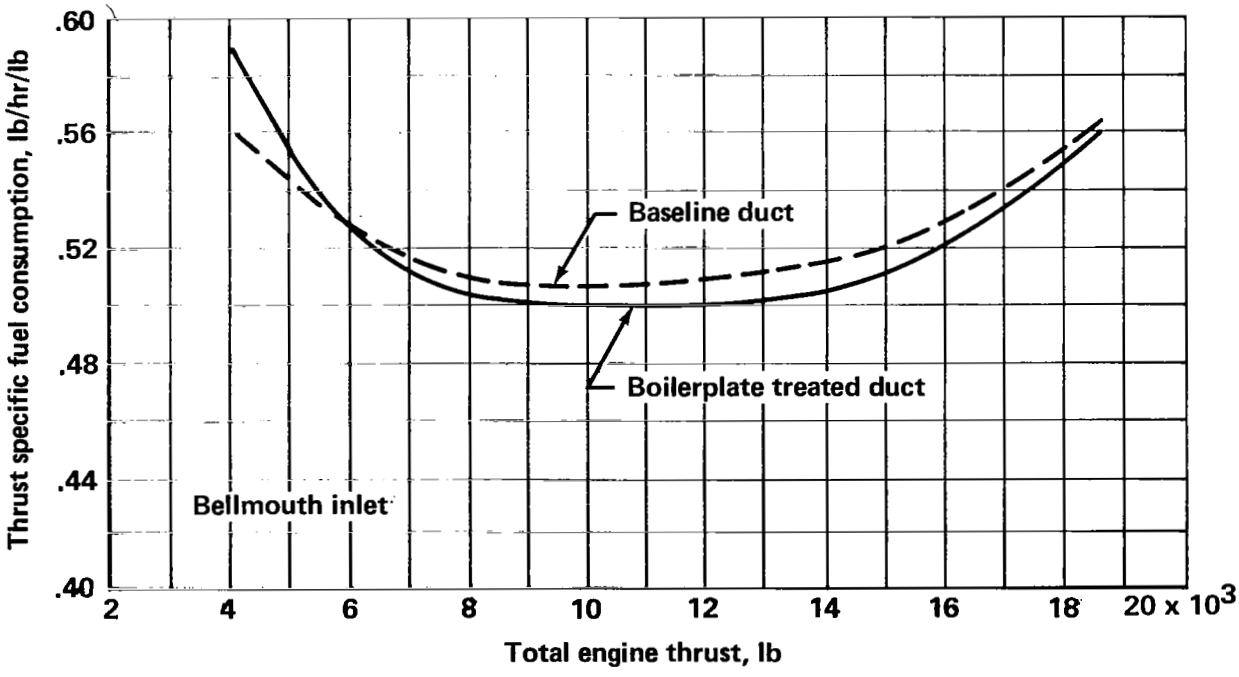

FIGURE 63.—SPECIFIC FUEL CONSUMPTION COMPARISON

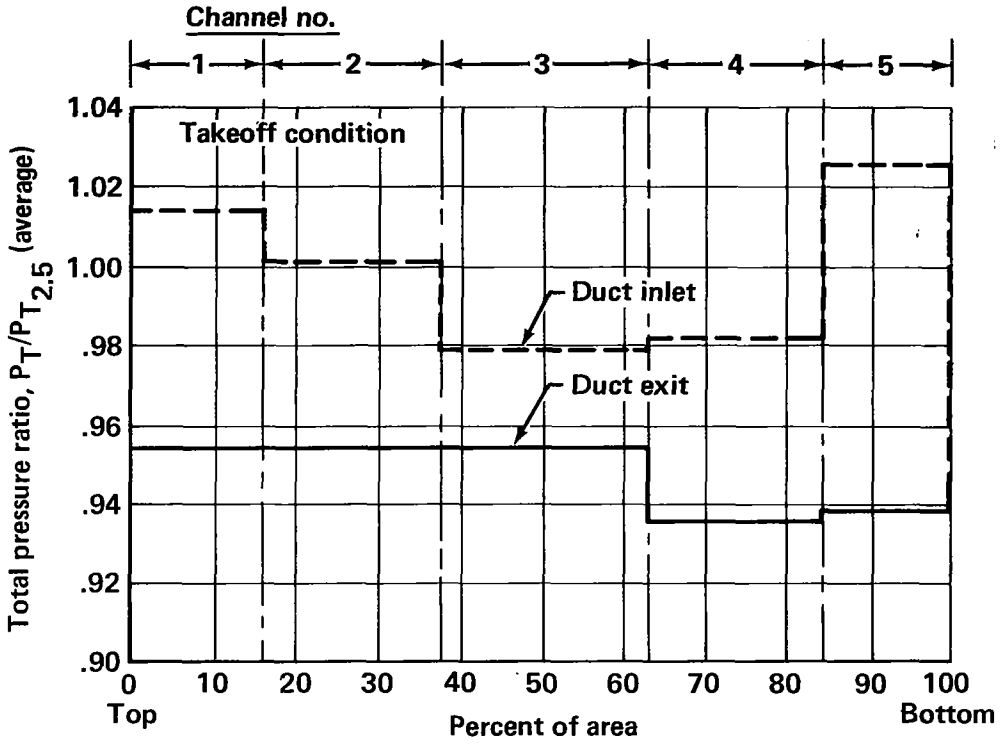

FIGURE 64.–TOTAL PRESSURE DISTRIBUTION

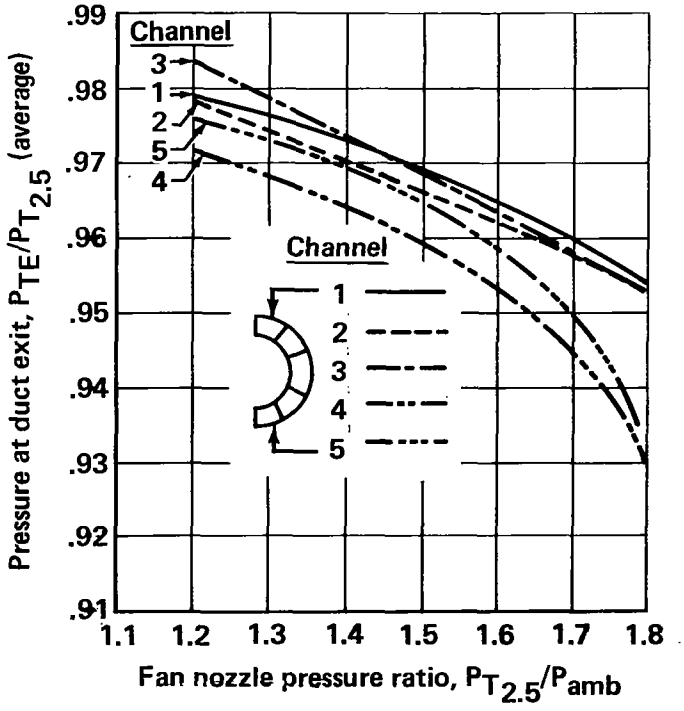

FIGURE 65.–PRESSURE AT NOZZLE EXIT

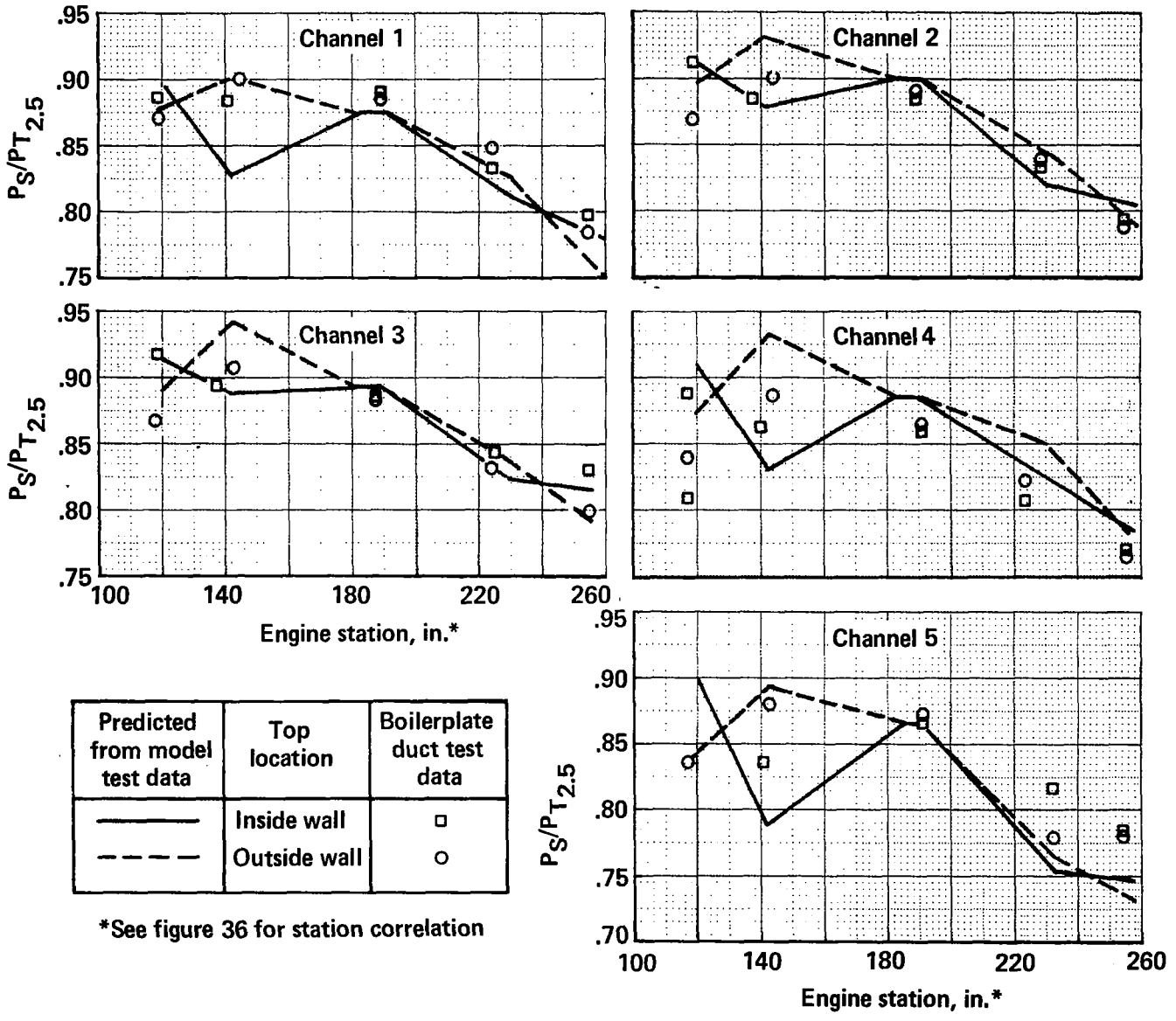

FIGURE 66.–FAN DUCT STATIC PRESSURE DISTRIBUTIONS, TAKEOFF THRUST